Cell Biology
Cancer Biology

mitoBK$_{Ca}$ is functionally expressed in murine and human breast cancer cells and potentially contributes to metabolic reprogramming

Reviewed Preprint

Revised by authors after peer review.

About eLife's process

Reviewed preprint version 2
April 8, 2024 (this version)

Reviewed preprint version 1
December 11, 2023

Posted to preprint server
October 4, 2023

Sent for peer review
September 21, 2023

Helmut Bischof, Selina Maier, Piotr Koprowski, Bogusz Kulawiak, Sandra Burgstaller, Joanna Jasińska, Kristian Serafimov, Monika Zochowska, Dominic Gross, Werner Schroth, Lucas Matt, David Arturo Juarez Lopez, Ying Zhang, Irina Bonzheim, Florian A. Büttner, Falko Fend, Matthias Schwab, Andreas L. Birkenfeld, Roland Malli, Michael Lämmerhofer, Piotr Bednarczyk, Adam Szewczyk, Robert Lukowski

Department of Pharmacology, Toxicology and Clinical Pharmacy, Institute of Pharmacy, University of Tuebingen, Auf der Morgenstelle 8, 72076 Tuebingen, Germany • Dr Margarete Fischer-Bosch Institute of Clinical Pharmacology, Auerbachstraße 112, 70376 Stuttgart, Germany • Laboratory of Intracellular Ion Channels, Nencki Institute of Experimental Biology, Polish Academy of Sciences, 3 Pasteur Street, 02-093 Warsaw, Poland • NMI Natural and Medical Sciences Institute at the University of Tuebingen, Markwiesenstraße 55, Reutlingen 72770, Germany • Institute of Clinical Anatomy and Cell Analysis, University of Tuebingen, Oesterbergstraße 3, 72074 Tuebingen, Germany • Institute of Pharmaceutical Sciences, Pharmaceutical (Bio-)Analysis, University of Tuebingen, Auf der Morgenstelle 8, 72076 Tuebingen, Germany • University of Tuebingen, Tuebingen, Germany • Medical Clinic IV, University Hospital Tuebingen, Otfried-Müller-Straße 10, 72076 Tuebingen, Germany • Institute of Pathology and Neuropathology, University Hospital Tuebingen, 72076 Tuebingen, Germany • Image-Guided and Functionally Instructed Tumor Therapies Cluster of Excellence (iFIT), University of Tuebingen, Roentgenweg 11, 72076 Tuebingen, Germany • Department of Clinical Pharmacology, University of Tuebingen, Auf der Morgenstelle 8, 72076 Tuebingen, Germany • Department of Biochemistry and Pharmacy, University of Tuebingen, Auf der Morgenstelle 8, 72076 Tuebingen, Germany • German Cancer Consortium (DKTK), German Cancer Research Center, Partner Site Tuebingen, Auf der Morgenstelle 15, 72076 Tuebingen, Germany • Gottfried Schatz Research Center, Molecular Biology and Biochemistry, Medical University of Graz, Neue Stiftingtalstraße 6, 8010 Graz, Austria • BioTechMed Graz, Mozartgasse 12, 8010 Graz, Austria • Department of Physics and Biophysics, Warsaw University of Life Sciences (SGGW), Nowoursynowska St. 159 02-776 Warsaw, Poland

Abstract

Summary

Alterations in the function of K^+ channels such as the voltage- and Ca^{2+} activated K^+ channel of large conductance (BK$_{Ca}$) reportedly promote breast cancer (BC) development and progression. Underlying molecular mechanisms remain, however, elusive. Here, we provide electrophysiological evidence for a BK$_{Ca}$ splice variant localized to the inner mitochondrial membrane of murine and human BC cells (mitoBK$_{Ca}$). Through a combination of genetic knockdown and knockout along with cell permeable BK$_{Ca}$ channel blocker, we show that mitoBK$_{Ca}$ modulates overall cellular and mitochondrial energy production and mediates the metabolic rewiring referred to as the “Warburg effect”, thereby promoting BC cell

proliferation in the presence and absence of oxygen. Additionally, we detect mitoBK$_{Ca}$ and BK$_{Ca}$ transcripts in low or high abundance, respectively, in clinical BC specimens. Together, our results emphasize, that targeting mitoBK$_{Ca}$ could represent a treatment strategy for selected BC patients in future.

eLife assessment

The large-conductance Ca2+ activated K+ channel BKCa has been reported to promote breast cancer progression. The present study presents **convincing** evidence that an intracellular subpopulation of this channel reprograms breast cancer cells towards the Warburg phenotype, one of the metabolic hallmarks of cancer. This **important** finding advances the field of cancer cell metabolism and has potential therapeutic implications.

Introduction

Cancer represents a complex disease characterized by unconstrained cell proliferation and the spread of malignant cells in the body (Kalia, 2015; Seyfried and Shelton, 2010). It is one of the leading causes of death worldwide, with millions of new cases diagnosed each year (Sung et al., 2021). Globally, the most prevalent form of cancer represents breast cancer (BC) (Sung et al., 2021). Despite many available anti-cancer treatments which largely depend on the steroid and epidermal growth factor (HER2) receptor status (Dunnwald et al., 2007), cancer cells frequently escape from existing therapies due to adaptions (P. Wu et al., 2021). Therefore, the identification of novel targets and therapeutic strategies that confer benefits for at least a subset of patients, whose cancer displays specific molecular or cellular features, is of utmost relevance.

Important factors that emerged as new cancer targets are ion channels (Li and Xiong, 2011). Especially alterations in the expression levels and function of potassium ion (K^+) channels are critically related to cancer malignancy and progression (Li et al., 2023, p. 0). One of these channels represents the calcium ion (Ca^{2+}) and voltage-activated K^+ channel of large conductance (BK$_{Ca}$) (Mohr et al., 2022). Canonical BK$_{Ca}$ channels usually localize in the plasma membrane (PM) of cells, and contribute to the regulation of the cytosolic K^+ content, the PM potential ($\Delta\Psi_{PM}$), cell cycle, and cell motility, as well as regulatory volume, changes (Burgstaller et al., 2022a). Opening of BK$_{Ca}$ channels results in K^+ efflux, increasing the electrochemical driving force for Ca^{2+} entry into the cancer cell and affecting pathological cell growth and death (Ouadid-Ahidouch and Ahidouch, 2013). Accordingly, in BC cells (BCCs), an upregulation of BK$_{Ca}$ has been associated with increased malignancy (Huang and Jan, 2014; Mohr et al., 2022; Oeggerli et al., 2012). However, besides their localization in the PM, several K^+ channels, including BK$_{Ca}$, have also been identified in the inner mitochondrial membrane (IMM) (mitoBK$_{Ca}$), a topic which has been extensively reviewed recently (Checchetto et al., 2021; Kulawiak and Szewczyk, 2022; Szabo and Szewczyk, 2023; Szewczyk et al., 2009; Wrzosek et al., 2020). mitoBK$_{Ca}$ was first described by Siemen et al. in a human glioma cell line more than 20 years ago (Siemen et al., 1999). So far, mitoBK$_{Ca}$ has further been found e.g. in bronchial epithelial cells (Dabrowska et al., 2022), neurons (Douglas et al., 2006), skeletal muscle cells (Skalska et al., 2008), and in cardiac myocytes (Xu et al., 2002). In the latter, a splice variant, the BK$_{Ca}$-DEC isoform containing a unique C-terminal exon of 50 amino acids forms the functional mitoBK$_{Ca}$ channel at the IMM (Singh et al., 2013). Little, however, is known about the molecular identity of mitoBK$_{Ca}$ in other cell types, and mitochondrial localization of BK$_{Ca}$ in BCCs has not been demonstrated so far.

Cancer cells show increased energy demands due to their high proliferation rates. Thus, tumor cells compensate for their elevated energy demand by increasing metabolic activities and adapting to nutrient-poor metabolic niches in the tumor microenvironment, allowing them to overcome oxygen (O_2)-dependent mitochondrial metabolism (Eales et al., 2016; Gross et al., 2022; Jang et al., 2013; Nazemi and Rainero, 2020). This metabolic switch from oxidative phosphorylation to glycolysis, frequently referred to as the "Warburg effect", describes the phenomenon that cancer cells rather secrete lactate to the extracellular matrix (ECM), instead of utilizing pyruvate to fuel the TCA cycle (Warburg, 1924). This lactate secretion towards the ECM was shown to promote multiple microenvironmental cues causing tumor progression (de la Cruz-López et al., 2019). Interestingly, extracellular K^+ may also impair effector T-cell function, and, thus, the anti-tumor immune response (Eil et al., 2016), while, within the cancer cell, functions of several glycolytic enzymes rely on K^+ (Bischof et al., 2021; Gohara and Di Cera, 2016). Further, the presence of mitoBK$_{Ca}$ contributes to the K^+ entry into the mitochondrial matrix to interfere with mitochondrial volume changes and the mitochondrial membrane potential ($\Delta\Psi_{mito}$) (Krabbendam et al., 2018). Consequently, (mito)/BK$_{Ca}$-dependent mechanisms may severely affect energy production pathways and the resulting energy supply of cancer cells.

To elucidate how BK$_{Ca}$ contributes to increasing BCC malignancy (Oeggerli et al., 2012), we utilized BK$_{Ca}$ pro- and deficient human BCC lines including MDA-MB-453 and MCF-7 cells, and primary murine BCCs derived from the mouse mammary tumor polyoma middle T-antigen (MMTV-PyMT)-induced wild type (WT) or BK$_{Ca}$ knock-out (BK-KO) BC model (Mohr et al., 2022). In these cells, either isoforms of BK$_{Ca}$ were expressed, or BK$_{Ca}$ was pharmacologically blocked by paxilline or iberiotoxin, two frequently used inhibitors of BK$_{Ca}$ that either penetrate the cell or act exclusively at PM localized channels, respectively (Candia et al., 1992; Zhou and Lingle, 2014). These approaches were complemented by patch-clamp experiments, and by measuring the cellular ion homeostasis and metabolism with fluorescence live-cell imaging, extracellular flux analysis and liquid chromatography-mass spectrometry (LC-MS)-based approaches.

Our results emphasize that the presence of BK$_{Ca}$ in the IMM affects mitochondrial bioenergetics, thereby increasing BCC malignancy. This effect was specifically mediated by the DEC isoform of BK$_{Ca}$, i.e., mitoBK$_{Ca}$. Functional expression of BK$_{Ca}$-DEC was validated by single-channel patch-clamp recordings BCC-derived mitoplasts. Importantly, we also identified BK$_{Ca}$-DEC expression in a subset of BC patient biopsies using nanostring-based mRNA expression analysis. Finally, mitoBK$_{Ca}$ crucially contributed to murine and human BCC proliferation and hypoxic resistance, and its activity increased lactate secretion resulting in higher extracellular acidification rates, even in the presence of O_2.

Combined, our analyses provide, for the first time, a mechanistic link between functionally relevant mitochondrial BK$_{Ca}$ isoforms in cancer cells and the promotion of the Warburg effect.

Results

Functional characterization of BK$_{Ca}$ expression in BCCs

First, we assessed the functional expression of BK$_{Ca}$ in established human BCC lines by performing whole-cell patch-clamp experiments. Primary BCCs obtained from transgenic, BC-bearing MMTV-PyMT WT or BK-KO mice were used as positive or negative controls, respectively (Mohr et al., 2022). Patch-clamp experiments revealed that depolarizing stimuli delivered in 20 mV increments induced K^+ outward currents that were larger in MMTV-PyMT WT compared to BK-KO cells (**Figs. 1A** and **1B**, and **Figs. S1A** and **S1B**). To validate that these increased currents were elicited by BK$_{Ca}$, we pharmacologically inhibited the channel by using either paxilline or iberiotoxin (Candia et al., 1992; Zhou and Lingle, 2014). While the current remained unaffected by these treatments in MMTV-PyMT BK-KO cells (**Fig. 1B** and **Fig. S1B**), peak currents

(I_{max}) were drastically reduced in MMTV-PyMT WT cells (**Fig. 1A** and **Fig. S1A**). Further, we analyzed the plasma membrane potential ($\Delta\Psi_{PM}$) in these cells using the voltage-sensitive fluorescent dye Dibac4(3) (Adams and Levin, 2012) as well as current clamp experiments. The $\Delta\Psi_{PM}$ was more polarized in MMTV-PyMT WT compared to BK-KO cells (**Fig. 1C and Fig. S1C**), as expected, due to the presence of hyperpolarizing BK_{Ca} channels in WT cells (N'Gouemo, 2014). Current clamp experiments unveiled a basal $\Delta\Psi_{PM}$ of -44.0 ± 2.4 mV and -32.2 ± 2.1 mV for MMTV-PyMT WT and BK-KO cells, respectively (**Fig. S1C**). Iberiotoxin treatment equalized the $\Delta\Psi_{PM}$ of the two genotypes (**Fig. S1C**). In line with these findings, using a recently developed, genetically encoded K^+ sensor, NES lc-LysM GEPII 1.0 (Bischof et al., 2017), we found reduced cytosolic K^+ concentrations ($[K^+]_{cyto}$) in MMTV-PyMT WT cells under basal conditions (83.07 ± 5.8 mM for WT ctrl vs. 121.2 ± 7.1 mM for BK-KO ctrl), which increased to the BK-KO cell level in response to iberiotoxin treatment (109.8 ± 10.8 mM for WT + IBTX vs. 114.6 ± 9.8 mM for BK-KO + IBTX) (**Figs. S1D** and **Fig. S1E**), explaining the PM depolarization. Subsequently, we recorded current-voltage relationships using the human BCC lines MDA-MB-453 and MCF-7, expressing either high or low levels of BK_{Ca} mRNA transcripts, respectively (Mohr et al., 2022). Analysis of the outward currents activated by depolarization demonstrated a paxilline- and iberiotoxin-sensitive current in MDA-MB-453 cells (**Fig. 1D** and **Fig. S1F**), indicative for functional BK_{Ca} channels in their PM, but not in MCF-7 cells (**Fig. 1E** and **Fig. S1G**), which is well in line with previous studies (Mohr et al., 2022). Based on the almost non-existent level of BK_{Ca}-mediated PM currents in MCF-7 cells, we utilized these cells to express different BK_{Ca} isoforms fused to a red fluorescent protein (RFP). Therefore, we either used an earlier identified mitoBK_{Ca} isoform (Singh et al., 2013), namely BK_{Ca}-DEC^{RFP}, or the same channel lacking C-terminal amino acids including the DEC exon, hereinafter referred to as BK_{Ca}^{RFP} (**Fig. 1F**). We hypothesized, that, in analogy to cardiac myocytes (Singh et al., 2013), the expression of BK_{Ca}-DEC^{RFP} in MCF-7 cells may yield a functional channel present in the IMM. To test this, MCF-7 cells were first transiently transfected either with RFP fused to a glycosylphosphatidylinositol (GPI)-anchor (RFP-GPI) directing RFP to the PM, or linked to a cytochrome c oxidase subunit 8 (COX8) mitochondrial leading sequence, yielding a mitochondrial targeted fusion protein (mtRFP) (**Fig. S1H** and grey dotted lines in **Fig. 1G**). Analysis of the colocalization of mtRFP with MitoGREEN, a dye that specifically stains the mitochondrial matrix, resulted in high colocalization scores, while a low overlap was observed for RFP-GPI transfected MCF-7 cells (**Fig. S1H** and **Fig. 1G**, grey dotted lines). Subsequently, the same experiments were performed with MCF-7 cells expressing BK_{Ca}^{RFP} or BK_{Ca}-DEC^{RFP}. Although the mitochondrial localization score was lower for BK_{Ca}-DEC^{RFP} compared to mtRFP (compare **Fig. 1G** and **Fig. S1H**), this BK_{Ca} variant showed a significantly higher overlap with the mitochondrial dye than BK_{Ca}^{RFP} (**Fig. 1G and Fig. S1I**). Despite rather moderate colocalization scores of BK_{Ca}-DEC^{RFP} with MitoGREEN, on the level of single mitochondria, the RFP signal derived from BK_{Ca}-DEC^{RFP} surrounded the MitoGREEN fluorescence signal originating from the mitochondrial matrix, as expected for a K^+ channel located in the IMM (**Fig.1G** and **Fig. S1I**). As not all RFP signal in the BK_{Ca}-DEC^{RFP} overexpressing MCF-7 originated from mitochondria, we investigated the PM localization of the two channel isoforms by patch-clamp. Compared to native MCF-7 cells (**Fig. 1E**), both, BK_{Ca}^{RFP} and BK_{Ca}-DEC^{RFP}, increased the PM outward current (**Fig. 1H** and **Figs. S1J** and **S1K**). Despite comparable expression levels of the RFP signals (**Fig. 1L**), presence of BK_{Ca}^{RFP} caused significantly bigger currents across the PM compared to BK_{Ca}-DEC^{RFP} (**Fig. 1H**), indicative either for i) higher intracellular abundance or ii) major functional differences of BK_{Ca}-DEC^{RFP}. Importantly, the conductance of both channels was sensitive to the BK_{Ca} blockers paxilline and iberiotoxin, as treatment of the cells with both compounds resulted in PM conductance values comparable to those of native MCF-7 cells (**Figs. 1E** and **1H** and **Figs. S1J** and **S1K**).

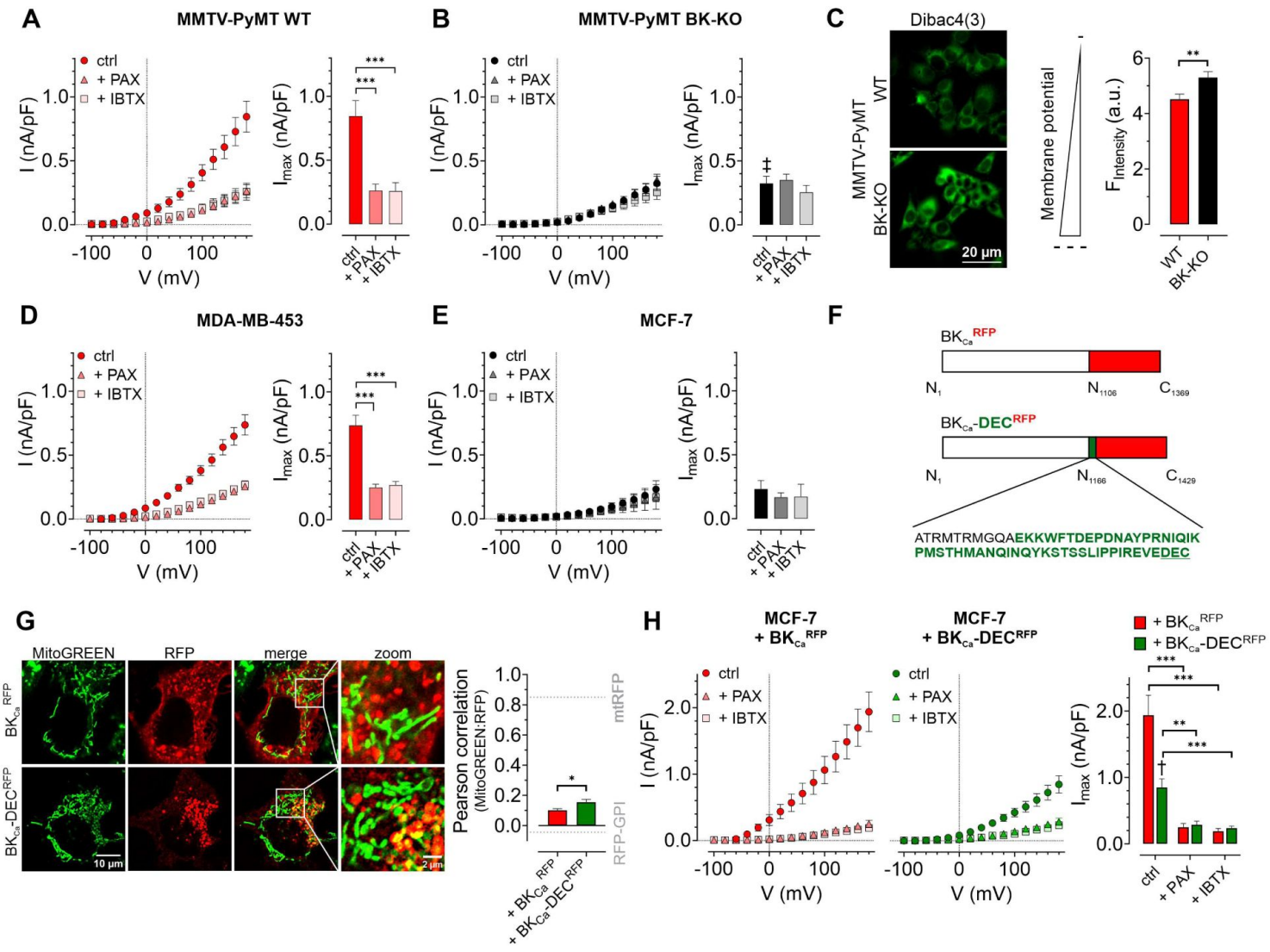

Figure 1

Characterization of BKCa channels in murine and human BCCs.

(**A; B**) I-V curves (left) and corresponding maximal currents (right) of MMTV-PyMT WT (**A**) and MMTV-PyMT BK-KO cells (**B**), either under control conditions, or in the presence of paxilline or iberiotoxin. Data represents average ± SEM. n (cells) = 15 WT ctrl, 17 WT + PAX, 17 WT + IBTX, 16 BK-KO ctrl, 17 BK-KO + PAX, 19 BK-KO + IBTX. ***p≤0.001, Brown-Forsythe and Welch ANOVA test followed by Games-Howell's multiple comparison test. ‡p≤0.001 compared to respective WT condition, Welch's t-test. (**C**) Representative fluorescence images (left) and statistics (right) of MMTV-PyMT WT and BK-KO cells loaded with the ΔΨPM sensitive dye Dibac4(3). N = 6 independent experiments, **p≤0.01, Unpaired t-test. (**D**) I-V curves (left) and maximal currents (right) of MDA-MB-453 cells, either under control conditions, or in the presence of paxilline or iberiotoxin. Data represents average ± SEM. n (cells) = 30 ctrl, 22 + PAX, 24 + IBTX. ***p≤0.001, Kruskal-Wallis test followed by Dunn's multiple comparison test. (**E**) I-V curves (left) and maximal currents (right) of MCF-7 cells, either under control conditions, or in the presence of paxilline or iberiotoxin. Data shows average ± SEM. n (cells) = 16 ctrl, 20 + PAX, 15 + IBTX. (**F**) Schematic representation of constructs used for over-expression in MCF-7 cells. The DEC exon is indicated in green. (**G**) Representative images (left) of MCF-7 cells either expressing $BKCa^{RFP}$ (upper) or $BKCa\text{-}DEC^{RFP}$ (lower), additionally stained with MitoGREEN. Average Pearson correlations ± SEM of MitoGREEN and RFP of BKCa or BKCa-DEC are shown. n (cells) = 17 BKCa – RFP, 22 $BKCa\text{-}DEC^{RFP}$. *p≤0.05, Unpaired t-test. (**H**) I-V curves (left and middle) and corresponding maximal currents (right) of MCF-7 cells expressing BKCa (left) or BKCa-DEC (middle), respectively, either under control conditions, or in the presence of paxilline or iberiotoxin. Data represents average ± SEM. n (cells) = 18 $BKCa^{RFP}$ ctrl, 14 $BKCa^{RFP}$ + PAX, 19 $BKCa^{RFP}$ + IBTX, 18 $BKCa\text{-}DEC^{RFP}$ ctrl, 21 $BKCa\text{-}DEC^{RFP}$ + PAX, 18 $BKCa\text{-}DEC^{RFP}$ + IBTX. **p≤0.01, ***p≤0.001, Brown-Forsythe and Welch ANOVA test followed by Games-Howell's multiple comparison test. †p≤0.01 between ctrl conditions, Welch's t-test.

BK_{Ca} modulates global and subcellular Ca^{2+} homeostasis in BCCs

As BK_{Ca} potentially affects cellular Ca^{2+} fluxes (Ouadid-Ahidouch and Ahidouch, 2013), we next investigated the cytosolic (**Figs. 2A-C**), endoplasmic reticulum (ER) (**Figs. 2D-F**), and mitochondrial (**Figs. 2G-I**) Ca^{2+} homeostasis in these cells. First, we assessed changes in the cytosolic Ca^{2+} concentration ($[Ca^{2+}]_{cyto}$) over-time in response to cell stimulation with the purinergic receptor agonist adenosine-5'-triphosphate (ATP) (Müller et al., 2020) using the fluorescent Ca^{2+} indicator Fura-2 (Grynkiewicz et al., 1985). Of note, extracellular ATP, released for example from necrotic cells in the tumor microenvironment, could be of pathophysiological relevance for BCCs (Di Virgilio et al., 2018), and all cell lines used in our study were previously reported to respond to ATP stimulation with a significant increase in intracellular Ca^{2+} (Chadet et al., 2014; Gross et al., 2022; Klijn et al., 2015). These experiments were either performed under control conditions (**Fig. 2A**) or in the presence of paxilline (**Fig. S2A**) or iberiotoxin (**Fig. S2B**). Analysis of the Fura-2 fluorescence emission ratio showed significantly elevated basal (**Fig. 2A**) and ATP-elicited maximal $[Ca^{2+}]_{cyto}$ responses (**Fig. S2C**) in MMTV-PyMT WT compared to BK-KO cells under control conditions. Interestingly, the elevated basal $[Ca^{2+}]_{cyto}$ of WT cells was reduced to the BK-KO cell level in response to paxilline (**Fig. 2A** and **Fig. S2A**), but not by iberiotoxin (**Fig. 2A** and **Fig. S2B**), which is a peptide-based pore-blocking toxin that cannot pass the PM (Candia et al., 1992). To validate the observed basal differences in $[Ca^{2+}]_{cyto}$, we additionally performed ionomycin-based calibrations by chelating intracellular Ca^{2+}, followed by Fura-2 saturation (**Fig. S2F-H**). These experiments confirmed the observed differences in basal $[Ca^{2+}]_{cyto}$, with $[Ca^{2+}]_{cyto}$ of 170.2 ± 8.0 nM, 98.40 ± 4.8 nM and 178.5 ± 13.5 nM for MMTV-PyMT WT, and 102.3 ± 4.9 nM, 96.49 ± 3.3 nM and 114.9 ± 4.3 nM for MMTV-PyMT BK-KO cells, under control conditions, or in the presence of paxilline or iberiotoxin, respectively. Subsequently, basal and ATP-elicited maximal $[Ca^{2+}]_{cyto}$ transients were recorded in the human BCC line MDA-MB-453, where both BK_{Ca} blockers reduced the basal $[Ca^{2+}]_{cyto}$ (**Fig. 2B**), while maximal $[Ca^{2+}]_{cyto}$ was not altered by these treatments (**Fig. S2D**). Again, ionomycin-based experiments confirmed the BK_{Ca}-modulation dependent reduction of $[Ca^{2+}]_{cyto}$ (**Fig. S2I**), with $[Ca^{2+}]_{cyto}$ of 110.7 ± 8.0 nM, 64.1 ± 4.8 nM and 78.2 ± 13.5 nM under control, paxilline- or iberiotoxin-treated conditions, respectively. Eventually, $[Ca^{2+}]_{cyto}$ was assessed in MCF-7 cells expressing or lacking the different BK_{Ca} isoforms (**Fig. 2C**). These experiments confirmed previous findings with the other BCC lines, as the expression of both splice variants increased the basal (**Fig. 2C** and **Fig. S2J**) and maximal $[Ca^{2+}]_{cyto}$ (**Fig. S2E**). $[Ca^{2+}]_{cyto}$ in MCF-7 cells was found to be 31.5 ± 3.7 nM, 58.1 ± 6.4 nM and 52,9 ± 5.6 nM in MCF-7 control cells expressing RFP, or MCF-7 cells expressing BK_{Ca}^{RFP} or BK_{Ca}-DEC^{RFP}, respectively.

Next, we visualized changes in the ER $[Ca^{2+}]$ ($[Ca^{2+}]_{ER}$). Therefore, BCCs were transfected with D1ER, an established genetically encoded, FRET-based Ca^{2+} sensor targeted to the lumen of the ER (Palmer et al., 2004). $[Ca^{2+}]_{ER}$ was depleted by extracellular Ca^{2+} removal and chelation by EGTA, followed by inhibition of the sarcoplasmic endoplasmic reticulum Ca^{2+} ATPase (SERCA) with BHQ and activation of inositol 1,4,5-trisphosphate (IP_3) receptors upon purinergic receptor stimulation with ATP (Lape et al., 2008; Müller et al., 2020; Salter and Hicks, 1995). Experiments were either performed under control conditions (**Figs. 2D-F**), or in the presence of paxilline or iberiotoxin for MMTV-PyMT (**Fig. 2D** and **Figs. S2K** and **S2L**), MDA-MB-453 (**Fig. 2E**), and MCF-7 cells expressing BK_{Ca}^{RFP} or BK_{Ca}-DEC^{RFP} (**Fig. 2F**). Throughout all BCCs investigated, expression of BK_{Ca} reduced $[Ca^{2+}]_{ER}$, potentially indicating that the channel was i.) functional in this cell compartment and ii.) involved in regulating the Ca^{2+} homeostasis of the ER. In MMTV-PyMT WT cells, $[Ca^{2+}]_{ER}$ was restored by the cell-permeable BK_{Ca} inhibitor paxilline (**Fig. 2D** and **Fig. S2K**) but not by the cell-impermeable iberiotoxin (**Fig. 2D** and **Fig. S2L**), while both inhibitors restored the $[Ca^{2+}]_{ER}$ in MDA-MB-453 cells (**Fig. 2E**). Accordingly, overexpression of both RFP-tagged BK_{Ca} isoforms in MCF-7 cells depleted the $[Ca^{2+}]_{ER}$ (**Fig. 2F**).

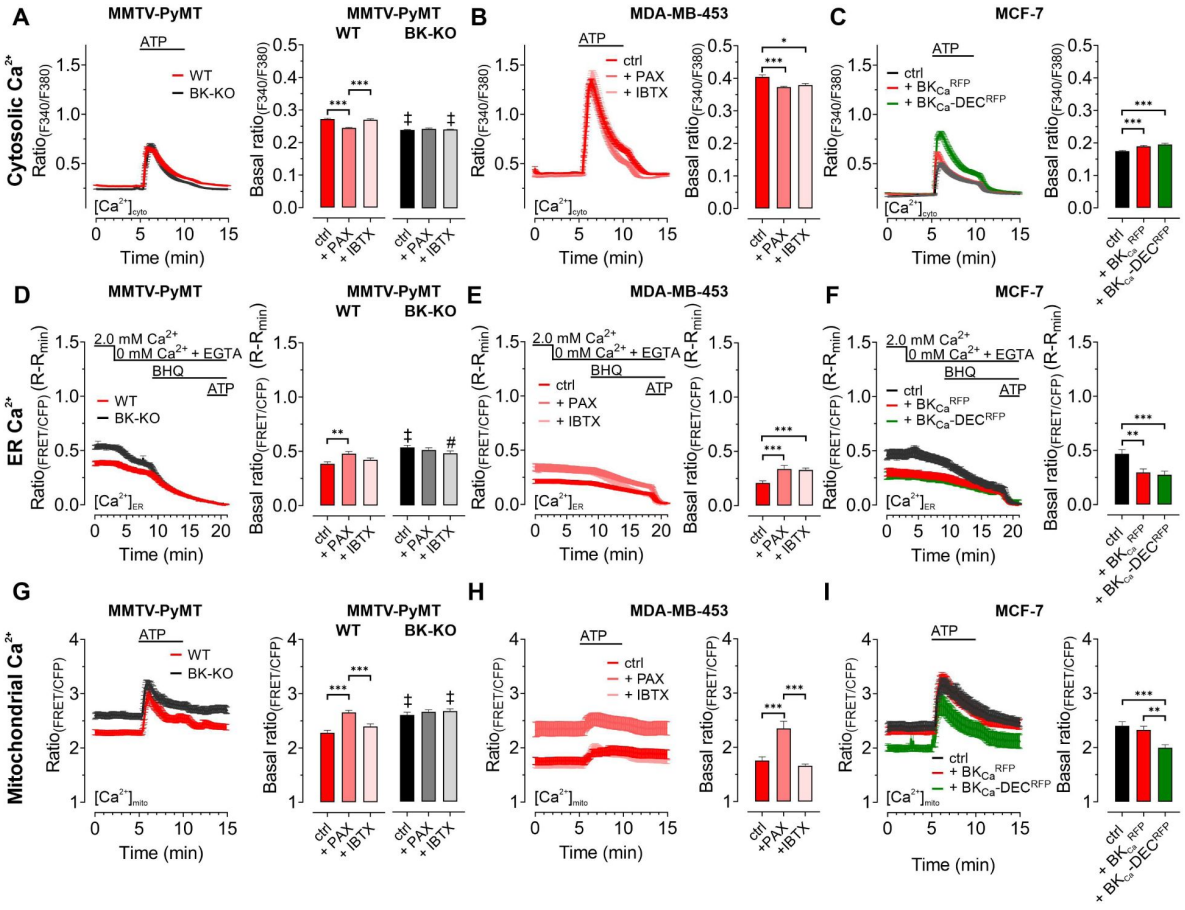

Figure 2

BKCa modulates the subcellular Ca^{2+} homeostasis in BCCs.

Cytosolic (**A – C**), endoplasmic reticulum (ER) (**D – F**), and mitochondrial Ca^{2+} dynamics (**G – I**) over-time of MMTV-PyMT WT and MMTV-PyMT BK-KO cells (**A, D, G**), MDA-MB-453 cells (**B, E, H**) or MCF-7 cells (**C, F, I**). All data represent average ± SEM. At time points indicated in the panels, cytosolic and mitochondrial Ca^{2+} alterations were evoked by extracellular stimulation with ATP (**A – C, G – I**), or by Ca^{2+} depletion of the ER using Ca^{2+}-free buffer containing the Ca^{2+} chelator EGTA, followed by administration of the SERCA inhibitor BHQ prior to ATP administration (**D – F**). MMTV-PyMT (**A, D, G**) and MDA-MB-453 (**B, E, H**) cells were either measured under control conditions, or in the presence of paxilline (+ PAX) or iberiotoxin (+ IBTX). MCF-7 cells (**C, F, I**) either expressed an RFP (ctrl), $BKCa^{RFP}$, or BKCa-DEC^{RFP}. N (independent experiments) / n (cells analyzed) = **A:** 17/784 WT ctrl, 18/857 BK-KO ctrl, 6/300 WT + PAX, 6/300 BK-KO + PAX, 5/318 WT + IBTX, 5/304 BK-KO + IBTX, **B:** 4/151 ctrl, 4/132 + PAX, 4/87 + IBTX, **C:** 5/111 ctrl, 5/117 + $BKCa^{RFP}$, 5/91 + BKCa-DEC^{RFP}, **D:** 14/116 WT ctrl, 13/117 BK-KO ctrl, 8/71 WT + PAX, 8/92 BK-KO + PAX, 6/102 WT + IBTX, 6/86 BK-KO + IBTX, **E:** 7/44 ctrl, 9/34 + PAX, 5/49 + IBTX, **F:** 4/25 ctrl, 4/35 + BKC^{aRFP}, 4/38 + BKCa-DEC^{RFP}, **G:** 11/47 WT ctrl, 12/86 BK-KO ctrl, 6/46 WT + PAX, 6/58 BK-KO + PAX, 5/59 WT + IBTX, 4/43 BK-KO + IBTX, **H:** 8/33 ctrl, 8/28 + PAX, 5/22 + IBTX, **I:** 5/28 ctrl, 4/27 + $BKCa^{RFP}$, 4/24 + BKCa-DEC^{RFP}. **p≤0.01, ***p≤0.001. Kruskal-Wallis test followed by Dunn's MC test (**A, B, C, D, I**), One-Way ANOVA test followed by Tukey's MC test (**E, F, G**) or Brown-Forsythe ANOVA test followed by Games-Howell's MC test (**H**). #p≤0.05, ‡p≤0.001 compared to respective WT condition, Mann-Whitney test (**A, D,** ctrl in **G**), or Welch's t test (+ IBTX in **G**).

$[Ca^{2+}]_{cyto}$ and $[Ca^{2+}]_{ER}$ reportedly affect the mitochondrial $[Ca^{2+}]$ ($[Ca^{2+}]_{mito}$) (Wacquier et al., 2019). Since an accumulation of K^+ within the mitochondrial matrix may oppose mitochondrial Ca^{2+} uptake (Checchetto et al., 2021), we assessed the effects of functional BK_{Ca} expression on $[Ca^{2+}]_{mito}$ utilizing 4mtD3cpV, a genetically encoded Ca^{2+} sensor targeted to the mitochondrial matrix (Palmer et al., 2006). Again, BCCs were treated with ATP to investigate the $[Ca^{2+}]_{mito}$ upon cell stimulation. In MMTV-PyMT WT (**Fig. 2G**) as well as MDA-MB-453 cells (**Fig. 2H**), functional expression of BK_{Ca} reduced basal $[Ca^{2+}]_{mito}$. Interestingly, in these two BCC types, basal and maximally elicited $[Ca^{2+}]_{mito}$ peaks increased in response to paxilline (**Figs. 2G** and **2H** and **Figs. S2M-P**), but not iberiotoxin treatment (**Figs. 2G** and **2H** and **Figs. S2M-P**). These findings confirm a role of intracellular located BK_{Ca} channels in modulating $[Ca^{2+}]_{mito}$ dynamics. Importantly, in MCF-7 cells, basal $[Ca^{2+}]_{mito}$ was only affected upon expression of the mitochondrially targeted BK_{Ca}-DEC^{RFP}, but not BK ^{RFP} (**Fig. 2I**), whereas neither of the two isoforms affected the maximal $[Ca^{2+}]_{mito}$ (**Fig. S2Q**). Presumably, by facilitating K^+ fluxes across the IMM, BK_{Ca}-DEC^{RFP} expression reduces the driving force for Ca^{2+} uptake and thus the resulting Ca^{2+} signals in the mitochondrial matrix. Basal differences in all of the utilized cell lines under the different conditions were additionally validated by ionomycin treatment, followed by intracellular Ca^{2+} chelation (**Figs. S2R-V**).

In total, our $[Ca^{2+}]$ imaging approaches emphasize that different BK_{Ca} isoforms at different localizations, i.e. the PM or intracellular organelles, may either amplify or weaken $[Ca^{2+}]_{cyto}$ and $[Ca^{2+}]_{ER}$ signals, respectively. These opposing effects are expected, as BK_{Ca}-mediated uptake of K^+ into the ER should limit the Ca^{2+} uptake capacity of this subcellular compartment, while functional channel expression at the PM might increase the driving force for Ca^{2+} influx to fuel $[Ca^{2+}]_{cyto}$. $[Ca^{2+}]_{mito}$, however, seems to be exclusively and effectively suppressed by the activity of intracellularly located BK_{Ca} variants in MMTV-PyMT WT and MDA-MB-453 cells and solely by the expression of BK_{Ca}-DEC^{RFP} in MCF-7 cells.

The metabolic activity of murine and human BCCs is modulated by intracellular BK_{Ca}

Given the involvement of Ca^{2+} and K^+ in regulating key features of cellular metabolism (Bischof et al., 2021; Dejos et al., 2020; Gohara and Di Cera, 2016), we proposed, that BK_{Ca} may alter metabolic activities of BCCs (Rossi et al., 2019). Hence, we analyzed the extracellular acidification rate (ECAR) as a measure of lactate secretion, i.e. glycolytic activity in MMTV-PyMT and MDA-MB-453 cells (Burgstaller et al., 2021a). ECAR measurements unveiled an increased basal ECAR of MMTV-PyMT WT compared to BK-KO cells (**Figs. 3A** and **3B**). Subsequently, we performed a mitochondrial stress test by injection of Oligomycin-A, FCCP, and Antimycin-A, which increased ECARs in both cell types due to ATP-synthase inhibition, mitochondrial uncoupling and complex III blockade, respectively (**Fig. 3A**). Maximal ECAR, received upon FCCP injection, was elevated in WT compared to BK-KO cells (**Fig. 3C**). Besides this evidence derived from a gene-targeted BK_{Ca} channel-deficient model, we used paxilline or iberiotoxin as pharmacological BK_{Ca} modulators (**Figs. S3A** and **S3B**). Interestingly, only paxilline, but not iberiotoxin treatment equalized basal (**Fig. 3B**) and maximal ECARs (**Fig. 3C**) between WT and BK-KO, suggesting that intracellular BK_{Ca} channels stimulate the glycolytic activity of BCCs. Moreover, in MDA-MB-453 cells iberiotoxin treatment did neither affect basal (**Fig. 3D** and **3E**) nor maximal ECARs (**Fig. 3F**). Contrary to MMTV-PyMT WT cells, however, paxilline increased basal and maximal ECAR in these cells (**Figs. 3E** and **3F**), suggesting that the cell lines examined strongly differ in their metabolic settings or in other H^+ releasing processes contributing to extracellular acidification.

Next, we investigated the oxygen consumption rates (OCRs) (Burgstaller et al., 2021a). (**Fig. 3G**). Interestingly, the increased basal and maximal ECAR (**Figs. 3A-C**) in MMTV-PyMT WT cells correlated with a higher basal (**Fig. 3H**) and maximal (**Fig. 3I**) OCR compared to BCCs lacking BK_{Ca}. Paxilline treatment reduced the basal and maximal OCR of BK_{Ca} proficient MMTV-

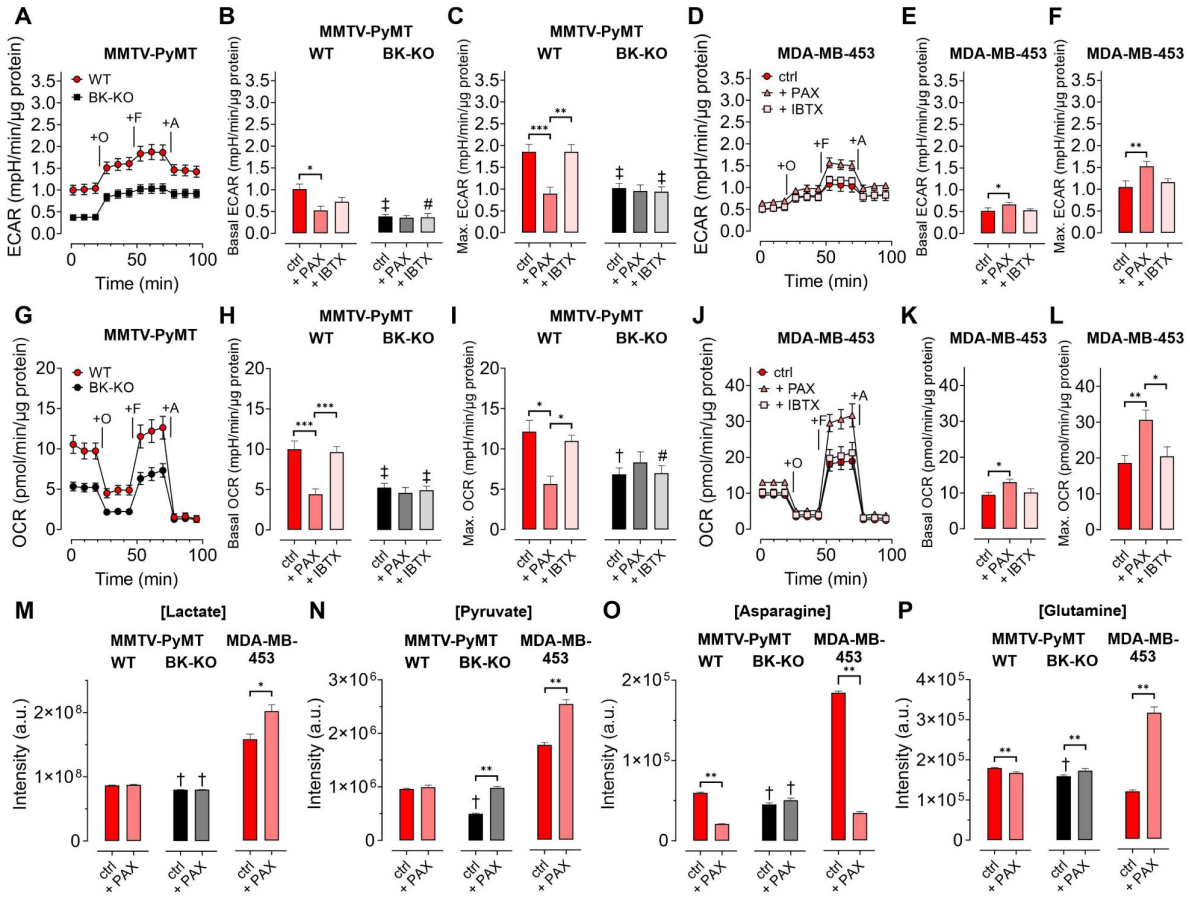

Figure 3

BKCa channels alter the metabolic activity of BCCs.

(**A, D**) Average ECAR over-time ± SEM of MMTV-PyMT WT (**A,** red) and BK-KO cells (**A,** black), or MDA-MB-453 cells (**D**) in response to administration of Oligomycin-A (+O), FCCP (+F) and Antimycin-A (+A) at time points indicated. (**B, E**) Average basal and (**C, F**) maximal ECAR ± SEM of MMTV-PyMT WT (**B, C,** left) and BK-KO cells (**B, C,** right), or MDA-MB-453 cells (**E, F**) under control conditions, or in the presence of paxilline or iberiotoxin. (**G, J**) Average OCR over-time ± SEM of MMTV-PyMT WT (**G,** red) and BK-KO cells (**G,** black), or MDA-MB-453 cells (**J**) in response to administration of Oligomycin-A (+O), FCCP (+F) and Antimycin-A (+A) at time points indicated. (**H, K**) Average basal and (**I, L**) maximal OCR ± SEM of MMTV-PyMT WT (**H, I,** left) and BK-KO cells (**H, I,** right), or MDA-MB-453 cells (**K, L**) under control conditions, or in the presence of paxilline or iberiotoxin. (**M – P**) LC-MS-based determination of major glycolytic and mitochondrial metabolites in particular Lactate (**M**, [Lactate]), Pyruvate (**N**, [Pyruvate]), Asparagine (**O**, [Asparagine]) and Glutamine (**P**, [Glutamine]) of MMTV-PyMT WT (left panels), BK-KO (middle panels) and MDA-MB-453 cells (right panels), either under control conditions or after cell cultivation with paxilline. N (independent experiments) = **A, B, C, G, H, I:** 7 WT ctrl and BK-KO, 3 for all others, **D, E, F, J, K, L:** 3 for all, **M – P:** 7 for BK-KO ctrl, 6 for all others. *p≤0.05, **p≤0.01, ***p≤0.001, Kruskal-Wallis test followed by Dunn's MC test (**B, E, F, I**), Brown-Forsythe and Welch ANOVA test followed by Games-Howell's MC test (**C, H**), One-Way ANOVA test followed by Tukey's MC test (**K, L**) or Mann-Whitney test (**M – P**). #p≤0.05, †p≤0.01, ‡p≤0.001, to respective WT condition, Mann-Whitney test (**B, C,** + IBTX in **I**, **M – P**), Welch's t-test (ctrl in **H** and **I**) or Unpaired t-test (+ IBTX in **H**).

PyMT cells to the BK-KO level (**Figs. 3H** and **3I** and **Fig. S3C**), while iberiotoxin did not have any effect (**Figs. 3H** and **3I** and **Fig. S3D**) again suggesting that that the latter toxin cannot reach the metabolism-relevant population of intracellular BK_{Ca} channels. Again, in MDA-MB-453 cells, paxilline treatment had an opposite effect to the observations that were made in MMTV-PyMT WT cells, as paxilline treatment increased the OCR (**Figs. 3J-L**), potentially due to the increased supply of oxidative phosphorylation with glycolytic substrates (**Figs. 3D-F**). More importantly, regardless of this difference between the BCC lines iberiotoxin treatment did consistently not affect the OCR of MDA-MB-453 cells (**Figs. 3J-L**).

To confirm that BK_{Ca} regulates the bioenergetic profile of BCCs, we subsequently applied LC-MS-based metabolomics according to the workflow presented in **Figure S3E**. We included typical analytes of glycolysis such as lactate (**Fig. 3M**) and pyruvate (**Fig. 3N**), as well as selected metabolites of mitochondrial metabolism including asparagine (**Fig. 3O**) and glutamine (**Fig. 3P**). Single time-point measurements confirmed the metabolic differences between MMTV-PyMT WT and BK-KO cells and further demonstrated that BK_{Ca} inhibition by paxilline directly affected the concentrations of these metabolites (**Figs. 3M-P**). As observed before by the ECAR and OCR measurements, MMTV-PyMT and MDA-MB-453 cells responded, however, differently to paxilline treatment (**Figs. 3M-P**). In summary, our data strengthen the notion that intracellular BK_{Ca} modulates the cellular energy balance of murine and human BCCs.

BK_{Ca} alters the mitochondrial function of BCCs

To clarify how BK_{Ca} regulates BCC cell metabolic activities, we examined cellular bioenergetics in real time using single-cell fluorescence microscopy. First, we assessed the mitochondrial membrane potential ($\Delta\Psi_{mito}$) of MMTV-PyMT and MDA-MB-453 cells using TMRM under control and BK_{Ca} inhibitor-treated conditions, followed by depolarization of $\Delta\Psi_{mito}$ using the proton ionophore FCCP (Joshi and Bakowska, 2011). These measurements unveiled, however, a less polarized $\Delta\Psi_{mito}$ of MMTV-PyMT WT cells compared to BK-KO cells under control conditions (**Figs. 4A** and **4B**). Paxilline, but not iberiotoxin, equalized $\Delta\Psi_{mito}$ between MMTV-PyMT WT and BK-KO cells (**Fig. 4B**). Identical results were obtained in MDA-MB-453 cells (**Figs. 4C** and **4D**).

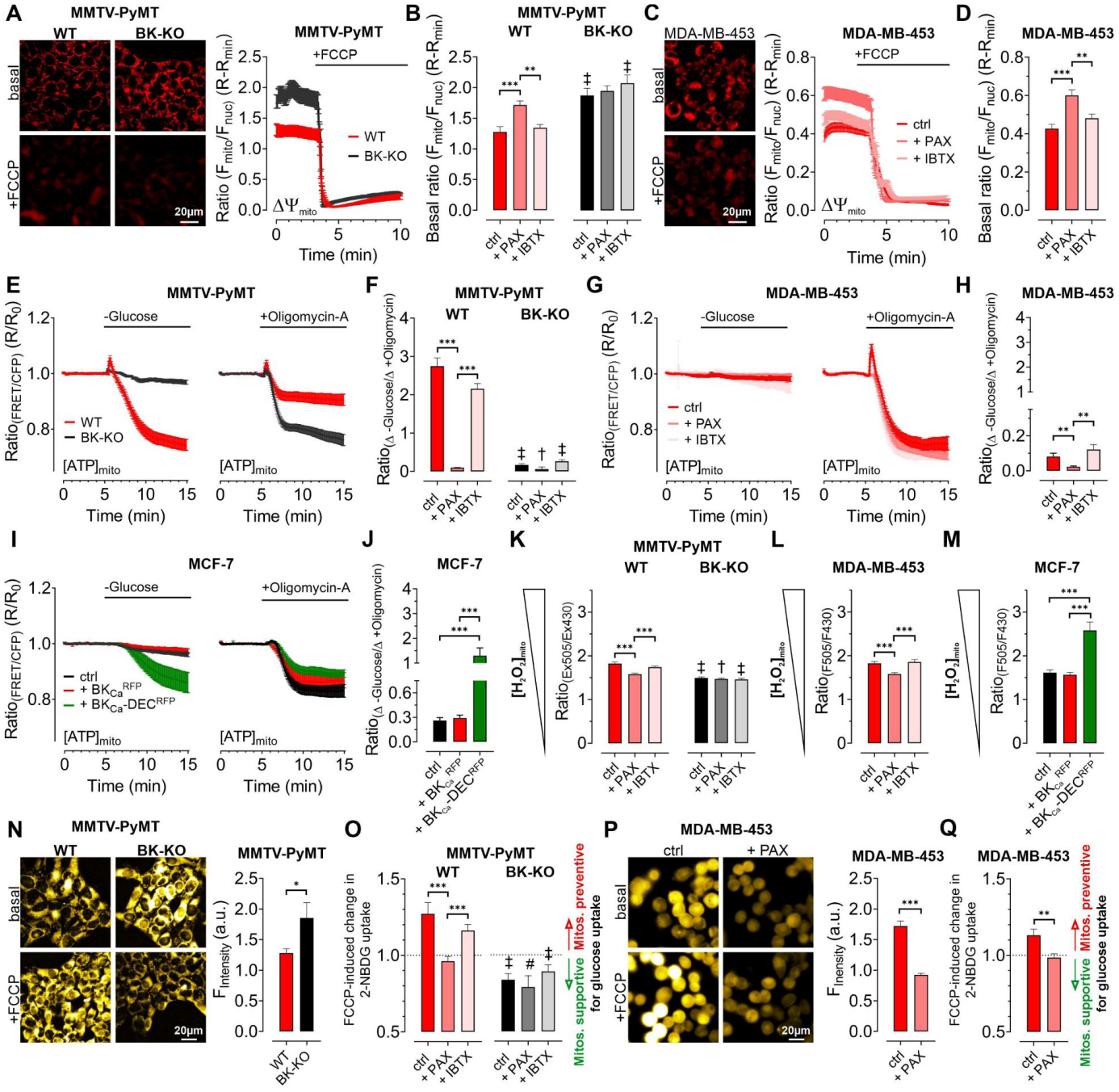
A
MMTV-PyMT
WT
BK-KO
basal
+FCCP
20µm
MMTV-PyMT
+FCCP
WT
BK-KO
Ratio (F_mito/F_nuc) (R-R_min)
ΔΨ_mito
Time (min)
B
MMTV-PyMT
WT
BK-KO
Basal ratio (F_mito/F_nuc) (R-R_min)
ctrl
+ PAX
+ IBTX
C
MDA-MB-453
basal
+FCCP
20µm
MDA-MB-453
+FCCP
ctrl
+ PAX
+ IBTX
Ratio (F_mito/F_nuc) (R-R_min)
ΔΨ_mito
Time (min)
D
MDA-MB-453
Basal ratio (F_mito/F_nuc) (R-R_min)
E
MMTV-PyMT
-Glucose
+Oligomycin-A
Ratio_(FRET/CFP) (R/R_0)
WT
BK-KO
[ATP]_mito
Time (min)
F
MMTV-PyMT
WT
BK-KO
Ratio_(Δ -Glucose/Δ +Oligomycin)
G
MDA-MB-453
-Glucose
+Oligomycin-A
Ratio_(FRET/CFP) (R/R_0)
ctrl
+ PAX
+ IBTX
[ATP]_mito
Time (min)
H
MDA-MB-453
Ratio_(Δ -Glucose/Δ +Oligomycin)
I
MCF-7
-Glucose
+Oligomycin-A
Ratio_(FRET/CFP) (R/R_0)
ctrl
+ BK_Ca^RFP
+ BK_Ca-DEC^RFP
[ATP]_mito
Time (min)
J
MCF-7
Ratio_(Δ -Glucose/Δ +Oligomycin)
ctrl
+ BK_Ca^RFP
+ BK_Ca-DEC^RFP
K
MMTV-PyMT
WT
BK-KO
[H2O2]_mito
Ratio_(Ex505/Ex430)
L
MDA-MB-453
[H2O2]_mito
Ratio_(F505/F430)
M
MCF-7
[H2O2]_mito
Ratio_(F505/F430)
N
MMTV-PyMT
WT
BK-KO
basal
+FCCP
20µm
MMTV-PyMT
F_Intensity (a.u.)
O
MMTV-PyMT
WT
BK-KO
FCCP-induced change in 2-NBDG uptake
Mitos. preventive
Mitos. supportive
for glucose uptake
P
MDA-MB-453
ctrl
+ PAX
basal
+FCCP
20µm
Q
MDA-MB-453
FCCP-induced change in 2-NBDG uptake
Mitos. preventive
Mitos. supportive
for glucose uptake

Figure 4

Expression of BKCa modulates mitochondrial function and glucose uptake of BCCs.

(**A – D**) Representative fluorescence images and -ratios (Fmito/Fnuc) over-time (**A, C**), and corresponding statistics ± SEM (**B, D**) representing ΔΨmito of TMRM-loaded MMTV-PyMT WT and BK-KO (**A, B**) and MDA-MB-453 cells (**C, D**) under basal conditions (**A, C**, upper images) and upon administration of FCCP for mitochondrial depolarization (**A, C** lower images). (**E – J**) [ATP]mito dynamics ± SEM over-time of MMTV-PyMT WT and BK-KO cells (**E**), MDA-MB-453 cells (**G**) and MCF-7 cells (**I**) in response to extracellular glucose removal (left panels) or upon administration of Oligomycin-A (right panels). **F, H** and **J** show changes of [ATP]mito induced by glucose removal to Oligomycin-A administration ± SEM, under control conditions, or in the presence of paxilline or iberiotoxin (**F, H**), or upon expression of $BKCa^{RFP}$ or BKCa-DEC^{RFP} (**J**). (**K – M**) Basal mitochondrial H2O2 concentrations ± SEM of MMTV-PyMT WT (**K**, left), BK-KO (**K**, right), MDA-MB-453 (**L**) and MCF-7 cells (**M**), either under control conditions, in the presence of paxilline or iberiotoxin (**K, L**), or upon expression of $BKCa^{RFP}$ or BKCa-DEC^{RFP} (**M**). (**N, P**) Representative fluorescence wide-field images (left) and corresponding statistics ± SEM (right) of MMTV-PyMT WT (**N,** left images and red bars) and BK-KO cells (**N,** right images and black bars) or MDA-MB-453 cells (**P**) incubated with 2-NBDG, either in the absence (upper images) or presence of FCCP (lower images). (**O, Q**) Average ± SEM of FCCP induced change in 2-NBDG uptake of MMTV-PyMT WT (**O**, left) and BK-KO cells (**O**, right), or MDA-MB-453 cells (**Q**) either under control conditions, or in the presence of paxilline or iberiotoxin. Values above 1 indicate that mitochondria prevent, values below 1 that mitochondria support glucose uptake. N (independent experiments) / n (cells analyzed) = **A**, **B:** 4/75 WT ctrl, 4/90 WT + PAX, 4/86 WT + IBTX, 4/91 BK-KO ctrl, 4/89 BK-KO + PAX, 4/100 BK-KO + IBTX, **C, D:** 4/113 ctrl, 4/97 + PAX, 4/103 + IBTX, **E, F:** [-Glucose]: 8/55 WT ctrl, 6/45 WT + PAX, 7/27 WT + IBTX, 8/65 BK-KO ctrl, 6/57 BK-KO + PAX, 7/28 BK-KO + IBTX, [+ Oligomycin-A]: 11/52 WT ctrl, 7/53 WT + PAX, 7/34 WT + IBTX, 8/87 BK-KO ctrl, 6/35 BK-KO + PAX, 5/45 BK-KO + IBTX. **G, H:** [-Glucose]: 5/14 ctrl, 3/13 + PAX, 5/13 + IBTX, [+ Oligomycin-A]: 5/33 ctrl, 3/21 + PAX, 8/27 + IBTX, **I, J:** [-Glucose]: 6/48 ctrl, 5/23 + BK^{RFP}, 5/20 + BK -DEC^{RFP}, [+ Oligomycin-A]: 5/27 ctrl, 5/23 + BK^{RFP}, 5/37 + BK -DEC^{RFP}, **K:** 3/33 WT ctrl, 4/51 WT + PAX, 4/54 WT + IBTX, 4/55 BK-KO ctrl, 4/51 BK-KO + PAX, 4/54 BK-KO + IBTX, **L:** 4/31 ctrl, 4/39 + PAX, 4/31 + IBTX, **M:** 4/29 ctrl, 4/17 + $BKCa^{RFP}$, 4/21 + BKCa-DEC^{RFP}, **N – Q:** 4 for all. *p≤0.05, **p≤0.01, ***p≤0.001, Kruskal-Wallis test followed by Dunn's MC test (**B, D, F, H, J, K, O**), Brown-Forsythe and Welch ANOVA test followed by Games-Howell's MC test (**L, M**), Mann-Whitney test (**N**), Unpaired t-test (**P**) or Welch's t-test (**Q**). #p≤0.05, †p≤0.01, ‡p≤0.001, to respective WT condition, Mann-Whitney test (**B, F,** + PAX and + IBTX in **K,** ctrl in **O**), Unpaired t-test (ctrl in **K,** + PAX and + IBTX in **O**).

Interestingly, we found that $\Delta\Psi_{mito}$ of MMTV-PyMT cells was tightly dependent on the extracellular glucose concentration ($[GLU]_{ex}$) (**Fig. S4A**). Under high $[GLU]_{ex}$ conditions (25.0 mM), the difference in $\Delta\Psi_{mito}$ between MMTV-PyMT WT and BK-KO cells disappeared, as $\Delta\Psi_{mito}$ increased significantly in WT and decreased significantly in BK-KO cells compared to low $[GLU]_{ex}$ (2.0 mM). Because F_OF_1-ATP-synthase (ATP Synthase) may hydrolyze ATP in an attempt to maintain $\Delta\Psi_{mito}$, these results strongly suggest that the forward (ATP producing) *vs* reverse (ATP consuming) mode of the ATP synthase is affected by the BK_{Ca} status of the cells (Naguib et al., 2018).

To unravel the substrate dependency of these BCCs for maintaining their energy homeostasis in dependency of BK_{Ca}, we measured the mitochondrial ATP concentration ($[ATP]_{mito}$) using a genetically encoded ATP sensor targeted to the mitochondrial matrix, mtAT1.03 (Imamura et al., 2009). Mitochondrial ATP reportedly responds most dynamically to energy metabolism perturbations (Depaoli et al., 2018). To assess the sources of ATP in the cells, we either deprived the cells of $[GLU]_{ex}$, or administered Oligomycin-A to inhibit the ATP-synthase (Depaoli et al., 2018) (**Figs. 4E-J** and **Figs. S4B-G**). In MMTV-PyMT cells, glucose removal as well as ATP-synthase inhibition reduced $[ATP]_{mito}$, albeit the effect was more pronounced upon $[GLU]_{ex}$ depletion (**Figs. 4E** and **4F** and **Figs. S4B** and **S4C**). Remarkably, paxilline, but not iberiotoxin treatment reduced the glucose, and increased ATP-synthase dependency of MMTV-PyMT WT cells for maintaining $[ATP]_{mito}$ (**Figs. 4E** and **4F** and **Figs. S4B** and **S4C**). These observations were

confirmed in MDA-MB-453 cells, even though i.) these cells showed an overall higher dependency on the ATP-synthase, and ii.) the paxilline-sensitivity of $[ATP]_{mito}$ maintenance was much less pronounced (**Figs. 4G** and **4H** and **Figs. S4D** and **S4E**).

To validate these findings in a BK_{Ca} minimal to depleted model, these experiments were performed with MCF-7 cells either expressing exclusively RFP as control, BK_{Ca}^{RFP}, or BK_{Ca}-DEC^{RFP} (**Fig. 4I**). Expression of BK_{Ca}-DEC^{RFP}, but not BK_{Ca}^{RFP}, resulted in a high dependency on $[GLU]_{ex}$ to maintain $[ATP]_{mito}$ while the $[ATP]_{mito}$ rundown in the presence of Oligomycin A was identical for both BK_{Ca} splice variants. This suggests that BK_{Ca}-DEC^{RFP} specifically triggers a high $[GLU]_{ex}$ sensitivity and simultaneously an independency on ATP derived from ATP-synthase for maintaining $[ATP]_{mito}$ as demonstrated by the ratio of the respective changes under these experimental conditions (**Figs. 4I** and **4J** and **Figs. S4F** and **S4G**). These findings suggest that intracellular (mitochondrial) BK_{Ca} contributes to the metabolic reprogramming of BCCs.

In an extension to extracellular flux analyses, single time-point LC-MS metabolomics (**Fig. 3**), and high-resolution live-cell imaging experiments (**Figs. 4A-J**), pointing to a BK_{Ca}-dependent "oncometabolic" phenotype, we assessed the concentrations of mitochondrial hydrogen peroxide ($[H_2O_2]_{mito}$) using mitoHyPer3 (Bilan et al., 2013), a genetically encoded fluorescent indicator for monitoring H_2O_2 in the mitochondrial matrix (**Figs. 4K-M**). These experiments demonstrated increased levels of $[H_2O_2]_{mito}$ in MMTV-PyMT WT (**Fig. 4K**) and MDA-MB-453 cells (**Fig. 4L**), or specifically upon BK_{Ca}-DEC^{RFP} expression in MCF-7 cells (**Fig. 4M**). Excessive reactive oxygen species (ROS) synthesis is caused by uncoupling of the respiratory chain and it is considered as an indicator of mitochondrial stress, which, among other reasons, promotes mutagenesis and BCC progression. In this regard, $mitoBK_{Ca}$ may serve as an "uncoupling" protein (Gałecka et al., 2021), triggering ATP synthase to operate in reverse mode to consume instead of producing ATP, thereby counteracting the dissipation of the proton gradient and consequently the loss of $\Delta\Psi_{mito}$. Consequently, the lack of ATP must be compensated, e.g. by accelerating glycolysis. To investigate this assumption, we performed glucose uptake measurements using 2-NBDG, a fluorescent glucose analogue, which is taken up via glucose transporters (GLUTs), phosphorylated by hexokinase (HK) isoforms to generate 2-NBDG-6-phosphate and subsequently remains within the cell (Bischof et al., 2021) (**Figs. S4H** and **S4I**). Unexpectedly, we found that MMTV-PyMT BK-KO cells showed a higher rate of glucose uptake and phosphorylation compared to WT cells under basal conditions (**Fig. 4N**). To unravel the role of mitochondria in contributing to glucose uptake by supplying ATP to HKs, we next performed these experiments in the presence of FCCP, which disrupts mitochondrial ATP production (Losano et al., 2017). If ATP-synthase works in forward mode, FCCP treatment should reduce or even prevent oxidative ATP production, and, subsequently, ATP-dependent 2-NBDG phosphorylation (**Fig. S4H**). Contrary, if ATP-synthase works in reverse mode, it may compete with HKs for ATP, and FCCP treatment should abolish this competition, leading to increased 2-NBDG phosphorylation in BCCs (**Fig. S4I**). Interestingly, our experiments unveiled increased 2-NBDG uptake in MMTV-PyMT WT and reduced uptake in BK-KO cells upon mitochondrial depolarization (**Fig. 4N** and **Figs. S4J** and **S4K**). To facilitate the interpretation, we calculated the FCCP-induced change in 2-NBDG uptake. These analyses revealed that mitochondria are less effective in assisting 2-NBDG uptake and phosphorylation in MMTV-PyMT WT cells, while they "support" these processes in BK-KO cells under control conditions (**Fig. 4O**). To test whether the changes in 2-NBDG uptake are sensitive to pharmacological modulation of BK_{Ca}, we performed a similar set of experiments in the presence of paxilline or iberiotoxin. While iberiotoxin treatment did not have any effect, paxilline treatment shifted the activity of the ATP-synthase to the ATP-supplying "forward" mode (**Fig. 4O** and **Figs. S4J** and **S4K**). Comparable effects were obtained in MDA-MB-453, despite paxilline treatment reduced basal accumulation of 2-NBDG in these cells (**Figs. 4P** and **4Q** and **Fig. S4L**). Overall, the experiments performed so far suggest that mitochondria rather consume than generate ATP if BK_{Ca} was functionally expressed intracellularly in BCCs.

BK_{Ca} locates functionally in the IMM of murine and human BCCs

So far, our data suggest an important contribution of intracellularly located BK_{Ca}, possibly mitoBK_{Ca}, in reprogramming cancer cell metabolism. Thus, we applied an electrophysiological approach to provide functional evidence for endogenous mitoBK_{Ca}. Single-channel patch-clamp experiments were conducted using mitoplasts isolated from MMTV-PyMT WT and BK-KO, MDA-MB-453, and MCF-7 cells. In MDA-MB-453- and MMTV-PyMT WT-derived mitoplasts we indeed detected channels of large conductance (**Fig. 5A** and **Fig. S5A**). For these channels, the open probability did not significantly vary with the voltage (**Fig. 5B**). Only at very negative and positive voltages of approximately -150 mV and +150 mV differences in the open probabilities were observed (**Fig. 5C**). The bursts of single-channel openings showed an average conductance of 212 ± 2 pS (**Fig. 5D**). This large conductance and the sensitivity towards Ca^{2+}-(**Figs. 5E** and **5F** and **Fig. S5B**) and paxilline (**Figs. 5E** and **5F** and **Fig. S5C**) pointed to mitoBK_{Ca} that exhibits the pharmacologic characteristics of canonical BK_{Ca} channels present at the PM. Overall, our electro-pharmacological experiments unveiled 3 different classes of channels with either small (≤100 pS), medium (≤150 pS) or large (~210 pS) conductance, where the latter conductance corresponds to mitoBK_{Ca} (Liu et al., 1999). The lower conductance values may represent mitochondrial IK_{Ca}, SK_{Ca}, or K_{ATP} channel activity, but this was not investigated further in our study. Notably, mitoBK_{Ca} was detected at a frequency of 15% in 210 patches of MDA-MB-453 mitoplasts and at a lower frequency of 6% in 127 mitoplast patches of MMTV-PyMT WT cells. These numbers may, however, underestimate the actual abundance of the channel, as only a small area of the mitoplast is examined with each patch. Importantly, this channel was absent in 76 mitoplast patches from MMTV-PyMT BK-KO and 58 mitoplast patches from MCF-7 cells (**Fig. 5G**). These findings provide evidence that the molecular entity for the K^+ channel derives from the nuclear *Kcnma1* gene, which is ablated in the MMTV-PyMT BK-KO.

These experiments were further corroborated by immunoblotting experiments using whole-cell lysates and sub-cellular homogenates of different purity. We detected BK_{Ca}, the Na^+/K^+ ATPase as a marker of the PM, cytochrome c oxidase subunit IV (COXIV) as a marker of mitochondria and TMX1, which localizes to ER membranes in these samples (**Fig. S5D**). A protein band corresponding to BK_{Ca} was identified not only in whole-cell lysates, but also in isolated mitochondria. Importantly, the Na^+/K^+ ATPase was absent in the latter protein fraction, confirming the purity of the mitochondrial preparation (**Fig. S5D**). These data confirm the presence of mitoBK_{Ca}, potentially BK_{Ca}-DEC, in the utilized BK_{Ca} proficient BCCs.

mitoBK_{Ca} promotes the Warburg effect, triggers cellular O_2 independency and stimulates BCC proliferation

Based on the observed influence of mitoBK_{Ca} on glycolysis and mitochondrial metabolism, we addressed, whether the channel contributes to the Warburg effect, commonly observed in cancer cells (Bischof et al., 2021; Warburg, 1924). Therefore, we assessed the Warburg index (WI) by investigating the cytosolic lactate concentration ($[LAC]_{cyto}$) over-time using Laconic, a FRET-based lactate sensor (San Martín et al., 2013). $[LAC]_{cyto}$ was followed in response to either inhibiting mitochondrial metabolism by administration of NaN_3, a complex IV inhibitor, to stop pyruvate consumption (Leary et al., 1998), or upon subsequent inhibition of lactate secretion towards the ECM via monocarboxylate transporter 1 (MCT-1) using BAY-8002 (Quanz et al., 2018) (**Figs. 6A** and **6B**). Indeed, MMTV-PyMT WT cells exhibited an increased WI compared to BK-KO cells under control conditions (**Fig. 6C**), indicating that the presence of BK_{Ca} favors lactate secretion rather than TCA-dependent utilization of pyruvate. Paxilline, but not iberiotoxin treatment reduced the WI in WT cells to the BK-KO level (**Fig. 6C**). The WI profiles of MDA-MB-453 (**Fig. 6D**) and MCF-7 cells (**Fig. 6E**) showed the same sensitivity towards paxilline, while in the latter the expression of BK_{Ca}-DEC^{RFP}, but not $BK_{Ca}{}^{RFP}$, stimulated the WI. To validate the contribution of the different BK_{Ca} isoforms, endogenous BK_{Ca} transcripts in MMTV-PyMT and

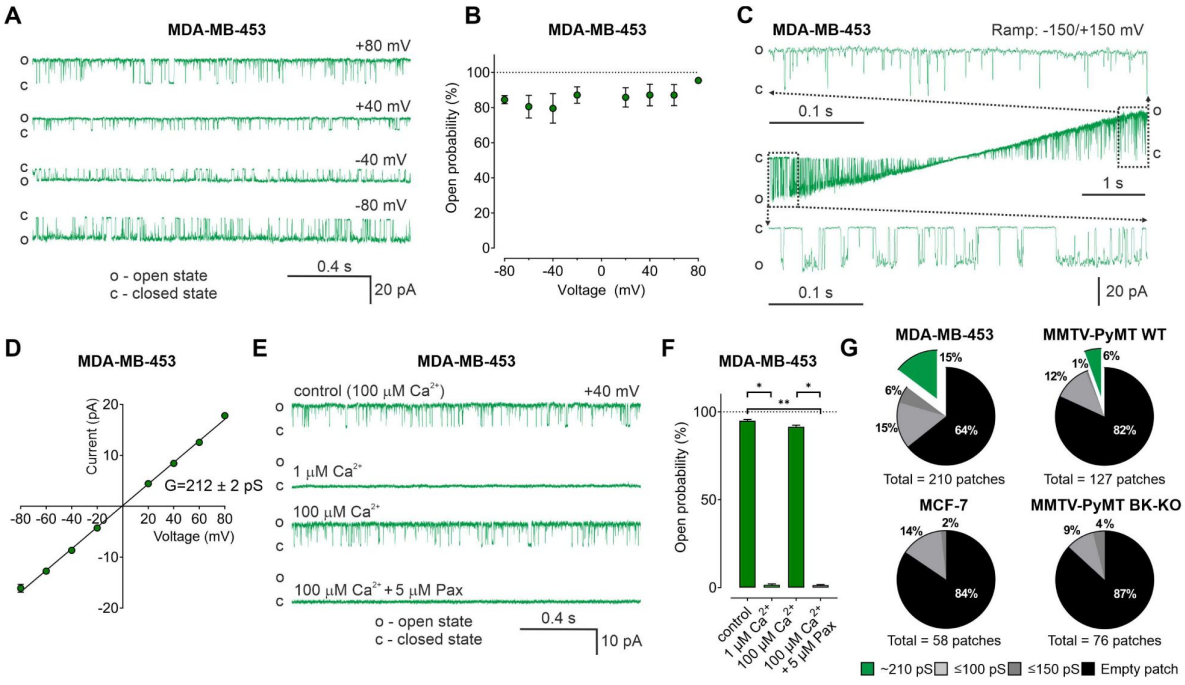

Figure 5

BKCa activity is present in the inner mitochondrial membrane (IMM) of BCCs.

(**A**) Representative BKCa single-channel recordings of the IMM of mitoplasts isolated from MDA-MB-453 cells using a symmetric 150/150 mM isotonic KCl solution containing 100 µM Ca^{2+} at voltages ranging from -80 to +80 mV as indicated in the panel. (**B**) Open probability analysis of mitoBKCa at different voltages received from experiments as performed in (**A**). N = 8. (**C**) Single-channel currents of the IMM of mitoplasts isolated from MDA-MB-453 cells recorded using a voltage ramp protocol ranging from −150 to +150 mV. Above and below the ramp are enlarged excerpts of the records shown in rectangles. (**D**) Current-voltage (I-V) plot based on single-channel recordings of MDA-MB-453 cells as performed in **a**, using a symmetric 150/150 mM KCl isotonic solution containing 100 µM Ca^{2+}. N = 11. (**E, F**) Representative single-channel recordings of the IMM of mitoplasts isolated from MDA-MB-453 cells (**E**) and corresponding open probabilities at +40 mV in a symmetric 150/150 mM KCl isotonic solution under control conditions (100 µM Ca^{2+}), after reducing Ca^{2+} to 1 µM, re-addition of 100 µM Ca^{2+} and finally after application of 5 µM paxilline in the presence of 100 µM Ca^{2}. Data in (**F**) show average ± SEM. *p≤0.05, **p≤0.01 using Friedmann test followed by Dunn's multiple comparison test, n =7. (**G**) Pie chart displaying the percentage of mitoBKCa channel currents (green) possessing a conductance of ~210 pS, *versus* the total number of patch-clamp experiments performed using mitoplasts isolated from MDA-MB-453 cells (upper left), MMTV-PyMT WT cells (upper right), MCF-7 cells (lower left) and MMTV-PyMT BK-KO cells (lower right). Black segments represent empty patches, bright- and dark grey fraction demonstrate percentage of channels possessing smaller conductances of ≤100 pS and ≤150 pS, respectively. All recordings were low-pass filtered at 1 kHz. "c" and "o" indicate the closed- and open state of the channel, respectively.

MDA-MB-453 cells were targeted using specific siRNAs targeting either the major BK_{Ca} isoforms or specifically the DEC exon of BK_{Ca} (**Fig. S6A**). Cell treatment with the respective siRNAs reduced the expression of BK_{Ca} or BK_{Ca}-DEC (**Fig. S6B** and **S6C**). Interestingly, the knockdown of BK_{Ca} interfered with the WI in these cells (**Figs. 6F** and **6G**). This effect was reproduced by specific silencing of the BK_{Ca}-DEC isoform (**Figs. 6F** and **6G**), indicating that BK_{Ca}-DEC-derived mitoBK_{Ca} channels stimulate the Warburg effect in BCCs.

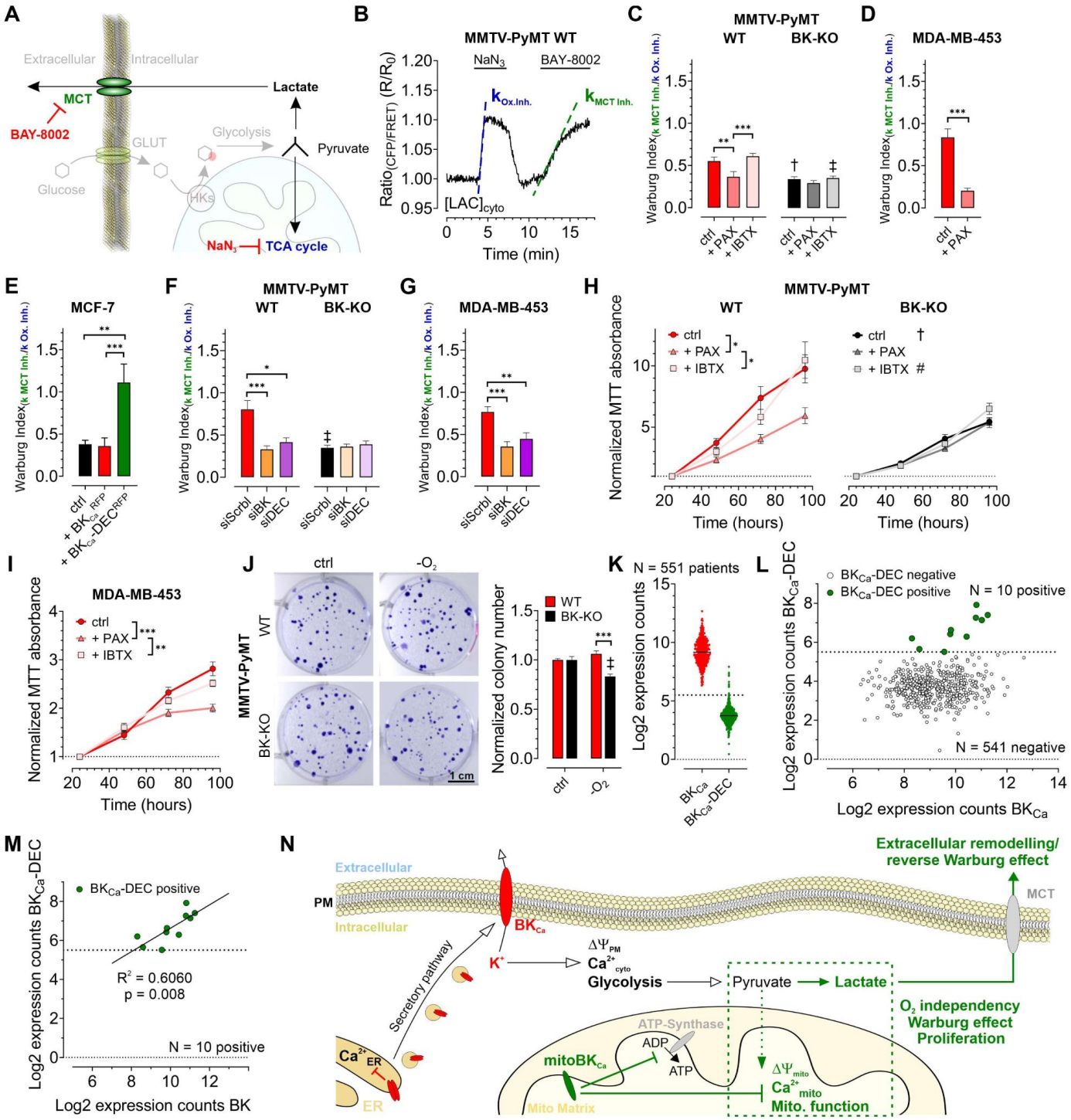
A
Extracellular
Intracellular
Lactate
MCT
BAY-8002
GLUT
Glycolysis
Pyruvate
Glucose
HKs
NaN3
TCA cycle
B
MMTV-PyMT WT
NaN3
BAY-8002
kOx.Inh.
kMCT Inh.
Ratio(CFP/FRET) (R/R0)
[LAC]cyto
Time (min)
C
MMTV-PyMT
WT
BK-KO
Warburg Index(k MCT Inh./k Ox. Inh.)
ctrl
+ PAX
+ IBTX
D
MDA-MB-453
E
MCF-7
F
MMTV-PyMT
WT
BK-KO
siScrbl
siBK
siDEC
G
MDA-MB-453
H
MMTV-PyMT
WT
BK-KO
Normalized MTT absorbance
Time (hours)
I
MDA-MB-453
J
ctrl
-O2
WT
BK-KO
MMTV-PyMT
1 cm
Normalized colony number
K
N = 551 patients
Log2 expression counts
BKCa
BKCa-DEC
L
BKCa-DEC negative
BKCa-DEC positive
N = 10 positive
N = 541 negative
Log2 expression counts BKCa-DEC
Log2 expression counts BKCa
M
BKCa-DEC positive
R2 = 0.6060
p = 0.008
N = 10 positive
Log2 expression counts BK
N
Extracellular
PM
Intracellular
BKCa
K+
ΔΨPM
Ca2+cyto
Glycolysis
Secretory pathway
Ca2+ ER
ER
Pyruvate
Lactate
MCT
Extracellular remodelling/
reverse Warburg effect
O2 independency
Warburg effect
Proliferation
ATP-Synthase
ADP
ATP
mitoBKCa
ΔΨmito
Ca2+ mito
Mito. function
Mito Matrix

Figure 6

BKCa-DEC expression contributes to the metabolic remodeling and growth of murine and human BCCs and is present in primary tumor samples.

(**A**) Schematic representation of the fate of glucose in glycolysis. The tricarboxylic acid (TCA) cycle or lactate secretion via monocarboxylate transporters (MCT) can be inhibited, either using NaN3 or BAY-8002. GLUT: Glucose transporter, HKs: Hexokinases. (**B**) Representative cytosolic lactate concentration ([LAC]cyto) of a MMTV-PyMT WT cell over-time in response to administration or removal of NaN3 and BAY-8002 at time points indicated. Dashed lines indicate slopes taken for assessment of the "Warburg index. (**C – G**) Average Warburg indices ± SEM of MMTV-PyMT WT (**C, F,** left), MMTV-PyMT BK-KO (**C, F**, right), MDA-MB-453 cells (**D, G**) and MCF-7 cells (**E**) calculated from the experiments as shown in (**B**), either under control conditions, in the presence of paxilline or iberiotoxin (**C, D**), upon expression of $BKCa^{RFP}$ or BKCa-DEC^{RFP} (**E**), or upon cell treatment with a scrambled siRNA (siScrbl), or siRNA against a common BKCa sequence targeting all known splice variants (siBK), or a siRNA specifically designed to knockdown BKCa-DEC (siDEC) (**F, G**). (**H, I**) Normalized MTT absorbance over-time of MMTV-PyMT WT (**H**, left) and BK-KO cells (**H**, right), and MDA-MB-453 cells (**I**), either under control conditions, or in the presence of paxilline or iberiotoxin. **J**, Representative images and corresponding statistics of colony formation assays using MMTV-PyMT WT or BK-KO cells in the presence or absence of O2. (**K – N**) mRNA expression of BKCa and BKCa-DEC as performed by Nanostring analysis of 551 BC patient samples. (**K**) Log2 expression counts of BKCa and BKCa-DEC. The threshold for positive expression level was set to log2 = 5.5 (dashed line). (**L**) Log2 expression counts of BKCa-DEC blotted over the log2 expression counts of BKCa. 10 of the 551 patient samples showed expression of BKCa-DEC above the threshold of log2 = 5.5 (dashed line), whereas 541 patient samples were BKCa-DEC negative. (**M**) Correlation of the log2 expression counts of BKCa-DEC positive samples with the log2 expression counts of BKCa in the primary human BC material. (**N**) Summarizing scheme of BKCa in cancer cell homeostasis. N (independent experiments)/ n (cells analyzed) = **C**: 4/26 WT ctrl, 6/28 WT + PAX, 4/39 WT + IBTX, 4/17 BK-KO ctrl, 5/18 BK-KO + PAX, 4/27 BK-KO + IBTX, **D:** 7/29 ctrl, 5/13 + PAX, **E:** 5/27 ctrl, 5/20 + BKCaRFP, 7/26 BKCa-DEC^{RFP}, **F:** 5/22 WT siScrbl, 5/28 WT siBK, 4/26 WT siDEC, 5/24 BK-KO siScrbl, 5/24 BK-KO siBK, 5/29 BK-KO siDEC, **G:** 5/21 siScrbl, 5/22 siBK, 5/19 siDEC, **H – J**: 4 for all. *p≤0.05, **p≤0.01, ***p≤0.001, Kruskal-Wallis test followed by Dunn's MC test (**C, E, F, G, I**), One-Way ANOVA test followed by Tukey's MC test (**H**) or Mann-Whitney test (**D**). †p≤0.01, ‡p≤0.001 compared to respective WT condition, Unpaired t-test (ctrl, **C, J**) or Mann-Whitney test (+ IBTX, **C, F**).

As glycolytic metabolites and ATP fuel cell proliferation, we investigated the proliferation rates of MMTV-PyMT WT, MMTV-PyMT BK-KO, and MDA-MB-453 cells over-time in the absence or presence of paxilline or iberiotoxin. Using MTT-assay, corroborating previous findings (Mohr et al., 2022), these analyses revealed faster proliferation of WT compared to BK-KO cells under control conditions (**Fig. 6H**). Interestingly, paxilline, but not iberiotoxin treatment, reduced the proliferation of MMTV-PyMT WT to the level of BK_{Ca}-deficient cells (**Fig. 6H**). These effects were also observed in MDA-MB-453 cells (**Fig. 6I**). Since the MTT assay is also a redout for mitochondrial function, we additionally performed immunofluorescence-based detection of Ki-67, a frequently used marker of cell proliferation (Dowsett et al., 2011). This approach confirmed the MTT data (**Figs. S6D-F**), establishing intracellular BK_{Ca}, possibly mitoBK_{Ca}, as key-player in mediating the metabolic rewiring. Next, we studied whether the increased WI affects the proliferation rate of these BCCs at low O_2 tension (Nazemi and Rainero, 2020). Colony formation assays (CFAs) revealed an increased hypoxic resistance of MMTV-PyMT WT compared to BK-KO cells, as the number and size of colonies lacking BK_{Ca} was reduced upon O_2-deprivation (**Fig. 6J** and **Fig. S6G**). In sum, these data demonstrate a malignancy-promoting effect of mitoBK_{Ca} in BCC.

mitoBK_{Ca} is of potential clinical relevance

To determine the clinical relevance of our findings, we investigated whether BK_{Ca}-DEC transcripts are present in primary BC tissue. Therefore, the mRNA expression of BK_{Ca} and BK_{Ca}-DEC was analyzed by nanostring analysis in bulk tumor biopsies isolated from 551 BC patients. Remarkably,

all 551 samples tested positive for BK_{Ca} mRNA expression, with 10 of the samples showing significant expression of BK_{Ca}-DEC above the log2 expression threshold of 5.5 (**Figs. 6K** and **6L**). Importantly, if BK_{Ca}-DEC was expressed, the expression of BK_{Ca} well correlated with the expression of BK_{Ca}-DEC (R^2 = 0.6060, p = 0.008) (**Fig. 6M**).

In sum, our experiments emphasize the presence of BK_{Ca} in different intracellular organelles including the ER and vesicles of the secretory pathway, yielding its PM localization. At these sites, BK_{Ca} modulates the Ca^{2+} homeostasis and regulates $\Delta\Psi_{PM}$. K^+ efflux across the PM may additionally affect glycolysis. Importantly, functionally relevant BK_{Ca} also locates in the IMM of BCCs, promoting, presumably by the K^+ accumulation in the matrix following channel activation, $\Delta\Psi_{mito}$ depolarization and consequently ATP-synthase activity in reverse mode as well as a depletion of $[Ca^{2+}]_{mito}$. These profound ionic and bioenergetic changes ultimately trigger the proliferation of BCCs in a low oxygen environment, as found in solid tumors (**Fig. 6N**). Taken together, functional expression of mitoBK_{Ca} could possibly denote a prognostic or therapeutic marker for BC patients, and its pharmacologic modulation could represent a novel anti-cancer treatment strategy.

Discussion

Here, we demonstrate for the first time that BK_{Ca}-DEC (mitoBK_{Ca}) is functionally expressed in BCCs. BK_{Ca}-DEC modulates BCC metabolism, stimulates the Warburg effect, and accelerates cell proliferation rates in the presence and absence of O_2. These tumor- and malignancy-promoting effects were sensitive to BK_{Ca} inhibition using the cell-permeable BK_{Ca} inhibitor paxilline (Zhou and Lingle, 2014), but not the cell-impermeable blocker iberiotoxin (Candia et al., 1992), indicating that intracellular BK_{Ca}, presumably mitoBK_{Ca}, mediates malignant BCC behavior and tumor development.

In line with recent single-cell RNA sequencing data of 26 primary breast tumors (S. Z. Wu et al., 2021), we found high transcript levels for BK_{Ca} throughout the analyzed BC samples, in addition to BK_{Ca}-DEC, albeit in a much smaller subset of BC. The analyzed BC samples were, however, all positive for hormone receptors. Whether BK_{Ca} expression is different in hormone receptor negative specimens hence needs to be further investigated. Further, we confirmed functional BK_{Ca} expression in the PM of MMTV-PyMT WT and MDA-MB-453 cells, while MMTV-PyMT BK-KO and MCF-7 cells showed no or very low PM BK_{Ca} currents. Therefore, MCF-7 cells represented a suitable model to investigate the effects of BK_{Ca} over-/expression on the metabolic homeostasis of human BCC. If the low BK_{Ca} expression correlates with hormonal receptor status or alternatively with human epidermal growth factor 2 (HER2) expression levels must be clarified by future studies. Interestingly, however, recent data have shown that BK_{Ca} is overexpressed in triple-negative BC, a fact that led the authors to draw similar conclusions to ours, that BK_{Ca} may represent a novel anti-cancer treatment strategy for selected BC patients (Sizemore et al., 2020). Nevertheless, similarly to cardiac myocytes (CM), expression of BK_{Ca}-DEC yielded mitochondrial localization of BK_{Ca}-DEC, although its abundance in the IMM appeared less pronounced compared to CM (Singh et al., 2013). While a direct comparison is difficult as plasmid transfections may have caused unexpected effects, our finding that BK_{Ca}-DEC^{RFP} caused significantly reduced currents across the PM compared to $BK_{Ca}{}^{RFP}$ putatively confirm its increased intracellular abundance.

Based on the potential impact of BK_{Ca} on the cellular $\Delta\Psi_{PM}$ and ion balance (Burgstaller et al., 2022a), we conducted an in-depth investigation of the (sub)cellular Ca^{2+} homeostasis. Across the BCCs examined, we observed that functional BK_{Ca} expression modulated $[Ca^{2+}]_{cyto}$ dynamics. These alterations showed, however, differential sensitivities to BK_{Ca} inhibitors in MMTV-PyMT WT and MDA-MB-453 cells. While basal $[Ca^{2+}]_{cyto}$ in MDA-MB-453 cells was reduced by both, paxilline and iberiotoxin treatment, MMTV-PyMT WT cells were only sensitive to paxilline. Examination of

$[Ca^{2+}]_{ER}$ confirmed the results from $[Ca^{2+}]_{cyto}$, as $[Ca^{2+}]_{ER}$ levels increased with paxilline and iberiotoxin in MDA-MB-453, but only upon paxilline exposure in MMTV-PyMT WT cells, suggesting differential effects of intracellular and PM-localized BK_{Ca} on Ca^{2+} handling in these cells. Interestingly, in MCF-7 cells, both BK_{Ca} splice variants mediated the opposing effects on the basal $[Ca^{2+}]_{cyto}$ and $[Ca^{2+}]_{ER}$ levels, which either in- or decreased, respectively, upon transient BK_{Ca}^{RFP} or BK_{Ca}-DEC^{RFP} expression. This is expected as the transitory hyperpolarization and the efflux of K^+ due to the opening of PM BK_{Ca} provides the driving force for Ca^{2+} entry into cytoplasm, while a BK_{Ca}-mediated K^+ increase within the ER, presumably through PM-directed channels crossing the ER membrane in the secretory pathway, would oppose the Ca^{2+} refiling (Burgstaller et al., 2022a). Moreover, these results are in line with the higher proliferative capability of BK_{Ca} proficient BCCs due to the manifold roles of Ca^{2+} as second messenger (Burgstaller et al., 2022a). Importantly, however, $[Ca^{2+}]_{mito}$ of BK_{Ca} proficient MMTV-PyMT WT and MDA-MB-453 cells was exclusively sensitive for paxilline, and it was specifically affected by the expression of BK_{Ca}-DEC^{RFP}, but not by BK_{Ca}^{RFP}, in MCF-7 cells, suggesting that this Ca^{2+} pool is exclusively controlled by intracellular BK_{Ca}.

Subcellular Ca^{2+} alterations could reportedly alter cellular bioenergetics, as Ca^{2+} directly regulates metabolic enzymes and activities (Rossi et al., 2019). Indeed, extracellular flux analysis, LC-MS-based metabolomics and fluorescence-based live-cell imaging confirmed, that the observed alteration in sub-cellular Ca^{2+} homeostasis caused by BK_{Ca}, especially mitoBK_{Ca}, has severe effects on cell metabolism. Our data further emphasize, that the presence of mitoBK_{Ca}, as confirmed by mitoplast patch-clamp and Western blot analysis of isolated mitochondria, depolarizes BCC mitochondria, which is in line with a previous study showing an impact of mitoBK_{Ca} activation on $\Delta\Psi_{mito}$ (Kicinska et al., 2016). mitoBKCa-dependent depolarization of $\Delta\Psi_{mito}$ in turn triggers cellular glucose dependency and reverses the activity of the mitochondrial ATP-synthase to consume ATP for restoring $\Delta\Psi_{mito}$. Finally, BK_{Ca}-DEC-derived mitoBK_{Ca} channels promote the Warburg effect and ultimately stimulated proliferation rates of BCCs. Our data fit earlier findings from glioma cells, where an O_2-sensitivity of mitoBK_{Ca} was observed, which probably increased the hypoxic resistance of these cancer cells (Gu et al., 2014). It may seem contradictory that mitoBK_{Ca} is highly expressed in CM, which are among one of the most oxidative cell types known. It is, however, important to mention, that CM, under physiologic conditions, do not show a metabolic Warburg setting, which is a common phenomenon of cancer cells propelling their O_2 independency, due to the hypoxic microenvironment. Moreover, it was demonstrated recently that the absence of (mito)BK_{Ca} does not alter physiologic cardiac function. Only upon induction of ischemia and reperfusion injury, a lack of (mito)BK_{Ca} promoted the susceptibility of the heart to cell death, resulting in increased infarction size (Frankenreiter et al., 2017). Hence, it can be concluded that (mito)BK_{Ca} only played a role under conditions where mitochondria are, due to the absence of O_2, not properly functioning. Taking this view into account, the results derived from CM are consistent with our findings in BCCs, as (mito)BK_{Ca} mediates the resistance to hypoxic stress to BCC.

Excessive production and release of lactate, a hallmark of the Warburg effect, leads to extracellular acidification, subsequently creating a microenvironment that promotes tumorigenesis and metastasis as well as the resistance to anti-tumor immune responses and therapy (de la Cruz-López et al., 2019; Nazemi and Rainero, 2020; P. Wu et al., 2021). Extracellular K^+ $[K^+]_{ex}$, in turn, accumulating within the necrotic core of solid tumors, was shown to interfere with effector T-cell function triggering immune escape of cancer cells (Eil et al., 2016). To elucidate whether mitoBK_{Ca} directly contributes to lactate-induced tumor aggressiveness or $[K^+]_{ex}$, live-cell imaging of extracellular metabolites in 3D BCC models should be applied in future investigations (Burgstaller et al., 2022b, 2021b).

Finally, our results demonstrate for the first time that BK_{Ca}-DEC transcripts are present in human BC biopsies. Although only a small proportion of patients was positive for BK_{Ca}-DEC expression, this finding could be of considerable clinical relevance considering the link between mitoBK_{Ca}

function and BCC metabolism. Importantly, the design of our study likely underestimates the incidental number of BK_{Ca}-DEC positive BC, as i.) only hormone-receptor positive BC specimens were included, and ii.) bulk-tumor mRNA was analyzed, hampering the detection of low-abundant or tightly regulated transcripts against a strong background of non-cancer cells present in bulk tumor tissues. Finally, due to the small number of positive hits (N=10 positive *versus* N=541 BK_{Ca}-DEC negative specimens) and the lack of (sufficient) follow-up information in some of these cases, we are currently unable to correlate BK_{Ca}-DEC expression with, for example, treatment response or survival. Thus, future studies are warranted to show how the tumor's BK_{Ca}-DEC status can help to predict or therapeutically improve standard chemo-endocrine treatments. The rather low abundance of BK_{Ca}-DEC in the clinical samples, however, is in agreement with our mitoplast patch clamp experiments with mitoBK_{Ca}-mediated K^+ currents being detected at frequencies between 6 to 15%, suggesting that either a small proportion of mitochondria express functional mitoBK_{Ca}, or that the abundance of the channel per mitochondrion is low, requiring sensitive mechanistic approaches for its detection.

In summary, our data highlight a potentially druggable mitoBK_{Ca} isoform in BCCs, whose molecular entity is mainly formed by the *Kcnma1* encoded BK_{Ca}-DEC splice variant. This channel promotes metabolic alterations in cancer cells, even under low-oxygen conditions, which may ultimately be of clinical interest for new anti-cancer therapies.

Material and Methods

Buffers and solutions

If not otherwise stated, all chemicals were purchased from Carl Roth GmbH, Karlsruhe, Germany.

Buffers used in this study comprised the following:

Physiologic buffer for single cell live recordings contained (in mM): 138 NaCl, 5 KCl, 2 $CaCl_2$, 1 $MgCl_2$, 2 glucose, 10 HEPES, pH set to 7.4 with NaOH. No glucose was added during glucose removal experiments, while glucose was increased to 25 mM to investigate glucose dependency of the mitochondrial membrane potential. 10 mM $CaCl_2$ instead of 2 mM $CaCl_2$ were added to obtain 10Ca buffer. 0.1 mM Ethylene glycol bis(2-aminoethylether)-N, N, N', N'-tetra acetic acid (EGTA) (Sigma Aldrich Chemie GmbH, Taufkirchen, Germany) instead of 2.0 mM $CaCl_2$ was added to obtain Ca^{2+} free buffer. For 0 mM K^+ buffer, 5 mM KCl was replaced by 5 mM NaCl. For 300 mM K^+ buffer, 300 mM KCl was added instead of 5 mM K^+ and addition of NaCl was omitted. The following compounds were added to yield the following final concentration: 3 µM Oligomycin-A, 200 nM Carbonyl cyanide-p-trifluoromethoxyphenylhydrazone (FCCP), 5 µM paxilline (all from (Santa Cruz Biotechnology, Dallas, USA), 30 nM iberiotoxin (Selleckchem, Planegg, Germany), 5 mM NaN_3, 3 µM BAY-8002, 15 µM 2,5-Di-(t-butyl)-1,4-hydroquinone (BHQ) (all from Sigma Aldrich Chemie GmbH), 100 µM adenosine-5'-triphosphate (ATP), 5 µM ionomycin (Alomone Labs, Jerusalem, Israel), 15 µM gramicidin (Sigma Aldrich Chemie GmbH). For H_2O insoluble compounds, final DMSO concentration in the buffer did not exceed 0.1%.

Intracellular buffer used for whole-cell patch-clamp experiments contained (in mM): 130 K-Gluconate, 5 KCl, 2 Mg-ATP, 0.1 $CaCl_2$, 0.2 Na_2-GTP, 0.6 EGTA, 5 HEPES, pH = 7.2 with KOH.

Cell equilibration buffer fluorescence microscopy-based contained (in mM): 135 NaCl, 5 KCl, 2 $CaCl_2$, 1 $MgCl_2$, 2.6 $NaHCO_3$, 0.44 KH_2PO_4, 0.34 Na_2HPO_4, 10 glucose, 10 HEPES, 2 GlutaMAX, 1 sodium pyruvate, with 1x MEM amino acids and 1x MEM vitamins added (both Thermo Fisher Scientific). pH was adjusted to 7.4 using NaOH.

Buffers used for mitochondrial isolation, mitoplast preparation, and single channel patch-clamp comprised the following: The preparation solution contained (in mM): 250 sucrose, 5 HEPES, pH = 7.2. The mitochondrial storage buffer contained (in mM): 150 KCl, 0.1 $CaCl_2$, 20 HEPES, pH = 7.2. The hypotonic buffer contained (in mM) 0.1 $CaCl_2$, 5 HEPES, pH = 7.2. The hypertonic buffer contained (in mM): 750 KCl, 0.1 $CaCl_2$, 30 HEPES, pH 7.2. Low-Ca^{2+} solution (1 µM Ca^{2+}) contained (in mM): 150 KCl, 1 EGTA, 0.752 CaCl2, 10 HEPES, pH = 7.2.

Cell culture and transfection

Mouse mammary tumor virus polyoma middle T antigen (MMTV-PyMT) cells were isolated from tumors of MMTV-PyMT transgenic FVB/N WT or BK-KO mice. Tumor growth *in vivo* and biopsies were authorized by the local ethics *Committee for Animal Research* (Regierungspräsidium Tuebingen, Germany), and were performed in accordance with the *German Animal Welfare Act*. Animals were kept on a 12-hour light/ dark cycle under temperature- and humidity-controlled conditions with unlimited access to food (Altromin, Lage, Germany) and water. MMTV-PyMT cells used in this study were isolated from 3 – 7 different female breast-cancer bearing WT and 3 – 4 different female breast-cancer bearing BK-KO animals at an age of ~ 12 – 14 weeks. Upon dissection, tumors were carefully minced into pieces using atraumatic forceps, lysed by 1 mg mL^{-1} Collagenase-D (Roche, Basel, Switzerland) for 10 min, and cultured as follows: Cells were grown in modified improved minimal essential medium (IMEM) supplemented with 5% fetal bovine serum (FBS), 1 mM sodium pyruvate and 100 U mL^{-1} penicillin and 100 µg mL^{-1} streptomycin (all purchased from Thermo Fisher Scientific) at 37°C and 5% CO_2 in a humidified incubator. Fibroblasts were removed by exposure of the cultures to 0.25% trypsin-EDTA in PBS (Thermo Fisher Scientific) and short incubation at 37°C (~ 1 minute). After gently tapping the plate, trypsin-EDTA with detached fibroblasts was removed and cells were further cultured in supplemented modified IMEM at 37°C and 5% CO_2 until subculturing.

MCF-7 and MDA-MB-453 cells were purchased from the Global Bioresource Center (ATCC). Cells were cultivated in Dulbecco's modified eagle's medium (DMEM) supplemented with 10% FBS, 1 mM sodium pyruvate and 100 U mL^{-1} penicillin and 100 µg mL^{-1} streptomycin (Thermo Fisher Scientific) at 37°C and 5% CO_2 in a humidified incubator.

Subculturing of cells was performed when cells reached a confluency of 80 – 90%. Therefore, cell culture medium was removed, cells were washed 1x with PBS, and trypsin-EDTA at a final concentration of 0.25% trypsin-EDTA in PBS was added. Subsequently, cells were incubated at 37°C and 5% CO_2 in a humidified incubator until cell detachment occurred (~ 2-5 minutes). Trypsinization was stopped by adding supplemented cell culture media and cells were pelleted at 300xg for 5 minutes. The supernatant was removed, and cells were seeded to new cell culture dishes as required. For fluorescence microscopic live-cell imaging experiments, cells were either seeded in 6-well plates containing 1.5 H 30 mm circular glass coverslips (Paul Marienfeld GmbH, Lauda-Königshofen, Germany). All other vessels and serological pipettes used for cell culture were ordered from Corning (Kaiserslautern, Germany).

Transfection of cells was performed according to manufacturer's instructions when cells showed a confluency of ~70%, either using PolyJET DNA transfection reagent (SignaGen Laboratories, Maryland, USA) for plasmid DNA transfection or Lipofectamine 2000 (Thermo Fisher Scientific) for siRNA transfection or co-transfection of siRNA with plasmid DNA. Plasmid DNA amount was reduced to 1/3 for transfection of mitochondrial-targeted probes to ensure proper mitochondrial localization of the probes. Plasmid transfections were performed 16 hours, siRNA transfections were performed 48 hours before the experiments. Paxilline or iberiotoxin were added 12 hours prior to the experiments to the respective cell culture medium. DMSO served as a control.

Whole-cell patch-clamp

For whole-cell patch-clamp experiments, 30,000 cells were seeded on the day before the experiment in 35 mm glass bottom µDishes (ibidi GmbH, Graefelfing, Germany) and cultivated in the respective supplemented cell culture medium over-night at 37°C and 5% CO_2 in a humidified incubator. The next day, cell culture medium was removed, and cells were washed 2x and maintained in prewarmed physiologic buffer. Subsequently, recordings were performed using borosilicate glass capillaries (0.86x1.5x100mm) (Science Products GmbH, Hofheim am Taunus, Germany), with a resistance of 4-6 MW, which were pulled using a model P-1000 flaming/ brown micropipette puller (Sutter Instruments, California, USA) and filled with intracellular buffer. A MP-225 micromanipulator served for pipette control (Sutter Instruments). Recordings were performed in whole-cell mode. Currents were evoked by 15 voltage square pulses (300 ms each) from the holding potential of -70 mV to voltages between -100 mV and +180 mV delivered in 20 mV increments. For amplifier control (EPC 10) and data acquisition, Patchmaster software (HEKA Elektronik GmbH, Lambrecht, Germany) was used. Voltages were corrected offline for the capacity. Data analysis was performed using Fitmaster software (HEKA Elektronik GmbH), Nest-o-Patch software (*http://sourceforge.net/projects/nestopatch*, written by Dr. V Nesterov), and Microsoft Excel (Microsoft, Washington, USA).

Cloning and plasmid preparation

Cloning was performed using conventional PCR-, restriction- and ligation-based procedures. BK_{Ca}-DEC was a gift from Michael J. Shipston and was N-terminally attached to an RFP (BK_{Ca}-DEC^{RFP}) using KpnI and BamHI restriction sites after PCR amplification (NEB Q5 High-Fidelity DNA-Polymerase, New England Biolabs (NEB), Ipswich, USA). For generation of BK_{Ca}^{RFP}, a PCR amplification of BK_{Ca}-DEC was performed, where the reverse primer omitted the last amino acids including the 50 amino acids encoding the DEC exon. Mitochondrial targeted TagRFP (mtRFP) was generated by fusing a double repeat of COX8 pre-sequence N-terminally to TagRFP. RFP-GPI was generated by fusing the membrane leading sequence (MLS) and the GPI-anchor signal of cadherin 13 N- and C-terminally to TagRFP, respectively. After PCR reactions, the DNA fragments were purified from gel electrophoresis using the Monarch DNA gel extraction kit (NEB), fragments and destination plasmid were digested using the respective restriction enzymes (NEB) and ligation (T4 DNA Ligase, NEB) and transformation (chemically competent NEB 5-alpha *E. coli*) were performed according to manufacturer's instructions. Plasmids were verified by sequencing (Microsynth AG, Balgach, Switzerland). DNA maxipreps were performed using the Nucleobond Xtra Maxi kit (Macherey Nagel GmbH & Co. KG, Düren, Germany). Purified DNA was stored at 4°C.

Confocal imaging

For confocal imaging of mtRFP, RFP-GPI, BK_{Ca}^{RFP} or BK_{Ca}-DEC^{RFP} colocalization with mitochondria, MCF-7 cells were seeded on circular 30 mm glass coverslips (Marienfeld GmbH) in 6-well plates (Corning). Cells were transfected using PolyJet transfection reagent according to the manufacturer's instructions. 16 hours after transfection medium was exchanged for fresh cell culture medium and cells were further cultivated for 24 hours. Subsequently, the medium was exchanged for cell equilibration buffer containing MitoGREEN (PromoCELL GmbH, Heidelberg, Germany) at a final concentration of 3 µM and cells were incubated at room temperature for 30 minutes. Subsequently, cells were washed 2x with physiologic buffer, and cells were analysed using confocal fluorescence microscopy Imaging was performed using a Zeiss LSM 980 equipped with an Airyscan 2 detector. A Zeiss C Plan-Apochromat 63x/1,4 Oil DIC M27 objective was used for all images. The ZEN 3.7 software (blue edition) was used for image acquisition and super resolution images were processed using the ZEN Airyscan module (Carl Zeiss AG). Tag-RFPs were excited at 561 nm and detected at 380-735 nm. MitoGREEN was excited at 488 nm and detected at 495-550 nm. Image analysis was performed using the colocalization test in ImageJ with Fay randomization after cell selection by ROIs.

Fluorescence live-cell imaging

Cells were either analyzed using a Zeiss AXIO Observer Z1 or a Zeiss Axiovert 200m microscope (Carl Zeiss AG, Oberkochen, Germany). The Zeiss AXIO Observer Z1 was connected to a LEDHub high-power LED light engine (OMICRON Laserage, Rodgau-Dudenhofen, Germany) and equipped with a EC Plan-Neofluar 40x/1.3 Oil DIC M27 objective (Carl Zeiss AG), an Optosplit II emission image splitter (Cairn Research Ltd, Faversham, UK), and a pco.panda 4.2 bi sCMOS camera (Excelitas PCO GmbH, Kelheim, Germany). The microscope possessed a BioPrecision2 automatic XY-Table (Ludl Electronic Products, Ltd., New York, USA). Optical filters included a 459/526/596 dichroic mirror and a 475/543/702 emission filter for FRET- and TMRM-based measurements, and a 409/493/573/652 dichroic mirror combined with a 514/605/730 emission filter for Dibac4(3), Fura-2 and 2-NBDG based measurements (all purchased from AHF Analysentechnik, Tuebingen, Germany). The Optosplit II emission image splitter was equipped with a T505lpxr long-pass filter (AHF Analysentechnik). The LEDHub high-power LED light engine was equipped with a 340 nm, 385 nm, 455 nm, 470 nm and 505-600 nm LED, followed by the following emission filters, respectively: 340x, 380x, 427/10, 473/10 and 510/10 or 575/15 (AHF Analysentechnik). The Zeiss Axiovert 200m microscope was connected to a pe340^{fura} light source (CoolLED, Andover, UK), an Optosplit II emission image splitter (Cairn Research Ltd.) and a pco.panda 4.2 sCMOS camera (Excelitas PCO GmbH) and equipped with 340/26, 380/14 and switchable 427/10, 485/20 or 575/15 excitation filters (AHF Analysentechnik) in the light source, respectively, a 40x Fluar 1.30 oil immersion objective (Carl Zeiss AG), a 459/526/596 or 515LP dichroic mirror and a 475/543/702 or 525/15 emission filter (AHF Analysentechnik) in the microscope, and a T505lpxr (AHF Analysentechnik) in the Optosplit II. Image acquisition and control of both microscopes was performed using VisiView software (Visitron Systems GmbH, Puchheim, Germany). Perfusion of cells was performed using a PC30 perfusion chamber connected to a gravity-based perfusion system (NGFI GmbH, Graz, Austria) and a vacuum pump.

Fura-2 based Ca^{2+} measurements

For fura-2 based Ca^{2+} measurements, cells were taken from the humidified incubator at 37°C and 5% CO_2, washed 1x with cell equilibration buffer and loaded with fura-2 AM (Biomol GmbH, Hamburg, Germany) at a final concentration of 3.3 µM in cell equilibration buffer for 45 minutes at room temperature. Subsequently, cells were washed 2x with cell equilibration buffer and stored in equilibration buffer for additional 30 minutes prior to the measurements. Paxilline or iberiotoxin treatment of the cells was performed 12 hours prior to the measurements and both inhibitors remained present during the fura-2 loading procedure and the measurement at concentrations of 5 µM and 30 nM, respectively. Imaging experiments were either performed on the Zeiss AXIO Observer Z1 or the Zeiss Axiovert 200m microscope (Carl Zeiss AG) in physiologic buffer using alternate excitations at 340 nm and 380 nm. Emissions were captured at roughly 514 nm (Zeiss AXIO Observer Z1) or 525 nm (Zeiss Axiovert 200m). To evoke intracellular Ca^{2+} signals, cells were perfused with physiologic buffer containing ATP (Carl Roth GmbH) at a final concentration of 100 µM.

Ca^{2+} and K^+ calibrations

Calibrations of $[Ca^{2+}]_{cyto}$ and $[K^+]_{cyto}$ were performed by initial superfusion of cells in physiologic buffer. Subsequently, buffer was exchanged to Ca^{2+} free buffer containing 5 µM of ionomycin (Alomone Labs), and subsequent switching to 10Ca buffer for Fura-2 saturation, or 0 mM K^+ buffer containing 15 µM gramicidin, followed by switching to 300 mM K^+ buffer for saturation of NES lc-LysM GEPII 1.0. For calculation of the $[Ca^{2+}]_{cyto}$ and $[K^+]_{cyto}$ in nM and mM, respectively, the following formula was used:

$$[Ion]_{cyto} = K_d * b * (\frac{R - Rmin}{Rmax - R})$$

Genetically encoded sensor-based measurements

Cells were grown on 1.5 H 30 mm circular glass coverslips (Paul Marienfeld GmbH) for perfusion-based experiments. Cells were taken from the incubator, cell culture medium was removed, and cells were equilibrated for at least 30 minutes in cell equilibration buffer in ambient environment. Sensor plasmids used in this study comprised the following: D1ER (Palmer et al., 2004) (Addgene plasmid #36325) for measurement of $[Ca^{2+}]_{ER}$ and 4mtD3cpV (Palmer et al., 2006) (Addgene plasmid #36324) for measurement of $[Ca^{2+}]_{mito}$ were a gift from Amy Palmer & Roger Tsien, mtAT1.03 (Imamura et al., 2009) for measurement of $[ATP]_{mito}$ was a gift from Hiromi Imamura, Laconic (San Martín et al., 2013) (Addgene plasmid #44238) for measurement of $[LAC]_{cyto}$ and assessment of the Warburg index was a gift from Luis Felipe Barros, mito-Hyper3 (Bilan et al., 2013) was a gift from Markus Waldeck-Weiermair and NES lc-LysM GEPII 1.0 (Bischof et al., 2017) was a gift from Roland Malli.. Experiments were either performed on the AXIO Observer Z1 or the Axiovert 200m microscope (Carl Zeiss AG). For experiments where paxilline (5 µM) or iberiotoxin (30 nM) were used, these compounds were added with the media change prior to the transfection with the PolyJet transfection reagent (SignaGen Laboratories) approximately 12 hours prior to the experiments. The compounds remained present throughout the experiment. FRET-based sensors were excited at 427/10 nm and emissions were collected simultaneously at roughly 475 and 543 nm. mito-Hyper3 was excited at 427/10 and 510/10 nm. Calibration of NES lc-LysM GEPII 1.0 was performed by superfusing cells with 15 µM Gramicidin (Sigma Aldrich Chemie GmbH) either in the absence of K^+ (0 mM K^+ buffer) or in the presence of 300 mM K^+. (300 mM K^+ buffer).

Extracellular flux analysis

Assessment of extracellular acidification rate (ECAR) and oxygen consumption rate (OCR) was performed using a Seahorse XFe24 analyzer (Agilent, Santa Clara, USA). The day before the assay, Seahorse XF24 cell culture microplates (Agilent) were coated with 0.5 mg mL^{-1} poly-L-lysine (Sigma Aldrich Chemie GmbH) for 30 minutes at 37°C, washed 2x with PBS followed by cell seeding of 50,000 MMTV-PyMT WT, 50,000 MMTV-PyMT BK-KO or 100,000 MDA-MB-453 cells per well of the 24-well plate in a final volume of 250 µL, either in the presence or absence of 5 µM paxilline, 30 nM iberiotoxin or an equivalent amount of DMSO. 4 wells contained medium without cells and served as blank. Cells were cultivated over-night at 37°C and 5% CO_2 in a humidified incubator. The Seahorse XFe24 sensor cartridges were equilibrated over-night at 37°C in Seahorse XF Calibrant solution according to manufacturer's instructions. The next day, cells were washed using Seahorse XF DMEM medium, pH 7.4 additionally supplemented with 5.5 mM glucose, 2 mM GlutaMAX and 1 mM sodium pyruvate (Thermo Fisher Scientific), with or without paxilline, iberiotoxin or DMSO according to manufacturer's instructions. With the last washing step, a final volume of 500 µL was adjusted per well and cells were incubated at 37°C in the absence of CO_2 for 30 minutes. Meanwhile the Seahorse XFe24 sensor cartridge was loaded with the following compounds: 55 µL of 20 µM Oligomycin-A, 62 µL of 3 µM FCCP and 69 µL of 25 µM Antimycin-A (Santa Cruz Biotechnology), yielding final concentrations of 2 µM, 300 nM and 2.5 µM upon injection, respectively. For analysis, ECAR and OCR rates were normalized for the protein concentration (µg) per well, which was assessed using the Pierce BCA protein assay kit (Thermo Fisher Scientific) according to manufacturer's instructions. Absorbance was measured at 540 nm using a TECAN multiplate reader (TECAN Group Ltd., Männedorf, Switzerland) and concentrations were assessed using a calibration curve.

LC-MS-based metabolomics

Formic acid, acetic acid, acetonitrile and methanol of Ultra LC-MS grade were supplied by Carl Roth (Karlsruhe, Germany). Ammonium hydroxide solution (Suprapur® quality 28.0 - 30.0% NH_3 basis) was purchased from Sigma-Aldrich (Merck, Taufkirchen, Germany). Deionized water was purified by a Purelab ultrapurification system (ELGA LabWater, Celle, Germany). Uniformly (U-)

^{13}C-labeled yeast extract of more than 2 × 109 Pichia pastoris cells (~15 mg; strain CBS 7435) was obtained from ISOtopic Solutions (Vienna, Austria). All standards used were purchased from Sigma-Aldrich Chemie GmbH. Stock solutions of the individual calibrants were prepared at concentrations of 1 mg mL^{-1} and used for further dilution. The individual stocks were stored at -80°C until use.

Targeted LC-MS analysis was performed using an Agilent 1290 Infinity II series UHPLC system from Agilent Technologies (Waldbronn, Germany) equipped with a binary pump, autosampler, thermostated column compartment and a QTrap 4500 mass spectrometer with a TurboIonSpray Source from SCIEX (Ontario, Canada). The samples were filled into homogenization tubes. Internal standards were added prior to sample preparation. For the extraction of the analytes, 1 mL of the ice-cold extraction solvent (50% methanol and 50% water) and 0.15 g of zirconia/glass beads were added to the cell pellets (which were slowly thawed on ice). The samples were homogenized (6,800 rpm, 1 min at 4 °C, 10 × 10 s, pause 30 s) with Cryolys Evolution using dry ice cooling (Bertin Technologies, France). The samples were then spun down for 5 min (16,100xg at 4 °C). The supernatant was carefully removed, transferred into fresh tubes and evaporated to dryness overnight under nitrogen using a high-performance evaporator (Genevac EZ-2) (Genevac, Ipswich, UK). The dry residue of the extract was reconstituted in 10 µL water and 90 µL acetonitrile, followed by 3 cycles of vortexing and sonication (30 seconds each). The samples were centrifuged at 18928xg for 5 min and the supernatant was used for further analysis.

Chromatographic separation was performed on a Waters (Eschborn, Germany) Premier BEH Amide column (150 x 2.1 mm, 1.7 µm). For metabolite analysis in ESI$^+$ mode, mobile phases A and B were adjusted to a pH of 3.5 with formic acid and consisted of 20 mM ammonium formate in water and acetonitrile, respectively. In ESI-, the chromatographic conditions differed. Mobile phase A and B were adjusted to a pH of 7.5 with acetic acid and consisted of 20 mM ammonium acetate in water and acetonitrile, respectively. The gradient elution profile was the same for both positive and negative ionization modes (0.0 min, 100% B; 13 min 70% B; 15 min 70% B; 15.1 min 100% B; 20 min 100% B) and was carried out at a flow rate of 0.25 mL min^{-1} and a constant column temperature of 35 °C. The injection volume was 5 µL. The autosampler was kept at 4°C. Ion source parameters were as follows: nebulizer gas (GS1, zero grade air) 50 psi, heater gas (GS2, zero grade air) 30 psi, curtain gas (CUR, nitrogen) 30 psi, source temperature (TEM) 450 °C, ion source voltage +5,500 V (positive mode) and - 4,500 V (negative mode). Due to the large number of transitions monitored simultaneously, the Scheduled-MRM function was enabled. A window of 30 seconds was set around the designated metabolite-specific retention time and the total cycle time was 1 s. Blank solvents (mobile phase A and B) followed by QCs were injected in the beginning of the chromatographic batch to ensure proper column and system equilibration.

Plasma- and mitochondrial membrane potential measurements

$\Delta\Psi_{PM}$ was determined using Bis-(1,3-dibutylbarbituric acid)trimethine oxonol (Dibac4(3)) (Thermo Fisher Scientific). Cells were cultivated on 30 mm glass coverslips. On the day of analysis, cells were equilibrated in cell equilibration buffer containing Dibac4(3) at a concentration of 0.25 µg mL^{-1} for 30 minutes and subsequently analyzed by fluorescence microscopy using 485/20 excitation at the Zeiss Axiovert 200m microscope. Emission was captured at roughly 525 nm.

$\Delta\Psi_{mito}$ was assessed using Tetramethylrhodamin-Methylester (TMRM) (Thermo Fisher Scientific). After cell cultivation on 30 mm glass coverslips in the presence or absence of paxilline, iberiotoxin or DMSO for 12 hours, the cell culture medium was replaced with cell equilibration buffer containing 200 nM TMRM and cells were incubated in ambient environment for 30 minutes. Subsequently, cells were washed with physiologic buffer containing 2 mM or 25 mM glucose and 200 nM TMRM, and cells were equilibrated for further 30 minutes. The glass coverslips were transferred to the PC30 perfusion chamber and experiments were started using the gravity-based perfusion system (NGFI GmbH). Paxilline, iberiotoxin or DMSO (control) and 200 nM TMRM remained present throughout the experiment. Mitochondrial depolarization was induced by the

perfusion of a buffer containing 200 nM FCCP. For analysis, the fluorescence emission at ≥600 nm upon excitation at 575/15 nm of a region of interest (ROI) above mitochondria was divided by a ROI in the nucleus (mitochondria free area) and the ratio was plotted over-time, or basal values were given.

2-NBDG based glucose uptake measurements

Glucose uptake was assessed using 2-(N-(7-Nitrobenz-2-oxa-1,3-diazol-4-yl)Amino)-2-Deoxyglucose (2-NBDG) (Biomol GmbH). Therefore, cells were seeded on 30 mm glass coverslips (Marienfeld GmbH) in 6-well plates (Corning) and cultivated over-night at 37°C and 5% CO_2 in a humidified incubator. The next day, cells were taken from the incubator, cell culture medium was replaced for cell equilibration buffer and cells were equilibrated for 30 minutes at ambient environment. Subsequently, cells were washed 3x with glucose free physiologic buffer, and glucose free physiologic buffer containing 100 µM 2-NBDG, with or without paxilline and 200 nM FCCP or an equivalent amount of DMSO, was added to the cells, followed by incubation at 37°C for 30 minutes. Next, cells were washed 3x with glucose free physiologic buffer to remove any residual 2-NBDG and were analyzed by fluorescence microscopy using 485/20 excitation light. Emission was captured at roughly 525 nm (Zeiss Axiovert 200m).

Mitochondrial single-channel patch-clamp measurements

For mitoplast electrophysiology, mitochondria were isolated from BCC grown to confluency (>90%). Adherent cells were washed 2x with PBS, scraped from the dish, collected in a tube and centrifuged at 400xg for 5 minutes. Subsequently, the cell pellet was resuspended in preparation solution, followed by homogenization using a glass-glass homogenizer. Next, the homogenate was centrifuged at 9,200xg for 10 minutes. The resulting pellet was resuspended in preparation solution and centrifuged at 780xg for 10 minutes. The supernatant was collected, followed by centrifugation at 9,200xg for 10 minutes and resuspension of the mitochondrial fraction in the mitochondrial storage buffer. All procedures were performed at 4°C.

An osmotic swelling procedure was used for the preparation of mitoplasts from the isolated mitochondria. Therefore, mitochondria were added to the hypotonic buffer for ~1 minute to induce swelling and breakage of the outer mitochondrial membrane. Subsequently, isotonicity of the solution was restored by the addition of hypertonic buffer at a dilution of 1:5.

Patch-clamp experiments on mitoplasts were performed as previously described (Bednarczyk et al., 2013). The experiments were carried out in mitoplast-attached single-channel mode using borosilicate glass pipettes with a mean resistance of 10-15 MΩ. The patch-clamp glass pipette was filled with mitochondrial storage buffer. This isotonic solution was used as a control solution for all experiments. The size of the pipettes and the formation of the gigaseal were monitored by measuring electrical resistance. Connections were made with Ag/AgCl electrodes and an agar salt bridge (3 M KCl) for the ground electrode. The current was recorded using an Axopatch 200B patch-clamp amplifier (Molecular Devices, California, USA). To apply substances, a self-made perfusion system containing a holder with a glass pipe, a peristaltic pump, and Teflon tubing was used. All channel modulators were added as dilutions in the isotonic solution containing 100 µM $CaCl_2$.

The presented single-channel current-time recordings are representative for the most frequently observed conductances under the given conditions. The conductance was calculated from the current-voltage relationship. The probability of channel openings and the current amplitude were determined using the Single-Channel Search mode of the Clampfit 10.7 software (Molecular Devices).

Western blotting

Mitochondria for western blotting were prepared as described earlier(Pallotti and Lenaz, 2007) with some modifications. Cells were washed and collected in PBS and centrifuged at 500xg for 10 min. The pellet was frozen in liquid nitrogen and stored at -80°C. The next day, pellet was resuspended in ice-cold isolation buffer containing (in mM): 210 mannitol, 70 sucrose, 1 PMSF, 5 HEPES and bovine serum albumin (2.5 mg mL^{-1}), pH 7.2. Digitonin was added to a final concentration of 0.02–0.04% for additional membrane permeabilization. After 1 min of incubation, digitonin was diluted with isolation buffer and the cells were centrifuged at 3,000xg for 5 min at 4°C. The pellet was resuspended in ice-cold isolation buffer. The cells were homogenized using a glass/glass homogenizer and centrifuged at 1,000xg for 5 min at 4°C followed by another homogenization. The homogenates were centrifuged at 1,000xg for 5 min at 4°C to remove cell remnants. The supernatants were collected and centrifuged for 60 min at 10,000xg, at 4°C. Next, the pellet was resuspended in the isolation buffer without BSA and centrifuged at 10,000xg for 30 min at 4°C, followed by resuspension in isolation buffer without BSA and centrifugation at 10,000xg for 15 min at 4°C. This step was repeated once more. The pellet containing crude mitochondria was resuspended in 0.8 mL of 15% Percoll (in isolation buffer without BSA) and layered on top of a Percoll step gradient (23% and 40% Percoll layers). The suspension was centrifuged at 30,000xg for 30 min at 4°C. Mitochondrial fraction located between the 23% and 40% Percoll layer was collected, diluted with isolation buffer without BSA and centrifuged at 10,000xg for 15 min at 4°C. The final mitochondrial pellet was resuspended in storage buffer containing 500 mM sucrose and 5 mM HEPES, pH 7.2. Each mitochondrial isolation was performed using between 15-30 x 10^6 cells.

A given amount of sample solubilized in Laemmli buffer (Bio-Rad) was separated by 10% Tris-tricine-SDS-PAGE and transferred onto polyvinylidene difluoride (PVDF) membranes (Bio-Rad). After protein transfer, the membranes were blocked with 10% nonfat dry milk solution in Tris-buffered saline with 0.2% Tween 20 and exposed to one of the following antibodies: anti-BKα antibody (NeuroMabs, USA, clone L6/60, diluted 1:200), anti-COXIV (Cell Signaling Technology, Leiden, Netherlands, no. 4844, 1:1,000), or anti-alpha 1 sodium potassium ATPase (Abcam, Berlin, Germany, no. ab7671, 1:1,000). This was followed by incubation with a secondary anti-rabbit (Thermo Fisher Scientific, no. 31460) or anti-mouse antibody (Thermo Fisher Scientific, no. SA1-100) coupled to horseradish peroxidase. The blots were developed using enhanced chemiluminescence solution (GE Healthcare). To estimate the molecular weight of the analyzed proteins PageRuler Prestained Protein Ladder (Thermo Fisher Scientific) was used.

qPCR analysis

mRNA was isolated from 6-well plates showing a cell confluency of ~90% using the Monarch Total RNA Miniprep kit (NEB). siRNA transfection was performed 48 hours prior to RNA isolation using the Lipofectamine 2000 transfection reagent (Thermo Fisher Scientific) according to manufacturer's instructions. qPCR reactions were performed using the GoTaq 1-Step RT-qPCR System (Promega GmbH, Walldorf, Germany). 100 ng of isolated mRNA were used per reaction. Primers were designed to span exon – exon junctions and to recognize both, human and murine BK_{Ca} sequences. Different primer pairs were used for human and murine b-tubulin. Primer and siRNA sequences are listed in **Supplementary Table 1** and **Supplementary Table 2**. Primers were purchased from Thermo Fisher Scientific, siRNAs were purchased from Microsynth AG. qPCR reactions were run in a CFX connect real-time PCR instrument (Bio-Rad Laboratories GmbH, Feldkirchen, Germany). Sample (Ct) values were normalized to Ct's of housekeeper gene (b-Tubulin) and calculated as $2^{-Ct\ (normalized)}$.

Proliferation assays

Proliferation assays were performed using 3-(4,5-dimethylthiazol-2-yl)-2,5-diphenyltetrazolium bromide (MTT) (Thermo Fisher Scientific) assay. For the assay, 2.500 MMTV-PyMT WT and BK-KO cells or 7.500 MDA-MB-453 cells were seeded per well in flat bottom 96-well cell culture plates (Corning) in their respective cell culture medium. Per run, condition, and time-point, 7 technical replicates were performed. One well served as a blank per time-point and condition and did not contain cells. The next day, medium was exchanged for fresh cell culture medium either containing 5 µM paxilline, 30 nM iberiotoxin or an equivalent amount of DMSO as a control and the MTT assay was started for time-point 24 hours directly thereafter. For each time-point (24, 48, 72 and 96 hours), MTT reagent was added with a medium change (10 µL + 100 µL / well) at a final concentration of 455 µg mL^{-1} and cells were incubated for 4 hours. Subsequently, 85 µL of medium were removed from each well, 85 µL of DMSO (Carl Roth GmbH) was added and wells were mixed by pipetting thoroughly. 85 µL of this mixture were transferred to a new 96-well plate (Corning) and absorbance was measured at 540 nm using a TECAN microplate reader (TECAN Group Ltd.). Absorbances at the different time-points (48, 72 and 96 hours) were normalized to the absorbances after 24 hours.

For KI-67 based assessment of cell proliferation rates, 20,000 MMTV-PyMT WT and BK-KO cells and 30,000 MDA-MB-453 cells were seeded in µ-slide 8 wells (ibidi GmbH). The next day, cells were washed 1x with PBS, and serum free cultivation medium was added. Cells were further cultivated for 48 hours, prior to addition of DMSO (ctrl) 5 µM paxilline or 30 nM iberiotoxin. After additional 24 hours, serum containing medium supplemented with DMSO, paxilline or iberiotoxin was re-added, and cell growth was allowed for another 48 hours. Finally, cells were washed 2x with PBS and fixed with ice cold methanol/aceton (50:50 v/v) for 15 minutes at -20°C. Subsequently, cells were washed thrice with PBS, and incubated in PBS containing 5% bovine serum albumin (BSA, Carl Roth GmbH) for 1 hours. Subsequently, anti Ki-67 rabbit monoclonal antibody (D3B5, Cell Signaling Technology) in 5% BSA-PBS was added at a dilution of 1:500. Wells without primary antibody served as a negative control. Slides were incubated over-night at 4°C. The next day, antibody solution was removed, cells were washed 3x with PBS, and subsequently incubated with Goat anti-Rabbit IgG (H+L) Cross-Adsorbed Secondary Antibody, Alexa Fluor 488 (Thermo Fisher Scientific) for 2 hours at room temperature, followed by washing 2x with PBS. During a 3rd washing step, Hoechst 33342 (Thermo Fisher Scientific) at a dilution of 1:2000 was added, cells were incubated for 10 minutes at room temperature and washed an additional time with PBS. Ultimately, cells were mounted in PermaFluor Mountant (Microm International GmbH, Dreieich, Germany), kept over-night at 4°C, and imaged using the Zeiss Axio Observer Z1 wide-field microscope. AlexaFluor 488 and Hoechst 33342 were illuminated using 473/10 and 380x filters, respectively. 2 images were captured per replicate. Image analysis was performed using ImageJ. Threshold positive area of Ki-67 (AlexaFluor488) was expressed as fraction of the threshold positive area of Hoechst 33342 per image, and the average of the 2 images per well was calculated.

Colony formation assays

For colony formation assays, cell suspensions containing 400 cells mL^{-1} of MMTV-PyMT WT or BK-KO cells were prepared. 1 mL of this suspension was spread drop-per-drop per well of a 6-well cell culture plate (Corning) already containing 1 mL of cell culture medium using 1 mL syringes and 23G needles. Culture plates were gently moved left/right and back/forth to equally distribute the cells across the well, plates were kept at room temperature for 20 minutes to ensure uniform cell settling, and cells were subsequently cultured over-night at 37°C and 5% CO_2 in a humidified incubator. The next day, medium was exchanged for 2 mL of fresh cell culture medium, and cells were kept in the presence or absence of O_2 at 37°C and 5% CO_2 in humidified incubators for 7 days. After 7 days, cells were washed carefully 2x with PBS and fixed for 30 minutes on ice using 2% PFA in PBS. Meanwhile, a solution of crystal violet (0.01% w/v) was prepared in ddH_2O, cells were washed 2x with PBS and incubated in the crystal violet solution (Sigma Aldrich Chemie

GmbH) for 60 minutes after fixation, followed by excessive washing with ddH_2O until a clear background was obtained. Plates were dried at room temperature for at least 12 hours before images were captured using an Amersham Imager 600 (GE Healthcare UK Limited, Buckinghamshire, UK). Analysis was performed using ImageJ.

Breast cancer patient study

A subset of 551 primary tumor specimens with available archival tumor blocks were obtained from a prospective, observational multicenter adjuvant endocrine treatment study of 1286 post-menopausal HR-positive breast cancer patients recruited between 2005 and 2011 (German Clinical Trial Register DRKS 00000605, "IKP211" study). Study inclusion and exclusion criteria have been previously described (Schroth et al., 2020). Patients had received standard endocrine treatment, i.e. tamoxifen, aromatase inhibitors, or switch regimens between both. Ethics approval was obtained from the Medical Faculty of the University of Tuebingen and the local ethics committees of all participating centers in Germany. Informed patient consent was obtained from all participants as required by institutional review boards and research ethics committees. All patient data were de-identified prior inclusion in this study.

Nanostring nCounter gene expression analysis

Gene expression analysis was performed according to manufacturer's protocol. In brief, total RNA from human primary tumors of the IKP211 study (Quick-DNA/RNA FFPE, ZymoResearch, Freiburg, Germany) was extracted from 10 µm sections of FFPE tissues with at least 20% tumor cell content. Samples were enriched for tumor tissue by microdissection. A total of 250 ng RNA was subsequently hybridized with target-specific capture and color-coded reporter probe sets in a pre-warmed thermal cycler at 65°C for 20 h. In the post-hybridization process, the total volume was increased to 32 µl with RNase-free water. Fluorescence count measurements were immediately conducted in the Nanostring nCounter System. Data were analyzed using nSolver 4.0 and normalized to housekeeping genes. ABCF1, NRDE2, POLR2A, PUM1 and SF3A1 served as housekeepers. Probes used for Nanostring nCounter gene expression analysis are listed in **Supplementary Table 3**.

Statistical analysis

Statistical analysis was performed using Prism8 software (GraphPad Software, Boston, USA). All data were tested for normal distribution using D'Agostino and Pearson omnibus normality test. A two-tailed Unpaired t-test or Welch's t-test were used for statistical comparison of normally distributed data, depending on whether the variances of the populations were comparable or significantly different as tested by an F-test. A two-tailed Mann-Whitney test was used for pairwise comparison of non-normally distributed data. Comparison of >2 data sets was done either using One-way ANOVA followed by Tukey's multiple comparison (MC) test or Brown-Forsythe and Welch ANOVA test followed by Games-Howell's MC test for normally distributed data, depending on whether the variances were comparable or significantly different. A Kruskal-Wallis test followed by Dunn's MC test was performed if data were not normally distributes. The statistical tests used are indicated in the figure legends. p-values of ≤0.05 were considered as significant, where * or #p≤0.05, ** or †p≤0.01 and *** or ‡p≤0.001. No priory sample size estimation was performed.

Acknowledgements

This work was funded by the Deutsche Forschungsgemeinschaft (DFG) with individual grants to RL and LM. RL is a member of the GRK2381: "cGMP: From Bedside to Bench", DFG grant number 335549539. SM, WS, MS and RL acknowledge financial support from the ICEPHA Graduate Program "Membrane-associated Drug Targets in Personalized Cancer Medicine". HB is a fellow of the Austrian Science Fund (FWF) funded Erwin-Schrödinger-Program, project number J-4457. SB

acknowledges financial support from the Fritz Thyssen Stiftung. The authors thank Clement Kabagema-Bilan, Michael Glaser and Antoni Wrzosek for excellent technical support and Peter Ruth for valuable discussions. This work was partially supported by the Nencki Institute of Experimental Biology, the Polish National Science Centre grant no. 2019/34/A/NZ1/00352 (AS), and by the FWF, project number I-3716 (RM).

Author contributions

HB and RL initiated and designed this study; HB, SM, PK, BK, SB, JJ, KS, YZ, WS and PB performed experiments and were involved in data curation; HB, SM, PK, BK, SB, JJ, KS and WS assisted in formal analysis; HB, SM, SB and PB visualized data; HB, SB, WS, LM, MS, PB, AS and RL acquired financial support; HB, SM, PK, BK, SB, KS, WS, ML and PB designed the methodology; HB and RL performed project administration; PK, WS, LM, MS, ALB, RM, ML, PB, AS and RL provided resources; RL supervised the project and the personnel; HB and RL wrote the original draft. All authors critically reviewed the manuscript and stated comments.

Data availability

Raw data for the graphs can be found in source data files.

Declaration of interests

The authors declare no competing interests.

References

Adams DS, Levin M (2012) **Measuring Resting Membrane Potential Using the Fluorescent Voltage Reporters DiBAC 4 (3) and CC2-DMPE** *Cold Spring Harb Protoc* **2012** https://doi.org/10.1101/pdb.prot067702

Bednarczyk P, Wieckowski MR, Broszkiewicz M, Skowronek K, Siemen D, Szewczyk A (2013) **Putative Structural and Functional Coupling of the Mitochondrial BKCa Channel to the Respiratory Chain** *PLoS ONE* **8** https://doi.org/10.1371/journal.pone.0068125

Bilan DS, Pase L, Joosen L, Gorokhovatsky AYu, Ermakova YG, Gadella TWJ, Grabher C, Schultz C, Lukyanov S, Belousov VV. (2013) **HyPer-3: A Genetically Encoded H 2 O 2 Probe with Improved Performance for Ratiometric and Fluorescence Lifetime Imaging** *ACS Chem Biol* **8**:535–542 https://doi.org/10.1021/cb300625g

Bischof H *et al.* (2021) **Potassium ions promote hexokinase-II dependent glycolysis** *iScience* **24** https://doi.org/10.1016/j.isci.2021.102346

Bischof H *et al.* (2017) **Novel genetically encoded fluorescent probes enable real-time detection of potassium in vitro and in vivo** *Nat Commun* **8** https://doi.org/10.1038/s41467-017-01615-z

Burgstaller S, Bischof H, Lukowski R, Graier WF, Malli R (2021) **Investigating the K+ sensitivity of cellular metabolism by extracellular flux analysis** *STAR Protoc* **2** https://doi.org/10.1016/j.xpro.2021.100876

Burgstaller S, Bischof H, Matt L, Lukowski R (2022) **Assessing K+ ions and K+ channel functions in cancer cell metabolism using fluorescent biosensors** *Free Radical Biology and Medicine* **181**:43–51 https://doi.org/10.1016/j.freeradbiomed.2022.01.026

Burgstaller S *et al.* (2021) **Immobilization of Recombinant Fluorescent Biosensors Permits Imaging of Extracellular Ion Signals** *ACS Sens* **6**:3994–4000 https://doi.org/10.1021/acssensors.1c01369

Burgstaller S *et al.* (2022) **Monitoring extracellular ion and metabolite dynamics with recombinant nanobody-fused biosensors** *iScience* **25** https://doi.org/10.1016/j.isci.2022.104907

Candia S, Garcia ML, Latorre R (1992) **Mode of action of iberiotoxin, a potent blocker of the large conductance Ca(2+)-activated K+ channel** *Biophys J* **63**:583–590 https://doi.org/10.1016/S0006-3495(92)81630-2

Chadet S, Jelassi B, Wannous R, Angoulvant D, Chevalier S, Besson P, Roger S (2014) **The activation of P2Y2 receptors increases MCF-7 breast cancer cells migration through the MEK-ERK1/2 signalling pathway** *Carcinogenesis* **35**:1238–1247 https://doi.org/10.1093/carcin/bgt493

Checchetto V, Leanza L, De Stefani D, Rizzuto R, Gulbins E, Szabo I. (2021) **Mitochondrial K+ channels and their implications for disease mechanisms** *Pharmacology & Therapeutics* **227** https://doi.org/10.1016/j.pharmthera.2021.107874

Dabrowska A, Zajac M, Bednarczyk P, Lukasiak A (2022) **Effect of Quercetin on mitoBKCa Channel and Mitochondrial Function in Human Bronchial Epithelial Cells Exposed to Particulate Matter** *IJMS* **24** https://doi.org/10.3390/ijms24010638

de la Cruz-López KG, Castro-Muñoz LJ, Reyes-Hernández DO, García-Carrancá A, Manzo-Merino J (2019) **Lactate in the Regulation of Tumor Microenvironment and Therapeutic Approaches** *Front Oncol* **9** https://doi.org/10.3389/fonc.2019.01143

Dejos C, Gkika D, Cantelmo AR (2020) **The Two-Way Relationship Between Calcium and Metabolism in Cancer** *Front Cell Dev Biol* **8** https://doi.org/10.3389/fcell.2020.573747

Depaoli MR *et al.* (2018) **Real-Time Imaging of Mitochondrial ATP Dynamics Reveals the Metabolic Setting of Single Cells** *Cell Rep* **25**:501–512 https://doi.org/10.1016/j.celrep.2018.09.027

Di Virgilio F, Sarti AC, Falzoni S, De Marchi E, Adinolfi E. (2018) **Extracellular ATP and P2 purinergic signalling in the tumour microenvironment** *Nat Rev Cancer* **18**:601–618 https://doi.org/10.1038/s41568-018-0037-0

Douglas RM, Lai JCK, Bian S, Cummins L, Moczydlowski E, Haddad GG (2006) **The calcium-sensitive large-conductance potassium channel (BK/MAXI K) is present in the inner mitochondrial membrane of rat brain** *Neuroscience* **139**:1249–1261 https://doi.org/10.1016/j.neuroscience.2006.01.061

Dowsett M *et al.* (2011) **Assessment of Ki67 in Breast Cancer: Recommendations from the International Ki67 in Breast Cancer Working Group** *JNCI Journal of the National Cancer Institute* **103**:1656–1664 https://doi.org/10.1093/jnci/djr393

Dunnwald LK, Rossing MA, Li CI (2007) **Hormone receptor status, tumor characteristics, and prognosis: a prospective cohort of breast cancer patients** *Breast Cancer Res* **9** https://doi.org/10.1186/bcr1639

Eales KL, Hollinshead KER, Tennant DA (2016) **Hypoxia and metabolic adaptation of cancer cells** *Oncogenesis* **5**:e190–e190 https://doi.org/10.1038/oncsis.2015.50

Eil R *et al.* (2016) **Ionic immune suppression within the tumour microenvironment limits T cell effector function** *Nature* **537**:539–543 https://doi.org/10.1038/nature19364

Frankenreiter S *et al.* (2017) **cGMP-Elevating Compounds and Ischemic Conditioning Provide Cardioprotection Against Ischemia and Reperfusion Injury via Cardiomyocyte-Specific BK Channels** *Circulation* **136**:2337–2355 https://doi.org/10.1161/CIRCULATIONAHA.117.028723

Gałecka S, Kulawiak B, Bednarczyk P, Singh H, Szewczyk A (2021) **Single channel properties of mitochondrial large conductance potassium channel formed by BK-VEDEC splice variant** *Sci Rep* **11** https://doi.org/10.1038/s41598-021-90465-3

Gohara DW, Di Cera E. (2016) **Molecular Mechanisms of Enzyme Activation by Monovalent Cations** *Journal of Biological Chemistry* **291**:20840–20848 https://doi.org/10.1074/jbc.R116.737833

Gross D, Bischof H, Maier S, Sporbeck K, Birkenfeld AL, Malli R, Ruth P, Proikas-Cezanne T, Lukowski R (2022) **IKCa channels control breast cancer metabolism including AMPK-driven autophagy** *Cell Death Dis* **13** https://doi.org/10.1038/s41419-022-05329-z

Grynkiewicz G, Poenie M, Tsien RY (1985) **A new generation of Ca2+ indicators with greatly improved fluorescence properties** *J Biol Chem* **260**:3440–3450

Gu XQ, Pamenter ME, Siemen D, Sun X, Haddad GG (2014) **Mitochondrial but not plasmalemmal BK channels are hypoxia-sensitive in human glioma: Glioma BK Channels are not Hypoxia Sensitive** *Glia* **62**:504–513 https://doi.org/10.1002/glia.22620

Huang X, Jan LY (2014) **Targeting potassium channels in cancer** *Journal of Cell Biology* **206**:151–162 https://doi.org/10.1083/jcb.201404136

Imamura H, Huynh Nhat KP, Togawa H, Saito K, Iino R, Kato-Yamada Y, Nagai T, Noji H (2009) **Visualization of ATP levels inside single living cells with fluorescence resonance energy transfer-based genetically encoded indicators** *Proc Natl Acad Sci USA* **106**:15651–15656 https://doi.org/10.1073/pnas.0904764106

Jang M, Kim SS, Lee J (2013) **Cancer cell metabolism: implications for therapeutic targets** *Exp Mol Med* **45**:e45–e45 https://doi.org/10.1038/emm.2013.85

Joshi DC, Bakowska JC (2011) **Determination of Mitochondrial Membrane Potential and Reactive Oxygen Species in Live Rat Cortical Neurons** *JoVE* **2704** https://doi.org/10.3791/2704

Kalia M (2015) **Biomarkers for personalized oncology: recent advances and future challenges** *Metabolism* **64**:S16–S21 https://doi.org/10.1016/j.metabol.2014.10.027

Kicinska A, Augustynek B, Kulawiak B, Jarmuszkiewicz W, Szewczyk A, Bednarczyk P (2016) **A large-conductance calcium-regulated K+ channel in human dermal fibroblast mitochondria** *Biochemical Journal* **473**:4457–4471 https://doi.org/10.1042/BCJ20160732

Klijn C *et al.* (2015) **A comprehensive transcriptional portrait of human cancer cell lines** *Nat Biotechnol* **33**:306–312 https://doi.org/10.1038/nbt.3080

Krabbendam IE, Honrath B, Culmsee C, Dolga AM (2018) **Mitochondrial Ca2+-activated K+ channels and their role in cell life and death pathways** *Cell Calcium* **69**:101–111 https://doi.org/10.1016/j.ceca.2017.07.005

Kulawiak B, Szewczyk A (2022) **Current Challenges of Mitochondrial Potassium Channel Research** *Front Physiol* **13** https://doi.org/10.3389/fphys.2022.907015

Lape M, Elam C, Versluis M, Kempton R, Paula S (2008) **Molecular determinants of sarco/endoplasmic reticulum calcium ATPase inhibition by hydroquinone-based compounds** *Proteins* **70**:639–649 https://doi.org/10.1002/prot.21542

Leary SC, Battersby BJ, Hansford RG, Moyes CD (1998) **Interactions between bioenergetics and mitochondrial biogenesis** *Biochimica et Biophysica Acta (BBA) - ssBioenergetics* **1365**:522–530 https://doi.org/10.1016/S0005-2728(98)00105-4

Li M, Tian P, Zhao Q, Ma X, Zhang Y (2023) **Potassium channels: Novel targets for tumor diagnosis and chemoresistance** *Front Oncol* **12** https://doi.org/10.3389/fonc.2022.1074469

Li M, Xiong Z-G (2011) **Ion channels as targets for cancer therapy** *Int J Physiol Pathophysiol Pharmacol* **3**:156–166

Liu H, Moczydlowski E, Haddad GG (1999) **O2 deprivation inhibits Ca2+-activated K+ channels via cytosolic factors in mice neocortical neurons** *J Clin Invest* **104**:577–588 https://doi.org/10.1172/JCI7291

Losano JDA, Padín JF, Méndez-López I, Angrimani DSR, García AG, Barnabe VH, Nichi M (2017) **The Stimulated Glycolytic Pathway Is Able to Maintain ATP Levels and Kinetic Patterns of Bovine Epididymal Sperm Subjected to Mitochondrial Uncoupling** *Oxidative Medicine and Cellular Longevity* **2017**:1–8 https://doi.org/10.1155/2017/1682393

Mohr CJ *et al.* (2022) **Subunits of BK channels promote breast cancer development and modulate responses to endocrine treatment in preclinical models** *British J Pharmacology* **179**:2906–2924 https://doi.org/10.1111/bph.15147

Müller CE, Baqi Y, Namasivayam V (2020) **Agonists and Antagonists for Purinergic Receptors In: Pelegrín P, editor. Purinergic Signaling, Methods in Molecular Biology. New York** *NY: Springer New York* :45–64 https://doi.org/10.1007/978-1-4939-9717-6_3

Naguib A *et al.* (2018) **Mitochondrial Complex I Inhibitors Expose a Vulnerability for Selective Killing of Pten-Null Cells** *Cell Reports* **23**:58–67 https://doi.org/10.1016/j.celrep.2018.03.032

Nazemi M, Rainero E (2020) **Cross-Talk Between the Tumor Microenvironment, Extracellular Matrix, and Cell Metabolism in Cancer** *Front Oncol* **10** https://doi.org/10.3389/fonc.2020.00239

N'Gouemo P (2014) **BK Ca channel dysfunction in neurological diseases** *Front Physiol* **5** https://doi.org/10.3389/fphys.2014.00373

Oeggerli M *et al.* (2012) **Role of KCNMA1 in Breast Cancer** *PLoS ONE* **7** https://doi.org/10.1371/journal.pone.0041664

Ouadid-Ahidouch H, Ahidouch A (2013) **K+ channels and cell cycle progression in tumor cells** *Front Physiol* **4** https://doi.org/10.3389/fphys.2013.00220

Pallotti F, Lenaz G (2007) **Isolation and Subfractionation of Mitochondria from Animal Cells and Tissue Culture LinesMethods in Cell Biology** *Elsevier* :3–44 https://doi.org/10.1016/S0091-679X(06)80001-4

Palmer AE, Giacomello M, Kortemme T, Hires SA, Lev-Ram V, Baker D, Tsien RY (2006) **Ca2+ indicators based on computationally redesigned calmodulin-peptide pairs** *Chem Biol* **13**:521–530 https://doi.org/10.1016/j.chembiol.2006.03.007

Palmer AE, Jin C, Reed JC, Tsien RY (2004) **Bcl-2-mediated alterations in endoplasmic reticulum Ca 2+ analyzed with an improved genetically encoded fluorescent sensor** *Proc Natl Acad Sci USA* **101**:17404–17409 https://doi.org/10.1073/pnas.0408030101

Quanz M *et al.* (2018) **Preclinical Efficacy of the Novel Monocarboxylate Transporter 1 Inhibitor BAY-8002 and Associated Markers of Resistance** *Molecular Cancer Therapeutics* **17**:2285–2296 https://doi.org/10.1158/1535-7163.MCT-17-1253

Rossi A, Pizzo P, Filadi R (2019) **Calcium, mitochondria and cell metabolism: A functional triangle in bioenergetics** *Biochimica et Biophysica Acta (BBA) - Molecular Cell Research* **1866**:1068–1078 https://doi.org/10.1016/j.bbamcr.2018.10.016

Salter M, Hicks J (1995) **ATP causes release of intracellular Ca2+ via the phospholipase C beta/IP3 pathway in astrocytes from the dorsal spinal cord** *J Neurosci* **15**:2961–2971 https://doi.org/10.1523/JNEUROSCI.15-04-02961.1995

San Martín A, Ceballo S, Ruminot I, Lerchundi R, Frommer WB, Barros LF (2013) **A Genetically Encoded FRET Lactate Sensor and Its Use To Detect the Warburg Effect in Single Cancer Cells** *PLoS ONE* **8** https://doi.org/10.1371/journal.pone.0057712

Schroth W *et al.* (2020) **Gene Expression Signatures of BRCAness and Tumor Inflammation Define Subgroups of Early-Stage Hormone Receptor–Positive Breast Cancer Patients** *Clinical Cancer Research* **26**:6523–6534 https://doi.org/10.1158/1078-0432.CCR-20-1923

Seyfried TN, Shelton LM (2010) **Cancer as a metabolic disease. Nutr Metab (Lond) 7:7. doi:10.1186/1743-7075-7-7 Siemen D, Loupatatzis C, Borecky J, Gulbins E, Lang F. 1999. Ca2+-Activated K Channel of the BK-Type in the Inner Mitochondrial Membrane of a Human Glioma Cell Line** *Biochemical and Biophysical Research Communications* **257**:549–554 https://doi.org/10.1006/bbrc.1999.0496

Singh H, Lu R, Bopassa JC, Meredith AL, Stefani E, Toro L (2013) **mitoBK Ca is encoded by the Kcnma1 gene, and a splicing sequence defines its mitochondrial location** *Proc Natl Acad Sci USA* **110**:10836–10841 https://doi.org/10.1073/pnas.1302028110

Sizemore G, McLaughlin S, Newman M, Brundage K, Ammer A, Martin K, Pugacheva E, Coad J, Mattes MD, Yu H-G (2020) **Opening large-conductance potassium channels selectively induced cell death of triple-negative breast cancer** *BMC Cancer* **20** https://doi.org/10.1186/s12885-020-07071-1

Skalska J *et al.* (2008) **A novel potassium channel in skeletal muscle mitochondria** *Biochimica et Biophysica Acta (BBA) - Bioenergetics* **1777**:651–659 https://doi.org/10.1016/j.bbabio.2008.05.007

Sung H, Ferlay J, Siegel RL, Laversanne M, Soerjomataram I, Jemal A, Bray F (2021) **Global Cancer Statistics 2020: GLOBOCAN Estimates of Incidence and Mortality Worldwide for 36 Cancers in 185 Countries** *CA A Cancer J Clin* **71**:209–249 https://doi.org/10.3322/caac.21660

Szabo I, Szewczyk A (2023) **Mitochondrial Ion Channels** *Annu Rev Biophys* **52**:229–254 https://doi.org/10.1146/annurev-biophys-092622-094853

Szewczyk A, Jarmuszkiewicz W, Kunz WS (2009) **Mitochondrial potassium channels** *IUBMB Life* **61**:134–143 https://doi.org/10.1002/iub.155

Wacquier B, Combettes L, Dupont G (2019) **Cytoplasmic and Mitochondrial Calcium Signaling: A Two-Way Relationship** *Cold Spring Harb Perspect Biol* **11** https://doi.org/10.1101/cshperspect.a035139

Warburg O (1924) **Über den Stoffwechsel der Carcinomzelle** *Naturwissenschaften* **12**:1131–1137 https://doi.org/10.1007/BF01504608

Wrzosek A, Augustynek B, Żochowska M, Szewczyk A. (2020) **Mitochondrial Potassium Channels as Druggable Targets** *Biomolecules* **10** https://doi.org/10.3390/biom10081200

Wu P, Gao W, Su M, Nice EC, Zhang W, Lin J, Xie N (2021) **Adaptive Mechanisms of Tumor Therapy Resistance Driven by Tumor Microenvironment** *Front Cell Dev Biol* **9** https://doi.org/10.3389/fcell.2021.641469

Wu SZ *et al.* (2021) **A single-cell and spatially resolved atlas of human breast cancers** *Nat Genet* **53**:1334–1347 https://doi.org/10.1038/s41588-021-00911-1

Xu W, Liu Y, Wang S, McDonald T, Van Eyk JE, Sidor A, O'Rourke B. (2002) **Cytoprotective Role of Ca 2+ - Activated K + Channels in the Cardiac Inner Mitochondrial Membrane** *Science* **298**:1029–1033 https://doi.org/10.1126/science.1074360

Zhou Y, Lingle CJ (2014) **Paxilline inhibits BK channels by an almost exclusively closed-channel block mechanism** *Journal of General Physiology* **144**:415–440 https://doi.org/10.1085/jgp.201411259

Article and author information

Helmut Bischof

Department of Pharmacology, Toxicology and Clinical Pharmacy, Institute of Pharmacy, University of Tuebingen, Auf der Morgenstelle 8, 72076 Tuebingen, Germany
ORCID iD: 0000-0003-2380-600X

Selina Maier
Department of Pharmacology, Toxicology and Clinical Pharmacy, Institute of Pharmacy, University of Tuebingen, Auf der Morgenstelle 8, 72076 Tuebingen, Germany, Dr Margarete Fischer-Bosch Institute of Clinical Pharmacology, Auerbachstraße 112, 70376 Stuttgart, Germany

Piotr Koprowski
Laboratory of Intracellular Ion Channels, Nencki Institute of Experimental Biology, Polish Academy of Sciences, 3 Pasteur Street, 02-093 Warsaw, Poland

Bogusz Kulawiak
Laboratory of Intracellular Ion Channels, Nencki Institute of Experimental Biology, Polish Academy of Sciences, 3 Pasteur Street, 02-093 Warsaw, Poland

Sandra Burgstaller
Department of Pharmacology, Toxicology and Clinical Pharmacy, Institute of Pharmacy, University of Tuebingen, Auf der Morgenstelle 8, 72076 Tuebingen, Germany, NMI Natural and Medical Sciences Institute at the University of Tuebingen, Markwiesenstraße 55, Reutlingen 72770, Germany, Institute of Clinical Anatomy and Cell Analysis, University of Tuebingen, Oesterbergstraße 3, 72074 Tuebingen, Germany

Joanna Jasińska
Laboratory of Intracellular Ion Channels, Nencki Institute of Experimental Biology, Polish Academy of Sciences, 3 Pasteur Street, 02-093 Warsaw, Poland

Kristian Serafimov
Institute of Pharmaceutical Sciences, Pharmaceutical (Bio-)Analysis, University of Tuebingen, Auf der Morgenstelle 8, 72076 Tuebingen, Germany

Monika Zochowska
Laboratory of Intracellular Ion Channels, Nencki Institute of Experimental Biology, Polish Academy of Sciences, 3 Pasteur Street, 02-093 Warsaw, Poland

Dominic Gross
Department of Pharmacology, Toxicology and Clinical Pharmacy, Institute of Pharmacy, University of Tuebingen, Auf der Morgenstelle 8, 72076 Tuebingen, Germany

Werner Schroth
Dr Margarete Fischer-Bosch Institute of Clinical Pharmacology, Auerbachstraße 112, 70376 Stuttgart, Germany, University of Tuebingen, Tuebingen, Germany

Lucas Matt
Department of Pharmacology, Toxicology and Clinical Pharmacy, Institute of Pharmacy, University of Tuebingen, Auf der Morgenstelle 8, 72076 Tuebingen, Germany

David Arturo Juarez Lopez
Medical Clinic IV, University Hospital Tuebingen, Otfried-Müller-Straße 10, 72076 Tuebingen, Germany

Ying Zhang
Department of Pharmacology, Toxicology and Clinical Pharmacy, Institute of Pharmacy, University of Tuebingen, Auf der Morgenstelle 8, 72076 Tuebingen, Germany

Irina Bonzheim
Institute of Pathology and Neuropathology, University Hospital Tuebingen, 72076 Tuebingen, Germany

Florian A. Büttner
Dr Margarete Fischer-Bosch Institute of Clinical Pharmacology, Auerbachstraße 112, 70376 Stuttgart, Germany, University of Tuebingen, Tuebingen, Germany

Falko Fend
Institute of Pathology and Neuropathology, University Hospital Tuebingen, 72076 Tuebingen, Germany

Matthias Schwab
Dr Margarete Fischer-Bosch Institute of Clinical Pharmacology, Auerbachstraße 112, 70376 Stuttgart, Germany, Institute of Pathology and Neuropathology, University Hospital Tuebingen, 72076 Tuebingen, Germany, Image-Guided and Functionally Instructed Tumor Therapies Cluster of Excellence (iFIT), University of Tuebingen, Roentgenweg 11, 72076 Tuebingen, Germany, Department of Clinical Pharmacology, University of Tuebingen, Auf der Morgenstelle 8, 72076 Tuebingen, Germany, Department of Biochemistry and Pharmacy, University of Tuebingen, Auf der Morgenstelle 8, 72076 Tuebingen, Germany, German Cancer Consortium (DKTK), German Cancer Research Center, Partner Site Tuebingen, Auf der Morgenstelle 15, 72076 Tuebingen, Germany

Andreas L. Birkenfeld
Medical Clinic IV, University Hospital Tuebingen, Otfried-Müller-Straße 10, 72076 Tuebingen, Germany
ORCID iD: 0000-0003-1407-9023

Roland Malli
Gottfried Schatz Research Center, Molecular Biology and Biochemistry, Medical University of Graz, Neue Stiftingtalstraße 6, 8010 Graz, Austria, BioTechMed Graz, Mozartgasse 12, 8010 Graz, Austria
ORCID iD: 0000-0001-6327-8729

Michael Lämmerhofer
Institute of Pharmaceutical Sciences, Pharmaceutical (Bio-)Analysis, University of Tuebingen, Auf der Morgenstelle 8, 72076 Tuebingen, Germany

Piotr Bednarczyk
Department of Physics and Biophysics, Warsaw University of Life Sciences (SGGW), Nowoursynowska St. 159 02-776 Warsaw, Poland

Adam Szewczyk
Laboratory of Intracellular Ion Channels, Nencki Institute of Experimental Biology, Polish Academy of Sciences, 3 Pasteur Street, 02-093 Warsaw, Poland

Robert Lukowski
Department of Pharmacology, Toxicology and Clinical Pharmacy, Institute of Pharmacy, University of Tuebingen, Auf der Morgenstelle 8, 72076 Tuebingen, Germany
For correspondence: robert.lukowski@uni-tuebingen.de

Copyright

Editors

Reviewing Editor
Alejandro San Martín
Centro de Estudios Científicos, Valdivia, Chile

Senior Editor
Caigang Liu
Shengjing Hospital of China Medical University, Shenyang, China

Reviewer #1 (Public Review):

Original Review:

Bischoff et al present a carefully prepared study on a very interesting and relevant topic: the role of ion channels (here a Ca2+-activated K+ channel BK) in regulating mitochondrial metabolism in breast cancer cells. The potential impact of these and similar observations made in other tumor entities has only begun to be appreciated. That being said, the authors pursue in my view an innovative approach to understanding breast cancer cell metabolism.

Considering the following points would further strengthen the manuscript:

Methods:

(1) The authors use an extracellular Ca2+ concentration (2 mM) in their Ringer's solutions that is almost twice as high as the physiologically free Ca2+ concentration (ln 473). Moreover, the free Ca2+ concentration of their pipette solution is not indicated (ln 487).

(2) Ca2+I measurements: The authors use ATP to elicit intracellular Ca2+ signals. Is this then physiological stimulus for Ca2+ signaling in breast cancer? What is the rationale for using ATP? Moreover, it would be nice to see calibrated baseline values of Ca2+i

(3) Membrane potential measurements: It would be nice to see a calibration of the potential measurements; this would allow to correlate IV relationship with membrane potential. Without calibration it is hard to compare unless the identical uptake of the dye is shown. Do paxilline or IbTx also induce a depolarization?

(4) mito-potential measurements: Why did the authors use such a long time course and preincubated cells mit channel blockers overnight? Why did they not perform paired experiments and record the immediate effect of the BK channel blockers in the mito potential?

(5) MTT assay are also based on mitochondrial function - since modulation of mito function is at the core of this manuscript, an alternative method should be used.

Results:

(1) Fig. 5G: The number of BK "positive" mitoplasts is surprisingly low - how does this affect the interpretation? Did the authors attempt to record mitoBK current in the "whole-mitoplast" mode? How does the mitoBK current density compare with that of the plasma membrane? Is it possible to theoretically predict the number of mitoBK channels per mitochondrium to elicit the observed effects? Can these results be correlated with immuno-localization of mitoBK channels?

(2) There are also reports about other mitoK channels (e.g. Kv1.3, KCa3.1, KATP) playing an important role in mitochondrial function. Did the authors observe them, too? Can the authors speculate on the relative importance of the different channels? Is it known whether they are expressed organ-/tumor-specifically?

Comments on revised version:

The authors responded to all of my comments - except for one - in a satisfactory way so that I have no further concerns. The authors have prepared a very interesting piece of work that advances the field.

However, I disagree with respect to their interpretation of statistics. Individually analyzed cells are not the best biological replicate per se. In my view a true replicate requires the use of an independent batch of cells derived from a new passage. The statistical analysis can only based on the total number of n cells, if each replicate contributes the same number of cells. If this is not the case, the authors will have to calculate the average of each replicate first so that they are equally weighted.

https://doi.org/10.7554/eLife.92511.2.sa2

Reviewer #2 (Public Review):

Summary:

The large-conductance Ca2+ activated K+ channel (BK) has been reported to promote breast cancer progression, but it is not clear how. The present study, carried out in breast cancer cell lines, concludes that BK located in mitochondria reprograms cells towards the Warburg phenotype, one of the metabolic hallmarks of cancer.

Strengths:

The use of a wide array of modern complementary techniques, including metabolic imaging, respirometry, metabolomics and electrophysiology. On the whole experiments are astute and well designed, and appear carefully done. The use of a BK knock out cells to control for the specificity of the pharmacological tools is a major strength. The manuscript is clearly written. There are many interesting original observations that may give birth to new studies.

Weaknesses: The main conclusion regarding the role of a BK channel located in mitochondria appears is not sufficiently supported. Other perfectible aspects are the interpretation of co-localization experiments and the calibration of Ca2+ dyes. These points are discussed in more detail in the following paragraphs:

(1) May the metabolic effects be ascribed to a BK located in mitochondria? Unfortunately not, at least with the available evidence. While it is clear these cells have a BK in mitochondria

(characteristic K+ currents detected in mitoplasts) and it is also well substantiated that the metabolic effects in intact cells are explained by an intracellular BK (paxilline effects absent in the BK KO), it does not follow that both observations are linked. Given that ectopic BK-DEC appeared at the surface, a confounding factor is the likely expression of BK in other intracellular locations such as ER, Golgi, endosomes, etc. To their credit authors acknowledge this limitation several times throughout the text ("...presumably mitoBK...") but not in other important places, particularly in title and abstract.

(2) mitoBK subcellular location. Pearson correlations of 0.6 and about zero were obtained between the locations of mitoGREEN on one side, and mRFP or RFP-GPI on the other (Figs. 1G and S1E). These are nice positive and negative controls. For BK-DECRFP however the Pearson correlation was about 0.2. What is the Z resolution of apotome imaging? Assuming an optimum optical section of 600 nm, as obtained a 1.4 NA objective with a confocal, that mitochondria are typically 100 nm in diameter and that BK-DECRFP appears to stain more structures that mitoGREEN, the positive correlation of 0.2 may not reflect colocalization. For instance, it could be that BK-DECRFP in not just in mitochondria but in a close underlying organelle e.g. the ER. Along the same line, why did BK-RFP also give a positive Pearson? Isnt that unexpected? Considering that BK-DEC was found by patch clamping at the plasma membrane, the subcellular targeting of the channel is suspect. Could it be that the endogenous BK-DEC does actually reside exclusively in mitochondria (a true mitoBK), but overflows to other membranes upon overexpression? Regarding immunodetection of BK in the mitochondrial Percoll preparation (Fig. S5), absence of NKA demonstrates absence of plasma membrane contamination, but does not inform about contamination by other intracellular membranes.

(3) Calibration of fluorescent probes. The conclusion that BK blockers or BK expression affects resting Ca2+ levels should be better supported. Fluorescent sensors and dyes provide signals or ratios that need be calibrated if comparisons between different cell types or experimental conditions are to be made. This is implicitly acknowledged here when monitoring ER Ca2+, with an elaborate protocol to deplete the organelle in order to achieve a reading at zero Ca2+.

(4) Line 203. "...solely by the expression of BKCa-DECRFP in MCF-7 cells". Granted, the effect of BKCa-DECRFP on the basal FRET ratio appears stronger than that of BK-RFP, but it appears that the latter had some effect. Please provide the statistics of the latter against the control group (after calibration, see above).

The revised version of the manuscript has incorporated my suggestions to a very reasonable degree, in several cases with new experiments. The details of these improvements can be found in the correspondence.

https://doi.org/10.7554/eLife.92511.2.sa1

Reviewer #3 (Public Review):

The original research article, titled "mitoBKCa is functionally expressed in murine and human breast cancer cells and promotes metabolic reprogramming" by Bischof et al, has demonstrated the underlying molecular mechanisms of alterations in the function of Ca2+ activated K+ channel of large conductance (BKCa) in the development and progression of breast cancer. The authors also proposed that targeting mitoBKCa in combination with established anti-cancer approaches, could be considered as a novel treatment strategy in breast cancer treatment.

The paper is modified according to the reviewer's comments. Most of the queries raised by this reviewer were answered. However, the preclinical implication of this study can also be

manifested in combinatorial treatment with known chemotherapeutic drugs which is lacking in this manuscript. Hopefully, the authors will consider this in their future study.

https://doi.org/10.7554/eLife.92511.2.sa0

Author Response

The following is the authors' response to the current reviews.

Our answer to the final point(s) raised is as follows:

"We thank the reviewer for the comment. We checked our datasets accordingly. Typically, the n of cells showed deviations of maximally 20% from experiment to experiment (e.g. 16-24 cells per experiment). Additionally, experiments were performed using different passages of the cells. Moreover, data were validated at different time-points during the study using newly thawed cell lines."

The following is the authors' response to the original reviews.

> ***Public Reviews:***
>
> ***Reviewer #1 (Public Review):***
>
> *Bischoff et al present a carefully prepared study on a very interesting and relevant topic: the role of ion channels (here a Ca2+-activated K+ channel BK) in regulating mitochondrial metabolism in breast cancer cells. The potential impact of these and similar observations made in other tumor entities has only begun to be appreciated. That being said, the authors pursue in my view an innovative approach to understanding breast cancer cell metabolism. Considering the following points would further strengthen the manuscript:*

We thank reviewer #1 for the overall positive feedback on our study.

> *Methods:*
>
> *(1) The authors use an extracellular Ca2+ concentration (2 mM) in their Ringer's solutions that is almost twice as high as the physiologically free Ca2+ concentration (ln 473). Moreover, the free Ca2+ concentration of their pipette solution is not indicated (ln 487).*

Indeed, we utilized 2 mM of Ca2+ in the physiologic live-cell imaging buffer. This concentration could actually be a little lower than the total Ca2+ concentration (ranging usually from 2.2 to 2.6 mM) in the body, while the free Ca2+ concentration is typically half as high. Nevertheless, we find multiple studies different from ours, which utilized 2 mM for their live-cell-based experiments. Please check the following studies, which represent only a small selection:

https://doi.org/10.1038/s41598-019-49070-8

https://doi.org/10.1016/j.bpj.2020.08.045

https://doi.org/10.1016/j.redox.2022.102319

However, to ensure that the applied conditions are physiologically relevant, we reperformed experiments using MMTV-PyMT WT and MMTV-PyMT BK-KO cells and compared cytosolic Ca2+ concentrations over time in response to cell stimulation with ATP, either in the presence of 1.0 mM (Author response image 1A) or 2.0 mM extracellular Ca2+ (Author response

image1B). The respective graphs are attached in the following for reviewer's inspection. As expected, we find that the intracellular Ca2+ concentration in MMTV-PyMT WT and BK-KO cells was dependent on the extracellular Ca2+ concentration. Importantly, however, irrespective of the exact Ca2+ concentration applied, we observed a similar difference in basal cytosolic Ca2+ between MMTV-PyMT WT and BK-KO cells (Author response image1C).

Author response image 1.

Cytosolic Ca2+ concentrations over-time in the presence of 1.mM or 2.0 mM extracellular Ca2+.

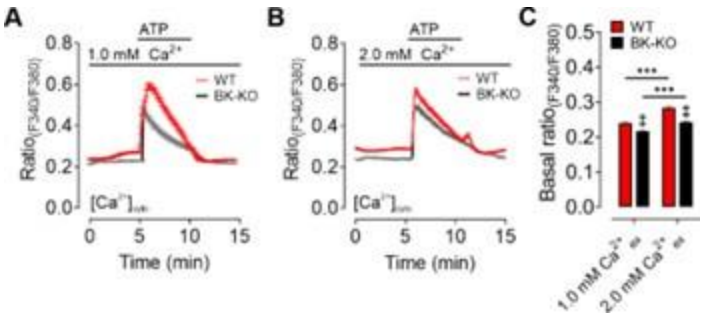

Concerning the Ca2+ concentration in the patch-pipette – we are very glad that you uncovered an error in our description and apologize for the mistake. Actually, the information the reviewer is referring to was already given in the previous version of the manuscript, but unclear because a comma was shifted (see line 487 in the originally submitted manuscript). The Ca2+ concentration of the patch-pipette was 0.1 mM in the presence of 0.6 mM EGTA, which should (according to Ca-EGTA calculator, https://somapp.ucdmc.ucdavis.edu/pharmacology/bers/maxchelator/CaEGTA-NIST.htm) be equivalent to ~30 nM of free Ca2+ in the patch pipette. We corrected the mistake in the manuscript and thank the reviewer again for spotting this inaccuracy.

> *(2) Ca2+I measurements: The authors use ATP to elicit intracellular Ca2+ signals. Is this then a physiological stimulus for Ca2+ signaling in breast cancer? What is the rationale for using ATP? Moreover, it would be nice to see calibrated baseline values of Ca2+i.*

We thank the reviewer for the comment and suggestion. Importantly, it was demonstrated recently, that all of the utilized cell lines respond to treatment with extracellular ATP with a prominent increase in Ca2+I, most probably indicating the expression of purinergic receptors, which was a prerequisite to observe ATP induced changes in [Ca2+]i.

https://doi.org/10.1038/s41419-022-05329-z,

https://doi.org/10.1093/carcin/bgt493

https://doi.org/10.1038/s41598-018-26459-5

Furthermore, ATP plays a crucial role in the tumor microenvironment, where high rates of cell death occur. Hence, ATP is of pathophysiologic relevance for the utilized cancer cell lines.

https://doi.org/10.1038/s41568-018-0037-0

https://doi.org/10.3390/cells9112496

https://doi.org/10.1002/jcp.30580

Following the suggestions by Reviewer #1 (and #2), we included calibrations of Ca2+cyto and Ca2+mito in the manuscript, by depleting the intracellular Ca2+ stores using Ionomycin in the absence of extracellular Ca2+ (EGTA) to validate the basal difference in Ca2+cyto and Ca2+mito. Additionally, Ca2+cyto was calibrated under basal and inhibitor treated conditions, and values in nM are given in the text (p. 5, lines 185-190, 193-195 and 199-200, in the tracked changes version of the MS). The new data can be found in new Figure S2F – Figure S2J and new Figure S2R – Figure S2V. Moreover, we calculated basal [Ca2+]cyto in the different BKCa pro- and deficient cell lines and under inhibitor treated conditions. We additionally added information about the pathophysiologic relevance of ATP in the tumor microenvironment in lines 175-178 in the tracked changes version of the manuscript.

> *(3) Membrane potential measurements: It would be nice to see a calibration of the potential measurements; this would allow us to correlate the IV relationship with membrane potential. Without calibration, it is hard to compare unless the identical uptake of the dye is shown. Does paxilline or IbTx also induce depolarization?*

We thank the reviewer for the suggestion. Indeed, membrane potential calibrations/ measurements using the membrane potential sensitive dye Dibac4(3) would be interesting, however, technically hardly feasible. The reason is that the principle of the dye is based on different uptake in response to differences in membrane potential, and not ratiometric as for most other dyes/ sensors used. Considering this limitation, we decided to perform membrane potential measurements by patch-clamp analysis. Additionally, we performed these experiments upon inhibition of PM-located BKCa by IBTX. Current-clamp experiments confirmed the difference in basal membrane potential between MMTV-PyMT WT and BK-KO cells (consult new Figure S1C and lines 127-130 in the tracked changes version of the manuscript). Interestingly, IBTX treatment depolarized the PM potential to the BK-KO cell level, which validates that BK activity and PM potential are connected. In addition to this approach, we utilized our recently developed genetically encoded K+ sensors revealing basal differences in [K+]cyto between MMTV-PyMT WT and BK-KO cells. Also this difference between both genotypes was equalized by IBTX as the respective treatment increased [K+]cyto only in WT cells, which most likely explains the cause of PM depolarization (consult lines 130-135 in the tracked changes version of the manuscript and new Figure S1D and Figure S1E).

> *(4) Mito-potential measurements: Why did the authors use such a long time course and preincubate cells with channel blockers overnight? Why did they not perform paired experiments and record the immediate effect of the BK channel blockers in the mito potential?*

We thank the reviewer for the suggestion. We performed TMRM-based experiments with MMTV-PyMT WT cells in response to short-term exposure to paxilline, which did not significantly affect the mitochondrial membrane potential, at least within 15 minutes of treatment (Author response image 2). This indicates, that further downstream processes subsequent to (mito) BKCa inhibition affect the mitochondrial membrane potential(MMP), most probably including remodeling processes of the respiratory chain, mitochondrial ion homeostasis or glycolytic activity, ultimately also delivering reduction equivalents to mitochondria. Our final goal was to validate potential differences between a BKCa pro-and deficient cell model, whereby the latter cells lacked the BKCa channel since its origination. Hence, “long-term” (~12h) BKCa inhibition as performed in our experiments rather reflects the BK-KO cell situation. Taken together with the new experiment (Author response image 2), we can now state that the effect of BK inhibition on the MMP is at least not the consequence of an acute (within minutes) channel blockade.

Author response image 2.

Mitochondrial membrane potential, as measured using TMRM, in response to acute short-term administration of 5µM paxilline, followed by mitochondrial depolarization using FCCP.

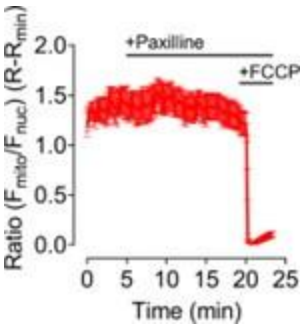

> *(5) MTT assays are also based on mitochondrial function - since modulation of mito function is at the core of this manuscript, an alternative method should be used.*

We thank the reviewer for the important comment. We performed additional, immunofluorescence-based experiments using Ki-67 staining to assess cell proliferation rates. The newly added data can be found in the text, lines 409-412 in the tracked changes version of the manuscript and new Figure S6D-F. The results obtained confirm the MTTbased results (Fig.6H-I).

> *Results:*
>
> *(1) Fig. 5G: The number of BK "positive" mitoplasts is surprisingly low - how does this affect the interpretation? Did the authors attempt to record mitoBK current in the "whole-mitoplast" mode? How does the mitoBK current density compare with that of the plasma membrane? Is it possible to theoretically predict the number of mitoBK channels per mitochondrion to elicit the observed effects? Can these results be correlated with the immuno-localization of mitoBK channels?*

Indeed, the number of BKCa-positive mitoplasts appears low on a first view. However, as these experiments were performed in a mitoplast-attached mode, it is important to keep in mind that only a very small area of the actual mitoplast is investigated with each patch. If no channel was detected in such region, the patch was depicted as “empty”, as presented in Fig.5G, which does, however, not mean that the entire mitochondria was actually BKCa negative. Hence, the density of BKCa in the IMM might be higher than expected from our experiments. Nevertheless, already earlier results using glioblastoma cell lines – considered to be one of the cell lines mostly enriched in mitoBKCa – demonstrated a quite low density of BKCa β4 regulatory subunit in mitochondria – please see figure 2B in the following paper: 10.1371/journal.pone.0068125 – which (based on 1:1 stoichiometry of α and β subunits) also suggests that the density of the alpha subunit of BKCa might be low in this compartment.

Author response image 3.

Author response image 3: Schematic representation of mitoplast attached patch-clamp experiments

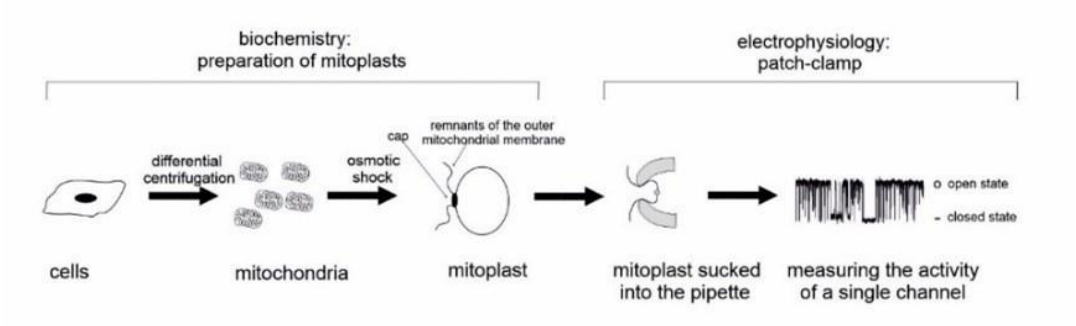

Theoretically, density predictions of mitoBK compared to PM localized BKCa would be possible if whole-mitoplast experiments were performed, however, we are unsure what added value this information would actually burst, allowing the pharmacologic modulation of structures originally located within the mitochondrial matrix. Please also consult Author response image 3. According to the most recent models, even if there are other views on this, mitoBKCa is oriented in a way, that the C-terminus with its Ca2+ binding bowl is located within the mitochondrial matrix. Hence, to allow Ca2+ sensitivity experiments of the channel, broken up (by swelling) mitoplasts are required to make the Ca2+ binding bowl accessible for Ca2+ manipulations in the bath solution. This approach does not allow us to compare the channel density to that of the PM.

Finally, to the best of our knowledge, a combination of immunofluorescence with mitoplast patch-clamp experiments is not feasible yet, and would probably be impossible due to the low density of the mitoBKCa as well as the lack of highly sensitive and specific antibodies.

> *(2) There are also reports about other mitoK channels (e.g. Kv1.3, KCa3.1, KATP) playing an important role in mitochondrial function. Did the authors observe them, too? Can the authors speculate on the relative importance of the different channels? Is it known whether they are expressed organ-/tumor-specifically?*

Author response image 4.

Representative single channels different to mitoBKCa detected in MDAMB-453 mitoplasts.

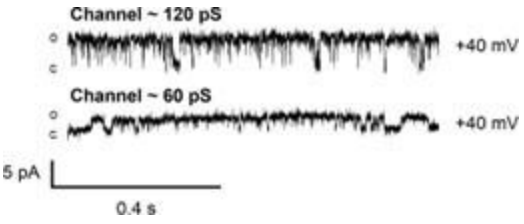

The reviewer is right, other K+ channels have been found in mitochondria and these also play a role in tumor cells. This is also consistent with our data (Fig.5G), where we observed other channels in the mitoplasts of BCCs as well. These all four cell lines tested. According to their conductance and our expectations from literature, these channels may e.g. include mitoIKCa, mitoSKCa, mitoKATP orothers (10.1146/annurev-biophys-092622-094853). As we focused, however, on patches containing a mitoBKCa, we did not further pharmacologically characterize these channels. Two examples of channels we found in these mitoplasts besides BKCa are presented for reviewers' inspection (Author response image 4). As our manuscript focusses on mitoBKCa, we did not further classify these channels in smaller subgroups according to their conductance, as we feel that a differentiation between BKCa (~210 pS), and

channels showing a conductance ≤150pS, or a conductance ≤100 pS is sufficient. Furthermore, this additional information would dilute our story too much making it difficult for the (non-specialist) reader to follow the red thread of the study. We added respective information in the manuscript, however. Please consult lines 365-366 in the tracked changes version of the manuscript.

Reviewer #1 is right, the observed the different K+ channels might of course be organ- or tumor-specific. For example, it has been reported that the expression of K+ channels is different in various cancer cell (lines) (https://doi.org/10.2174/1381612813199990032, 10.1016/j.pharmthera.2021.107874, 10.1038/nrc3635), a fact, which also according to our study might be exploited for pharmacological manipulation, aiming to affect proliferation/apoptosis of cancer cells. Further, a recently published single-cell and spatially resolved atlas of human breast cancer implies that the expression of different K+ channels (such as mitoIKCa, mitoSKCa, mitoKATP) might even differ between cancer- and non-cancer cells within a single tumour (https://doi.org/10.1038/s41588-021-00911-1).

> ***Reviewer #2 (Public Review):***
>
> *Summary:*
>
> *The large-conductance Ca2+ activated K+ channel (BK) has been reported to promote breast cancer progression, but it is not clear how. The present study carried out in breast cancer cell lines, concludes that BK located in mitochondria reprograms cells towards the Warburg phenotype, one of the metabolic hallmarks of cancer.*
>
> *Strengths:*
>
> *The use of a wide array of modern complementary techniques, including metabolic imaging, respirometry, metabolomics, and electrophysiology. On the whole, experiments are astute and well-designed and appear carefully done. The use of BK knock-out cells to control for the specificity of the pharmacological tools is a major strength. The manuscript is clearly written.*
>
> *There are many interesting original observations that may give birth to new studies.*
>
> *Weaknesses:*
>
> *The main conclusion regarding the role of a BK channel located in mitochondria appears is not sufficiently supported. Other perfectible aspects are the interpretation of co-localization experiments and the calibration of Ca2+ dyes. These points are discussed in more detail in the following paragraphs:*

We thank reviewer #2 for the thorough assessment of our study.

> *(1) May the metabolic effects be ascribed to a BK located in mitochondria? Unfortunately not, at least with the available evidence. While it is clear these cells have a BK in mitochondria (characteristic K+ currents detected in mitoplasts) and it is also well substantiated that the metabolic effects in intact cells are explained by an intracellular BK (paxilline effects absent in the BK KO), it does not follow that both observations are linked. Given that ectopic BKDEC appeared at the surface, a confounding factor is the likely expression of BK in other intracellular locations such as ER, Golgi, endosomes, etc. To their credit, authors acknowledge this limitation several times throughout the text ("...presumably mitoBK...") but not in other important places, particularly in the title and abstract.*

We thank the reviewer for this important comment and amended the title and abstract, respectively. The title of the manuscript was changed to “mitoBKCa is functionally expressed

in murine and human breast cancer cells and potentially contributes to metabolic reprogramming." Additionally, we changed appropriate passages in the text, to emphasize that mitoBKCa potentially mediates the metabolic reprogramming, but other intracellular channels could also contribute to these processes.

> *(2) MitoBK subcellular location. Pearson correlations of 0.6 and about zero were obtained between the locations of mitoGREEN on one side, and mRFP or RFP-GPI on the other (Figs. 1G and S1E). These are nice positive and negative controls. For BK-DECRFP however, the Pearson correlation was about 0.2. What is the Z resolution of apotome imaging? Assuming an optimum optical section of 600 nm, as obtained by a 1.4 NA objective with a confocal, that mitochondria are typically 100 nm in diameter and that BK-DECRFP appears to stain more structures than mitoGREEN, the positive correlation of 0.2 may not reflect colocalization. For instance, it could be that BK-DECRFP is not just in mitochondria but in a close underlying organelle e.g. the ER. Along the same line, why did BK-RFP also give a positive Pearson? Isnt that unexpected? Considering that BK-DEC was found by patch clamping at the plasma membrane, the subcellular targeting of the channel is suspect. Could it be that the endogenous BK-DEC does actually reside exclusively in mitochondria (a true mitoBK), but overflows to other membranes upon overexpression? Regarding immunodetection of BK in the mitochondrial Percoll preparation (Fig. S5), the absence of NKA demonstrates the absence of plasma membrane contamination but does not inform about contamination by other intracellular membranes.*

Indeed, it seems that BKCa-DEC is not an exclusive mitoBKCa, at least not upon (over-/)expression in MCF-7 cells. It is known from literature, that mitochondrial K+ channels are encoded by the nuclear genome, as no obvious gene for a K+ channel is found in the mitochondrial genome. Channel proteins are synthetized by cytosolic ribosomes and likely translocated into mitochondria via the TOM/TIM system. Although some K+ channels possess a mitochondrial targeting sequence at the N-terminus, their import is mostly far from a general mechanism, and this seems also to be true for BK channels. In the case of the K+ channel Kv1.3, an even more complex scenario is hypothesized, as the channel located in the PM could be transferred to mitochondria via mitochondria-associated membranes (MAM) structures of the ER (https://doi.org/10.3390/ijms20030734). Yet, the detailed mechanism for BK shuttling to mitochondria is not fully understood. Possibly, overflow is exactly what is happening, due to very high levels of BK-DEC expression upon transfection. However, that the channel translocates to the IMM upon transfection is not surprising and was also demonstrated for other cell models including HEK293 – see e.g. 10.1038/s41598-021-904653. Unfortunately, transfection efficiency of MCF-7 is quite low compared to HEK293 – hence, quantitative statements from mito-patches upon transfection are difficult.

In order to ensure that the mitochondrial colocalization is not a matter of poor microscope resolution, we reperformed these experiments using confocal imaging on a Zeiss LSM980 with an Airyscan 2 detector, yielding z resolutions of ~ 450 nm. These experiments confirmed the increased colocalization of BKCa-DEC with mitochondria compared to BKCa lacking the DEC exon. Furthermore, this imaging at higher resolution demonstrated, that, unfortunately, colocalization might not be the best analysis, as especially fragmented mitochondria showed a clear MitoGREEN stained matrix, surrounded by red fluorescence derived from BKCaDECRFP present in the IMM (revised Fig. 1G).

To validate the results derived from immunoblotting, we additionally stained the membranes for TMX1, a marker for the ER membrane. This analysis confirmed the high purity of the mitochondrial isolation without ER-membrane contamination after percoll purification, and hence validated the presence of BKCa in the mitochondrial membrane (revised Fig. S5D). The additional information can be found in lines 156-159 in the tracked changes version of the manuscript.

> *(3) Calibration of fluorescent probes. The conclusion that BK blockers or BK expression affects resting Ca2+ levels should be better supported. Fluorescent sensors and dyes provide signals or ratios that need to be calibrated if comparisons between different cell types or experimental conditions are to be made. This is implicitly acknowledged here when monitoring ER Ca2+, with an elaborate protocol to deplete the organelle in order to achieve a reading at zero Ca2+.*

We thank the reviewer for the important comment. Please note that at no point in the manuscript we aim to compare different cell lines concerning their intracellular Ca2+ concentration, but we only compare the same cell lines after the different treatments, as we are aware of this limitation of fluorescent probes. However, to validate the differences in intracellular Ca2+ concentrations, we calibrated the signals derived from Fura-2 and 4mtD3cpV using ionomycin in combination with cellular Ca2+ depletion/ saturation. The newly added data can be found in the text, lines 185-190, 192-195, 199-200, and 228-230 in the tracked changes version of the manuscript, as well as new Figure S2F – Figure S2J and new Figure S2R – Figure S2V

> *Line 203. "...solely by the expression of BKCa-DECRFP in MCF-7 cells". Granted, the effect of BKCa-DECRFP on the basal FRET ratio appears stronger than that of BK-RFP, but it appears that the latter had some effect. Please provide the statistics of the latter against the control group (after calibration, see above).*

Author response image 5.

Dot blot for data shown in Figure 2I.

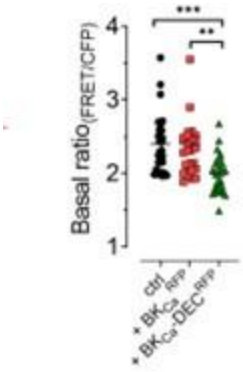

The reviewer is right, it seems that BKCaRFP may also affect [Ca2+]mito. However, the effect is not significant and shows a p-value of p>0.999 using Kruskal-Wallistest followed by Dunn's multiple comparison test, due to the non-normally distributed nature of the data. p=0.0002 for ctrl vs. BKCa-DECRFP and 0.0022 for BKCaRFP vs. BKCa-DECRFP, however. We added a scatter dot-blot of the respective data as Author response image 5 for reviewer's inspection. Additionally, first, even using a more stringent statistical test by only comparing ctrl vs BKCaRFP using Mann-Whitney test, the results are not significant, as the p-value was determined at 0.4467, and second, we performed the requested Ca2+calibration using ionomycin under these conditions, which confirmed the difference between ctrl cells and BKCa-DECRFP expressing cells, but not BKCaRFP expressing ones. Please see Figure S2V.

> ***Reviewer #3 (Public Review):***
>
> *The original research article, titled "mitoBKCa is functionally expressed in murine and human breast cancer cells and promotes metabolic reprogramming" by Bischof et al,*

has demonstrated the underlying molecular mechanisms of alterations in the function of Ca2+ activated K+ channel of large conductance (BKCa) in the development and progression of breast cancer. The authors also proposed that targeting mitoBKCa in combination with established anti-cancer approaches, could be considered as a novel treatment strategy in breast cancer treatment.

The paper is clearly written, and the reported results are interesting.

Strengths:

Rigorous biophysical experimental proof in support of the hypothesis.

Weaknesses:

A combinatorial synergistic study is missing.

We thank reviewer #3 for the positive summary of our study. Indeed, we propose that targeting of mitoBKCa in combination with established anti-cancer drugs may represent a novel anti-cancer treatment strategy. Unfortunately, we feel that the manuscript is very condensed already, and that adding respective required experiments and data to support this hypothesis will make the flow of the manuscript more complex or even incomprehensible. As no attempts linking mitoBKCa activity with anti-cancer therapies have been made so far, we removed the respective information from the abstract and only discuss this aspect.

Recommendations for the authors:

Reviewer #1 (Recommendations For The Authors):

(1) Statistics: Legends have to contain information about the number of biological replicates (N) and cells analysed (n). Statistics must be calculated with the averages of the replicates.

Author response image 6.

Representative single cell responses of Fura-2 loaded MMTV-PyMT WT cells.

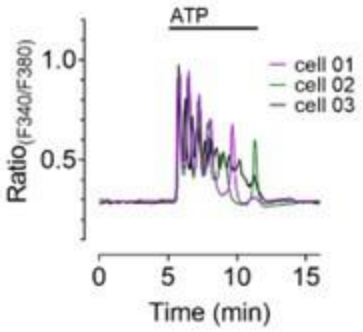

We thank the reviewer for the comment and added the missing details to all figure legends.

We feel that using each cell represents exactly the power of high-resolution live-cell imaging, as there is no better biological replicate than a single separated cell, which is observed by fluorescence microscopy. This analysis is also able to visualize cell-to-cell differences in the microscopy area, similarly to patch-clamp experiments, where each single cell or mitoplast patched is used as a single replicate. Please find a representative dataset derived from fluorescence microscopy of different responses of neighboring single cells in Author response image 6.

> *(2) Fig. 1G: This is a poor resolution figure, mostly because of its far too small size; in its current form it bears very little information.*

We agree with reviewer #1 and reperformed the imaging experiments using high resolution confocal imaging and exchanged the respective images. We feel that this increased the quality of the images significantly. Unfortunately, we were not able to increase the size of the images in the main figure, hence, we added magnifications of the respective images as new Figure S1I.

> *(3) Fig. 1H: What do the dotted grey lines and the labels stand for?*

We believe Reviewer #1 is probably referring to Figure 1G. As indicated in the figure panel and in the text, the grey dotted lines and labels indicate the colocalization scores of mtRFP and RFP-GPI with MitoGREEN, respectively. These data are also shown in Figure S1H, including error bars and statistics. We added additional information in the text to make the meaning of the lines clearer to the reader. Please consult lines 149 – 150 in the tracked changes version of the manuscript.

> ***Reviewer #2 (Recommendations For The Authors):***
>
> *(1) May the metabolic effects be ascribed to a BK located in mitochondria? Short of a way to tackle BK function and metabolism specifically in mitochondria, the conclusion may best be toned down to "intracellular BK". For the time being the term "mitoBK" appears too ambitious.*

We fell that you are right and that our previous overstatement requires adaptation as a clear (100%) attribution of the observed metabolic effects solely to mitoBKCa is not definitely possible. We have therefore amended all relevant passages in the entire MS accordingly.

> *(2) MitoBK subcellular location. Please address the points raised in the Public Review.*

As stated above we addressed the point raised in the public review accordingly (please consult new Figure S1I and revised Figure 1G).

> *(3) Calibration of fluorescent probes. Please provide calibrations for cytosolic and mitochondrial Ca2+, for example, the standard high Ca2+/ionophore/metabolic inhibition treatment to reach saturation followed by Ca2+ chelation to obtain zero Ca2+.*

We thank the reviewer for the comment. As you can see from our response to the public review, we performed the respective experiments, and datasets were added in the manuscript.

> *(4) Line 203. "...solely by the expression of BKCa-DECRFP in MCF-7 cells". Granted, the effect of BKCa-DECRFP on the basal FRET ratio appears stronger than that of BK-RFP, but it appears that the latter had some effect. Please provide the statistics of the latter against the control group (after calibration, see above).*

Please consult our response to the (same) comment in the public review.

> *(5) Line 228. The statement "Similar results were obtained in MDA-MB-453 cells" is confusing. As shown in Fig.3, pax reduced ECAR and OCR in MMTV-PyMT WT cells. As ibtx was without effect, it is suggested that intracellular BK support metabolism. However, the effect of pax on MDA cells was the opposite. Doesnt́ this divergence speak against a*

> *universal role of intracellular BKs in promoting metabolism in BCCs? A similar point may be made regarding metabolomics, which showed no effects of pax on lactate and pyruvate in MMTV-PyMT WT cells but stimulation in MDA cells. Perhaps the word "promotes" in the title of the figure should be replaced by something more neutral like "affects" or "alters", as used elsewhere,*

We thank the reviewer for pointing out the overstatement regarding intracellular BK functions and changed the title of the figure as suggested.

With regard to the experiments mentioned, we would like to point out the following aspects:

First, the cell lines used strongly differ in their metabolic settings under basal conditions. While both, MMTV-PyMT and MDA-MB-453 cells seem to show similar basal ECAR levels (if BKCa was present), their OCR seems to differ strongly. MMTV-PyMT cells seem to show a basal OCR which is almost at the maximum already, while MDA-MB-453 cells possess a tremendous capacity in their OCR, as observed upon mitochondrial uncoupling using FCCP. Of note, both, ECAR and OCR are indirect metabolic measures. On the one hand, ECAR measures extracellular acidification, which is accomplished by H+ along with lactate secretion. However, lactate secretion is not the only process leading to extracellular acidification, and ECAR may hence measure a variety of H+ releasing processes, including processes of vesicle secretion. On the other hand, OCR is not directly linked to ATP production, as mitochondrial complex IV is consuming O2, ATP, however, is produced by mitochondrial complex V. This becomes even more evident when having a look on OCRs after FCCP treatment – under these conditions, the H+ gradient is destroyed and ATP synthase activity is reduced, OCR, however, increases to the maximum due to increased supply of mitochondrial complex IV with H+.

Second, please note that the LC-MS-based metabolomics derive from a static single time point and not from an over-time “live” read-outs. Moreover, underlying dynamics of the parameters measured can not be assessed. Hence, as an example, increasing levels of pyruvate can e.g. indicate faster generation, or slower subsequent degradation/ metabolization. A clear in-depth statement about what is happening under basal and BKCa inhibitor treated conditions is hence not possible. The only conclusion possible to draw from these experiments is that paxilline treatment differentially affects metabolic pathways in these cells.

Based on these limitations of both methods, we decided to perform our in-depth fluorescence microscopy-based analysis, which provided strong evidence for intracellular BKCa channels on mitochondrial ATP production. Despite opposing effects of BKCa inhibition on OCR in MMTV-PyMT WT and MDA-MB-453 cells, mitochondrial ATP production was reduced, if BKCa-DECRFP was expressed/ intracellular BKCa was functional.

In line with these findings, mitoBKCa was recently described as an uncoupling protein, which could furthermore explain the differential effects of intracellular BKCa inhibition on OCR. https://doi.org/10.1038/s41598-021-90465-3

> *Minor*
>
> *(6) Fig. 1C. Average fluorescence intensity in 6 experiments was about 20% higher in BK-KO cells relative to WT. Such a small difference is significant but should not be evident to the eye. The pictures selected for illustration appear to show a much larger difference and therefore may not be representative. If this is the case, please omit them. The same goes for the other representative pictures.*

Author response image 7.

: Representative images at different brightnesses.

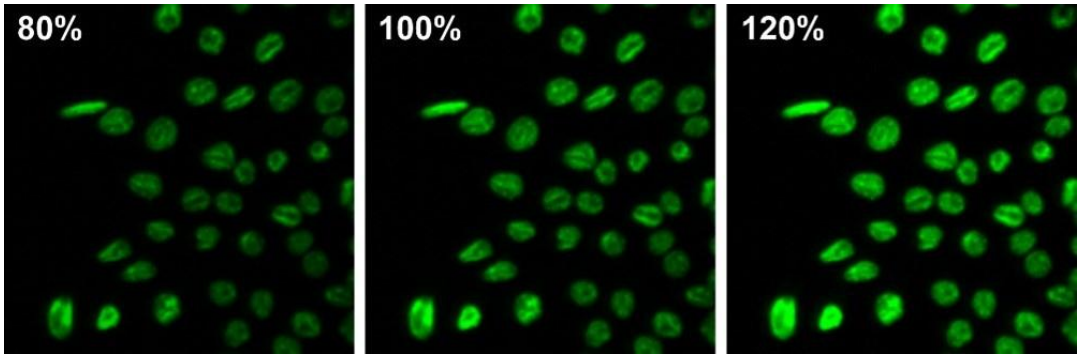

Please note, that the analysis of the images was done in an unbiased way using a Fiji macro. After analysis, we chose representative images, which were closest to the average.

Furthermore, we must kindly disagree with the reviewer as changes of 20% in fluorescence intensity are indeed evident to the eye (consult Author response image 7). This panels show the same image at different brightness levels with intensity differences of 20%. Hence, we feel, that all the images the reviewer was referring are representative for the values given.

> *(7) Line 130. The definition of "recent" is of course relative, but 10 years?*

We are very glad that you have discovered this “inconsistency", and reworded the respective phrase accordingly.

> *(8) Line 327. "conductivity" is the property of a medium, "conductance" is the property of a component, such as a channel.*

We thank the reviewer for the important comment. We revised the text accordingly.

> *(9) Various figures. FRET sensor data are expressed as Ratio(FRET/CFP). This is unusual, typically it should be FRET ratio (YFP/CFP), FRET ratio(mTFP/Venus), etc. Please note that the FRET partners differ between sensors.*

We acknowledge the comment of the reviewer. It is correct that fluorescent proteins vary widely between the sensors (used). Please note, however, the following: The emission measured from these sensors actually represents FRET, as CFP but not YFP is directly excited. Hence, emission is FRET, not the “intrinsic” fluorescence of the YFP. This is getting more and more important to differentiate, as there are probes existing, which can also be “alternately” excited, i.e. CFP and YFP separately, which will then yield the YFP/CFP ratio (https://doi.org/10.1021/acssensors.8b01599). In case of only CFP excitation, we feel, that the term FRET/CFP is preferable over other labelings such as YFP/CFP.

> *(10) BK-DEC makes BCCs cells less oxidative. However, BK-DEC was first described in cardiomyocytes, which are among the most oxidative cell types. It would be useful if authors could address this apparent contradiction in the Discussion Section.*

That is an exciting point that we addressed as follows in the revised MS:

First, it is important to mention that cardiac myocytes do not show a metabolic Warburg setting and are – under physiologic conditions – maintained in a high O2 environment.

Second, a recent study from our group addressed the question about the role of mitoBKCa in primary cardiac myocytes. Indeed, mitoBKCa was functionally expressed in these cells. Interestingly, under physiologic conditions, the channel did not alter (multiple) cell behaviours nor overall cardiac physiology in a mouse model. However, upon induction of ischemia/ reperfusion injury, a lack of BK increased cardiac susceptibility to cell death resulting in increased infarction size (https://doi.org/10.1161/CIRCULATIONAHA.117.028723). Hence, also in this cell model, BKCa only played a role under oxygen limited conditions/ conditions where mitochondria were not properly functioning. Thus, the results derived from cardiac myocytes support our recent findings in BCCs, as BKCa mediates BCC resistance to hypoxic stress/ makes BCCs more independent from oxidative metabolism.

Parts of this discussion were included in the revised MS. Please consult lines 490-500 in the tracked changes version of the manuscript.

> ***Reviewer #3 (Recommendations For The Authors):***
>
> *(1) The study is very well designed and most of the computational analyses were done rigorously.*

We highly appreciate the positive feedback by reviewer #3.

> *(2) The authors should discuss the expression of BKCa in different subsets of breast cancer. Authors may also debate on the level of steroid receptors and BKCa expressions.*

We thank reviewer #3 for the important suggestion and added the requested information in the discussion, lines 445-447 and 450-454 in the tracked changes version of the manuscript.

> *(3) In the discussion section, the authors mentioned that the MCF7 cell is the best model to study this hypothesis. Does it imply that triple-negative breast cancer cell lines express lower levels of BKCa? The authors should discuss this.*

We thank the reviewer for the interesting comment; we would like to point out that the ERα-positive MCF-7 cell line was used to study experimental overexpression of BKCa at an otherwise low baseline level. This does not imply that BKCa is expressed at lower levels in TNBC cell lines; in fact a recent study showed the opposite, i.e. overexpression of BKCa in TNBC patients (10.1186/s12885-020-07071-1). Consistent with our work, the authors conclude that the channel could even be a new strategy for development of a targeted therapy in TNBC. We also added this information in the discussion, lines 450-454 in the tracked changes version of the manuscript.

> *(4) The authors propose that combinatorial targeting of mitoBKCa along with known breast cancer chemotherapeutics can open a new horizon in breast cancer treatment. However, the authors did not perform any experiment to show the synergistic effect as mentioned.*

As already stated in the public reviews, we feel that the manuscript is very condensed already, and that adding the respective experiments and data will make the flow of the study even more complex. For the moment, we removed all information and statements linking mitoBKCa with anti-cancer treatment strategies from the abstract and only discuss this aspect. We hope that the reviewer agrees with us that an extensive analysis of the functional

mitoBKCa status in the context of established breast cancer therapies must be addressed by (our) future studies.

> *Minor Comments:*
>
> *There are several typos and grammatical errors that need further attention and rephrasing.*

We thank the reviewer for the comment and revised the text accordingly.